

CCEMC Project ID: **K130072**

Title of project: **Novel Internal Dry Reforming Solid Oxide Fuel Cell Technology for CO<sub>2</sub> Utilization**

Names and contact information of Principal Investigators:

**Jingli Luo and Tom Etsell**

12<sup>th</sup> Floor, Donadeo ICE

Department of Chemical and Materials Engineering

University of Alberta

Edmonton, AB T6G 1H9

e-mail: jingli.luo@ualberta.ca; Tel: 780 492 2232

e-mail: tom.etsell@ualberta.ca; Tel: 780 492 5594

Name of CCEMC Project Advisor: **Ms. Maureen Kolla**

Completion date of the project: **May 31, 2016**

Total CCEMC funds received: **\$500,000**

Amount of hold back: **\$0**

Submission date: **May 31, 2016**

## 2. TABLE OF CONTENTS

|        |  |    |
|--------|--|----|
| 2.     | Table of Contents  | 2  |
| 2.1.   | List of Tables   | 4  |
| 2.2.   | List of Figures  | 5  |
| 3.     | Executive Summary  | 8  |
| 4.     | Project Description  | 10 |
| 4.1.   | Introduction and background  | 10 |
| 4.2.   | Technical description  | 11 |
| 4.3.   | Project goals and work scope overview  | 11 |
| 5.     | Outcomes and Learnings   | 12 |
| 5.1.   | Literature review  | 12 |
| 5.2.   | Technology development, installation and commissioning   | 14 |
| 5.2.1. | Novel catalysts  | 14 |
| 5.2.2. | Design and testing of a short stack under CH <sub>4</sub> -CO <sub>2</sub> gas mixtures  | 15 |
| 5.2.3. | New current collector for anode  | 17 |
| 5.2.4. | Microwave sintering  | 18 |
| 5.2.5. | Using Ni as a pore former  | 19 |
| 5.2.6. | Thermally coupled SOFC dry reforming technology  | 20 |
| 5.3.   | Experimental procedures/methodology  | 21 |
| 5.3.1. | NiO-YSZ anode supported tubular fuel cell fabrication  | 21 |
| 5.3.2. | Proton conducting electrolyte (PCE) anode supported tubular fuel cell fabrication  | 22 |
| 5.3.3. | H-SOFC   | 23 |
| 5.3.4. | O-SOFC   | 26 |
| 5.4.   | Results, discussions and outcomes  | 29 |
| 5.4.1. | Lab scale extruder for tubular fuel cell manufacturing   | 29 |
| 5.4.2. | Development of the basic tubular fuel cell structure for a proton conducting solid electrolyte                                     | 32 |
| 5.4.3. | Redox and thermal cycling of the infiltrated electrodes and the suitability of the porous support to accommodate an anode catalyst | 34 |
| 5.4.4. | Impact of structure parameters of the porous support and the concentration and particle size of the infiltrate on the power output | 35 |

|   |    |
|---|----|
| 5.4.5. Evaluation of infiltrated $\text{Pr}_2\text{NiO}_4$ as a cathode material                                  | 39 |
| 5.4.6. Development of a fuel cell with higher performance in syngas compared to hydrogen                          | 39 |
| 5.4.7. In-situ dry reforming catalyst   | 40 |
| 5.4.8. Co-generating syngas-electricity from $\text{CO}_2\text{-CH}_4$ in an H-SOFC                               | 44 |
| 5.4.9. Co-generating syngas-electricity from $\text{CO}_2\text{-CH}_4$ in an O-SOFC                               | 47 |
| 5.4.10. Performance of a small stack using $\text{CH}_4\text{-CO}_2$  | 53 |
| 5.5. Summary and project outcomes   | 54 |
| 5.5.1. Summary of catalytic work  | 54 |
| 5.5.2. Project outcomes   | 55 |
| 5.6. Important lessons learned  | 56 |
| 5.7. References   | 56 |
| 6. Greenhouse Gas and Non-GHG Impacts   | 59 |
| 6.1. Greenhouse gas impact  | 59 |
| 6.1.1. Greenhouse gas impact of O-SOFC  | 59 |
| 6.1.2. Greenhouse Gas Impact of H-SOFC  | 61 |
| 6.1.3. Summary of Greenhouse Gas Impact   | 61 |
| 6.2. Non-GHG Impact   | 61 |
| 7. Overall Conclusions  | 63 |
| 8. Scientific Achievements  | 64 |
| 8.1. Refereed journal papers  | 64 |
| 8.1.1. Published  | 64 |
| 8.1.2. To be submitted/in preparation   | 64 |
| 8.2. Conference presentations   | 65 |
| 9. Next Steps   | 65 |
| 9.1. High level plan for Phase II and the road map of dry reforming SOFC technology for $\text{CO}_2$ utilization | 67 |
| 10. Communications Plan   | 70 |

**2.1. List of Tables**

|  |    |
|--|----|
| Table 5-1 Typical composition of extrusion paste   | 31 |
| Table 5-2 Porosity, surface area, pore size and shrinkage of the TY and CY anodes before and after reduction | 37 |

## 2.2. List of Figures

|  |    |
|--|----|
| Figure 4-1 (a) A conceptual comparison of the conventional and the proposed novel methods of CO <sub>2</sub> utilization for syngas production. (b) Schematic of the novel pathway proposed by Alberta researchers for conversion of CO <sub>2</sub> to electricity and value added industrial chemicals using internal dry reforming by a solid oxide fuel cell | 12 |
| Figure 5-1 (a) Tubular SOFC stack after test, (b) anode and cathode wire leads   | 15 |
| Figure 5-2 Individual fuel cell performance under humid hydrogen at (a) 600°C, (b) 650°C and (c) 700°C   | 16 |
| Figure 5-3 Electrochemical performance of the stack under different electrical arrangements at (a) 600°C, (b) 650°C and (c) 700°C  | 17 |
| Figure 5-4 Tubular SOFC stack containing 12 cells  | 17 |
| Figure 5-5 Impedance spectroscopy of both old and new current collectors   | 18 |
| Figure 5-6 Stability check of open ended configuration at 600°C and 0.7 V  | 18 |
| Figure 5-7 Hybrid microwave sintering. SiC rods are used to heat up the sample initially   | 19 |
| Figure 5-8 (a) Cross section of the anode after infiltration and labelling where EDX measurements were conducted, (b) corresponding composition of each label (1 is larger because it is taken from the most part of the anode)  | 20 |
| Figure 5-9 Dry reforming reactor embedded in a tubular solid oxide fuel cell   | 20 |
| Figure 5-10 Block diagram of integrated CO <sub>2</sub> capture and dry reforming SOFC technology for CO <sub>2</sub> utilization  | 21 |
| Figure 5-11 Cross section of the fuel cells used in the stack and the testing set up for a single cell   | 22 |
| Figure 5-12 (a) Drawing of 3-D assembly and (b) photograph of built lab scale piston extruder  | 30 |
| Figure 5-13 (a) Cross sectional view of the die for tube extrusion, (b) photograph of extrusion of the tube during operation and (c) photo of several extruded tubes using two different commercial modeling clays   | 31 |
| Figure 5-14 (a) Photograph of the modified extruder for manufacturing of tubular SOFCs, (b) SOFC researchers operating the extruder and (c) photograph of a YSZ extruded support tube during an extrusion run  | 32 |
| Figure 5-15 Performance of a proton conducting electrolyte based tubular SOFC under humid H <sub>2</sub> and its mixture with CO gas   | 33 |
| Figure 5-16 Impedance spectra of the proton conducting tubular SOFC  | 33 |
| Figure 5-17 SEM images of the cross section of the proton conducting fuel cell   | 34 |
| Figure 5-18 Performance of a proton conducting electrolyte tubular SOFC based on Ni-YSZ anode support under humid H <sub>2</sub>   | 34 |
| Figure 5-19 Porous YSZ microstructure infiltrated with 20 wt% NiO. (a) initial slip contained calcined-milled YSZ and graphite, (b) initial slip contained as received YSZ and was cast at pH 4  | 35 |

---

|   |    |
|---|----|
| Figure 5-20 Electrochemical galvanodynamic studies in SOFC and SOEC modes for the cell containing as received Tosoh YSZ (TY) and calcined YSZ (CY) in its anode structure. Solid symbols correspond to the CY cell and hollow symbols to the TY cell. Black: measured at 800°C using RT humidified hydrogen as fuel. All the rest were measured using 50% steam – 50% hydrogen as fuel. Red: measured at 800°C; Green: measured at 700°C; Blue: measured at 600°C. The inset corresponds to a magnification for both samples at low current densities (700°C) | 36 |
| Figure 5-21 SEM image of (a) TY anode before reduction, (b) TY anode after reduction, (c) CY anode before reduction, (d) CY anode after reduction, (e) pores of TY anode, (f) pores of CY anode   | 39 |
| Figure 5-22 Performance of a cell using 3YSZ in the anode under hydrogen and syngas   | 39 |
| Figure 5-23 Cross-section of cell with 3YSZ in the anode  | 40 |
| Figure 5-24 CH <sub>4</sub> conversion and CO selectivity for methane dry reforming over Ni-YSZ and NiM-Ce <sub>0.8</sub> Zr <sub>0.2</sub> O <sub>2</sub> catalysts at temperatures from 550°C to 800°C  | 41 |
| Figure 5-25 CH <sub>4</sub> conversion and CO selectivity for methane dry reforming over Ni-YSZ and NiM-Ce <sub>0.8</sub> Zr <sub>0.2</sub> O <sub>2</sub> catalysts after H <sub>2</sub> S treatment at temperatures ranging from 550°C to 800°C   | 42 |
| Figure 5-26 Raman spectra of fresh and H <sub>2</sub> S treated catalysts after exposing to dry CH <sub>4</sub> at 800°C for 30 min   | 43 |
| Figure 5-27 Electrochemical performance of conventional H-SOFC in various fuels at 700°C. (a) impedance spectra, (b) I-V and I-P curves, (c) galvanostatic test at a constant current of 1 A cm <sup>-2</sup> ; (d) XRD patterns of BZCYYb powder after 24 h exposure to either H <sub>2</sub> -CO or CH <sub>4</sub> -CO <sub>2</sub> at 700°C   | 44 |
| Figure 5-28 Schematic showing the configuration of the novel layered H-SOFC   | 46 |
| Figure 5-29 Stability test of in situ dry reforming in layered H-SOFC fueled with CH <sub>4</sub> -CO <sub>2</sub> at 700 °C. (a) galvanostatic test under a constant load of 1 A cm <sup>-2</sup> , (b) exhaust gas composition  | 46 |
| Figure 5-30 Schematically illustrating the CO <sub>2</sub> conversion process in a O-SOFC   | 47 |
| Figure 5-31 I-V and I-P curves of C-SOFC and TA-SOFC in various fuels at temperatures between 650°C and 800°C   | 48 |
| Figure 5-32 I-V and I-P curves of sulfured C-SOFC and TA-SOFC in various fuels at temperatures between 650°C and 800°C  | 49 |
| Figure 5-33 (a) Time dependent voltage of TA-SOFC in CH <sub>4</sub> -CO <sub>2</sub> atmosphere at 800°C and at 1.5 A cm <sup>-2</sup> and (b) the corresponding time dependent exhaust gas composition  | 50 |
| Figure 5-34 (a) SOFC for biogas conversion, (b) microstructure of the prepared LSM-YSZ composite cathode, (c) microstructure of the NiSn-YSZ anode, (d) EDX mappings showing the element distribution in the anode  | 51 |
| Figure 5-35 (a) CH <sub>4</sub> conversion and (b) CO selectivity during CH <sub>4</sub> -CO <sub>2</sub> (0 or 200 ppm H <sub>2</sub> S) dry reforming of biogas under various conditions [fresh cell (F-C) and the cell pre-treated in H <sub>2</sub> -500 ppm H <sub>2</sub> S (S-C)], (c) I-V and I-P curves of the cell in H <sub>2</sub> (0~200   | 52 |

ppm H<sub>2</sub>S), (d) I-V and I-P curves of the cell in CH<sub>4</sub>-CO<sub>2</sub> (0~200 ppm H<sub>2</sub>S), (e) CH<sub>4</sub> conversion and CO selectivity during dry reforming of biogas at open circuit condition, (f) voltage and outlet gas composition during dry reforming of biogas under 1.25 A cm<sup>-2</sup>. The feeding stream during the long term test is equal amounts of CH<sub>4</sub> and CO<sub>2</sub> balanced with 200 ppm H<sub>2</sub>S for a total flow rate of 20 mL min<sup>-1</sup>

Figure 5-36 The voltage-current/power curves of a stack based on three cells 53

Figure 9-1 Block diagram of integrated CO<sub>2</sub> capture and dry reforming SOFC technology for CO<sub>2</sub> utilization 67

Figure 9-2 Phase II technology development scheme 69

Figure 9-3 Multiyear development road map for dry reforming SOFC technology 70

### 3. EXECUTIVE SUMMARY

The escalating global warming effects are calling for immediate measures to reduce the level of greenhouse gases. To energy efficiently offset our carbon footprint, we herein developed a novel CH<sub>4</sub>-CO<sub>2</sub> dry reforming process to co-produce electricity and CO-concentrated syngas, which takes advantage of the selective oxidation of H<sub>2</sub> in novel solid oxide fuel cells (SOFCs). We designed three kinds of cells in this work.

In a high performance proton-conducting SOFC, a functional layer, consisting of Ni<sub>0.8</sub>Co<sub>0.2</sub>-La<sub>0.2</sub>Ce<sub>0.8</sub>O<sub>1.9</sub> (NiCo-LDC) composite, was successfully incorporated into the anode support, forming a layered SOFC configuration. In comparison to the conventional design, this layered SOFC demonstrated drastically improved CO<sub>2</sub> resistance as well as internal reforming efficiency (CO<sub>2</sub> conversion reached 91.5 % at 700°C), and up to 100 h galvanostatic stability in a CH<sub>4</sub>-CO<sub>2</sub> feed stream at 1 A cm<sup>-2</sup>. More importantly, H<sub>2</sub> was effectively and exclusively converted by electrochemical oxidation, yielding no CO<sub>2</sub> but CO concentrated syngas in the anode effluent. We also show that the layered design is beneficial in terms of decreasing coking as well as increasing CO<sub>2</sub> resistance of the SOFC in the mixed CO<sub>2</sub> and CH<sub>4</sub> feedstock.

The proton-conducting SOFC is very promising for the proposed application. Unfortunately, the commercialized SOFC is based on a Ni anode and oxygen-ion conducting electrolyte and suffers serious coking and sulfur poisoning in hydrocarbon environments containing H<sub>2</sub>S. We then demonstrated that the dry reforming of H<sub>2</sub>S-containing CH<sub>4</sub>-CO<sub>2</sub> can be efficiently conducted in conventional SOFCs via incorporating a coke/sulfur resistant catalyst layer. Through H<sub>2</sub> selective oxidation on the Ni-S anode catalyst, the released heat fully compensated that required for the reforming reaction with no CO<sub>2</sub> emissions. As an improvement on the Ni-S anode, we then developed NiSn alloys as effective reforming and H<sub>2</sub> selective catalysts for the oxygen ion-conducting SOFC. In this case, a novel on-cell micro reformer and NiSn bimetallic nanoparticles were introduced into a conventional Ni-based anode for efficient and durable internal reforming of CH<sub>4</sub>-CO<sub>2</sub>. With a constant current density of 1.25 A cm<sup>-2</sup>, the CH<sub>4</sub> conversion and CO selectivity remained constant at around 95 % while producing a steady output voltage (0.69 V), demonstrating excellent activity and coke/sulfur tolerance that have rarely been reported.

As it can accommodate a variety of fuels, the ceramic or solid oxide fuel cell (SOFC) is required to enable CO<sub>2</sub> to be eliminated via dry reforming of methane while simultaneously generating electricity rather than consuming heat. However, ceramic materials for engineering applications are always a concern due to their brittleness and low fracture toughness. We have successfully developed a robust tubular SOFC by fabricating a scaffold of yttria stabilized zirconia (YSZ) with very good mechanical properties consisting of a thick porous layer (for structural support), a thin dense electrolyte layer and a thin porous layer. The porous layers are subsequently infiltrated with anode and cathode materials, respectively. This cell has withstood many thermal and redox cycles with any cracking or structural damage.

The current project has enabled us to take this one step further. By making the porous layers of the scaffold out of partially stabilized zirconia with 3 mol%  $\text{Y}_2\text{O}_3$  (3YSZ) that has exceptional mechanical properties (the electrolyte must still be YSZ with 8 mol%  $\text{Y}_2\text{O}_3$  (8YSZ)), the ceramic cell should prove to be even more robust especially for large scale applications. Preliminary results showed the 3YSZ cell gave excellent performance in syngas. Proton conductors usually have poor mechanical properties. Advantage of this robust oxygen-ion conducting cell has been taken by coating a proton conductor onto the YSZ thick porous layer followed by adding a thin YSZ porous layer. In this manner, the proton conductor is not required for structural support.

Fabrication of the scaffold has been achieved via slip casting. As an alternative and perhaps more attractive for mass production, extrusion has been evaluated. A lab-scale extruder has been designed, built and tested to produce YSZ support tubes. A suitable paste formulation has been identified.

In part because they operate at high temperatures, long term stability of SOFCs is a worldwide problem, chiefly due to nickel agglomeration at the anode and current collection. A detailed study of the effect of porous support microstructure and the concentration and particle size of the infiltrate on nickel coarsening has been completed enabling us to minimize nickel agglomeration. Use of calcined powders to produce the scaffold played a large role. Fine copper mesh with optimum mechanical properties, especially formability, has proven an excellent anode current collector. Furthermore, we have studied two excellent cathode materials,  $\text{Nd}_2\text{NiO}_4$  and  $\text{Pr}_2\text{NiO}_4$ . This is critical to good performance since the major polarization losses on passage of current occur at the cathode. These improvements have enabled us to obtain the highest power densities ever reported for tubular cells with a YSZ electrolyte in both fuel cell and electrolysis modes.

Two further novel ideas related to fabrication have been initiated. Rather than graphite or polymethylmethacrylate as a pore former to generate sufficient porosity in the porous layers for infiltration and gas flow, use of nickel has been initiated via soaking of nickel nitrate into the structure, decomposition to nickel oxide, reduction to nickel and leaching with nitric acid. Upon subsequent infiltration of nickel, a uniform distribution and high loading efficiency resulted. Microwave sintering has been evaluated and may prove to be a rapid and cost effective method for fuel cell manufacture.

To scale up the process, both six- and 12-cell tubular stacks with both closed one end and open ended tubes have been built. Open ended tubes result in more complicated fabrication problems but improve current collection. Reasonable agreement has been realized between single cell results and the expected power outputs for series, parallel and series-parallel electrical configurations.

In summary, from the results achieved in this work on SOFC fabrication, behaviour of the

catalysts identified and electrochemical performance, the feasibility of feeding a CH<sub>4</sub>-CO<sub>2</sub> mixture into a fuel cell to simultaneously eliminate CO<sub>2</sub>, generate large amounts of electricity and produce CO as a valuable by-product has been clearly shown. This novel process promises to play a pivotal role in future CO<sub>2</sub> conversion and utilization. This study defines a new dimension of cogenerating CO<sub>2</sub>-derived synthesis gas and electrical power in the context of increasing interest for efficient utilization of H<sub>2</sub>S-containing CH<sub>4</sub> and CO<sub>2</sub>.

To potentially simplify the design and operating parameters, chemically decoupling dry reforming of CH<sub>4</sub> with CO<sub>2</sub> and the SOFC provides an interesting alternative. The heat generated while the fuel cell produces electricity (generally wasted) is used to overcome the heat absorbed by the strongly endothermic dry reforming reaction. This is usually viewed as a strong disincentive for the reforming of natural gas. In addition, this thermally-only coupled system could be integrated with a CO<sub>2</sub> capture system recently developed in Alberta.

Based on our own results, CO<sub>2</sub> reduction (including the CO<sub>2</sub> not generated by not burning CH<sub>4</sub>) would be 1.663 T/MWh and 4.541 T/MWh for an oxygen-ion conducting and proton conducting SOFC, respectively. Accordingly, while eliminating 1 MT of CO<sub>2</sub> per year, 6.0 x 10<sup>5</sup> MWh and 2.2 x 10<sup>5</sup> MWh of electrical energy would be generated, respectively, requiring 138 500 kW oxygen-ion conducting units or 51 500 kW proton conducting units.

## 4. PROJECT DESCRIPTION

### 4.1. Introduction and background

As a greenhouse gas, CO<sub>2</sub> contributes to global climate change and, therefore, anthropogenic emission of CO<sub>2</sub> is causing an increasing global concern. Human activities are altering the carbon cycle, both by adding more CO<sub>2</sub> to the atmosphere and by influencing the ability of natural sinks (e.g., forests) to remove CO<sub>2</sub> from the atmosphere. While CO<sub>2</sub> emissions come from a variety of natural sources, human-related emissions are responsible for the increase that has occurred in the atmosphere since the industrial revolution. With foreseeable new policies geared towards the reduction of carbon emissions, it is critical to develop new technologies capable of efficient chemical reduction of CO<sub>2</sub> to fuels and other useful products. In this context, dry reforming of methane (DRM),



an old yet both scientifically and industrially important process, is making a comeback contribution to the utilization of CO<sub>2</sub>. However, catalyst deactivation (sulfur poisoning and coke formation) and the associated high energy consumption remain the technological hurdles of its practical implementation.

## 4.2. Technical description

Solid oxide fuel cells (SOFCs), which typically operate at higher temperature (above 500°C) compared to other type of fuel cells, has received particular attention in recent years not only for power generation but also for the potential of performing simultaneous the DRM reaction in its anode compartment. The high operation temperature is favored by DRM, and at the same time, the heat released during the electro-oxidation process can partially compensate the energy required for DRM. Nonetheless, the conventional Ni-Y<sub>2</sub>O<sub>3</sub>-stabilized-ZrO<sub>2</sub> (YSZ) anode electro-catalyst does not show good *in-situ* dry reforming activity, nor does it exhibit excellent electrochemical performance in CH<sub>4</sub>-CO<sub>2</sub> mixtures, not to mention that sulfur impurities always significantly deactivate its reforming capability. On the one hand, the coke-sulfur resistant DRM catalyst resulting from recent advancement in this field has not been fully utilized in SOFC research due to many practical barriers, e.g., a sintering temperature as high as >1300°C in SOFC fabrication. On the other hand, a typical Ni-YSZ supported cell usually shows serious performance degradation when being directly fed with equal amounts of CH<sub>4</sub> and CO<sub>2</sub>, although performance could be improved by introducing noble metal catalysts or using novel fabrication methods. To combine the advantages of different processes and materials, we herein designed a novel SOFC reactor equipped with a highly coke/sulfur resistant triple-layer anode.

## 4.3. Project goals and work scope overview

We propose to develop a novel SOFC reactor for co-production of electricity and chemical feedstock CO through CO<sub>2</sub> reforming of methane (Figure 4-1). Such an approach offers the following:

- a) Effective elimination of 1.2 tonnes of CO<sub>2</sub> for every MWh of power generated by the proposed fuel cell.
- b) Simultaneous production of electrical power with CO<sub>2</sub> utilization. At 50% efficiency, the proposed fuel cell is able to generate 3,660 MWh of power while converting 1,000 tonnes of CH<sub>4</sub> and simultaneously consuming 2,750 tonnes of CO<sub>2</sub>.
- c) Production of an important chemical precursor CO which is a key raw material for the manufacture of many industrial chemicals and is used to provide a reducing atmosphere for the production of metals in metallurgical processes.

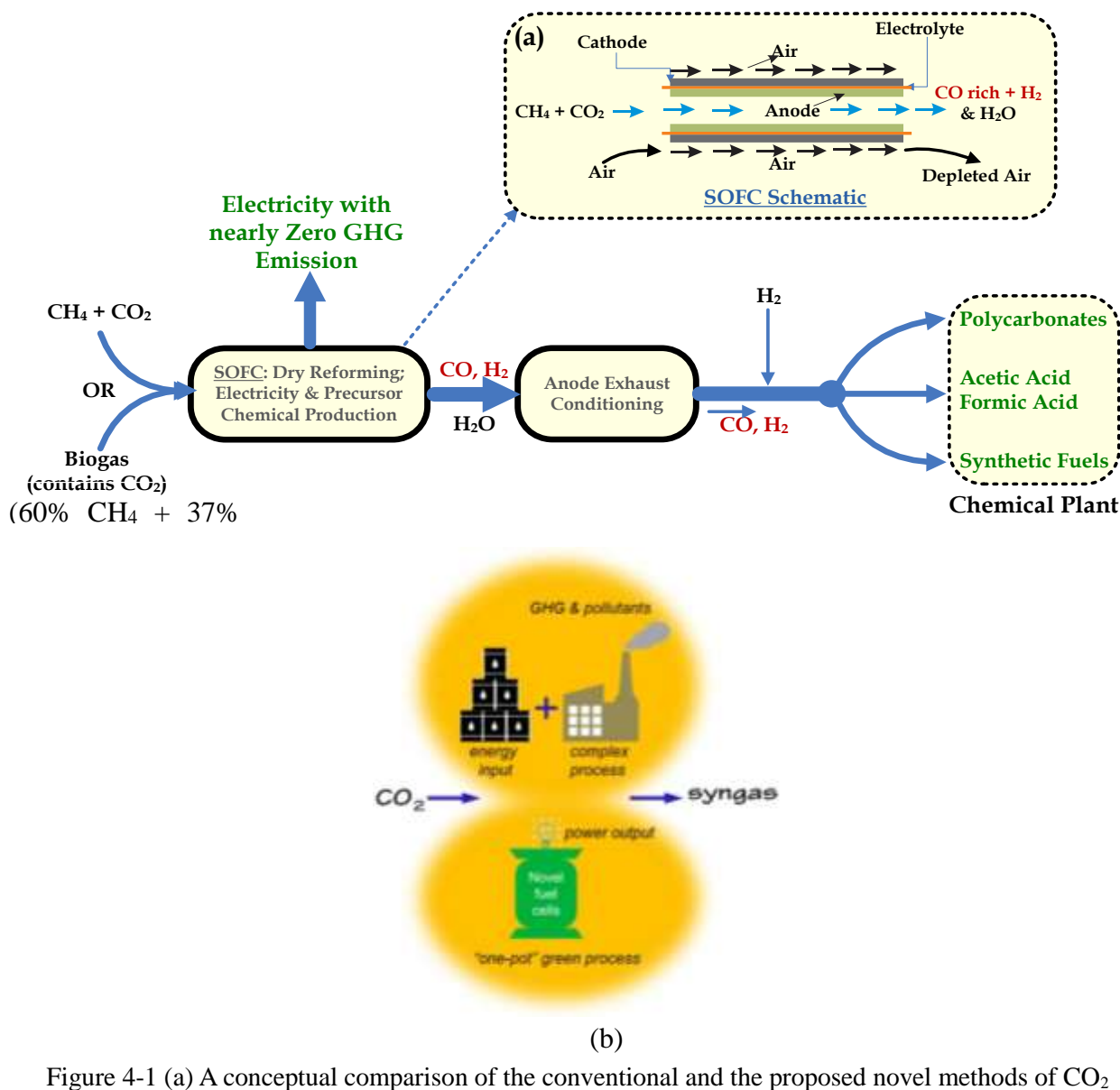


Figure 4-1 (a) A conceptual comparison of the conventional and the proposed novel methods of  $\text{CO}_2$  utilization for syngas production. (b) Schematic of the novel pathway proposed by Alberta researchers for conversion of  $\text{CO}_2$  to electricity and value added industrial chemicals using internal dry reforming by a solid oxide fuel cell

## 5. OUTCOMES AND LEARNINGS

### 5.1. Literature review

Although there are many papers studying dry reforming using homogenous or heterogeneous catalysts [1], literature studying fuel cells as a base for dry reforming are scarce. Guerra et al. performed a stability test for dry reforming using an SOFC and found that the ratio of carbon dioxide to methane should be between 1.5 to 2 at  $800^\circ\text{C}$  to prevent coke formation [2]. They observed long term stability for 70 h. One study concludes that except for

a narrow range of operating temperatures and only for methane, nickel based fuel cell anodes show a coking problem [3]. Lanzini et al. found out that both coarsening of nickel particles and carbon formation contribute to anode deactivation [4].

Most of these researches focus on using syngas and carbohydrates. They use carbon dioxide, steam and oxygen to reduce coke formation [5] but this has disadvantages such as diluting the fuel which lowers the performance and complicates the process.

Fabrication and testing of an SOFC which uses a mixture of methane and carbon dioxide with the main focus of reducing the amount of carbon dioxide to produce electricity and carbon monoxide as the output has not been performed previously.

SOFC is a promising device that allows CO<sub>2</sub> and CH<sub>4</sub> dry reforming *in situ* in the anode chamber [6-8]. Unlike the conventional dry reforming process, in this device, the heat required for the extremely endothermic reaction can be fully provided by the heat cogenerated during electrochemical oxidation, thus enabling a thermally autogenous process. Nonetheless, most SOFCs employed for dry reforming studies to date are based on oxygen ion-conducting electrolytes (O-SOFCs), in which O<sup>2-</sup> can readily oxidize both CO and H<sub>2</sub> (the main products of dry reforming), leading to CO<sub>2</sub> emission again in practice.



Another associated technical impediment is the insufficient reforming efficiency in this one-pot chemical/electrochemical combination; in most cases, the conventional Ni-based cermet anode suffers from relatively low catalytic activity, causing low conversion of both CO<sub>2</sub> and CH<sub>4</sub> [9,10].

Recently, many researchers have paid attention to proton-conducting SOFCs (H-SOFCs) which can effectively operate at intermediate temperatures (500~700°C) [9,11-15]. Theoretically, they show higher efficiency compared to O-SOFCs since H<sub>2</sub>O generation occurs at the cathode without fuel dilution effects at the anode [16-18]. In terms of CH<sub>4</sub> dry reforming, H-SOFC is considerably more advantageous than O-SOFC, since only protons can migrate through the electrolyte and no CO<sub>2</sub> will be electrochemically generated. Unfortunately, a technical problem arises if H-SOFC is used for dry reforming: although doped BaCeO<sub>3</sub>, the most widely applied electrolyte, has excellent proton conductivity, its chemical stability is, however, challenged in CO<sub>2</sub>-containing atmospheres [19,20]. For instance, although the composition of doping elements has been well-optimized, phase decomposition of BaZr<sub>0.1</sub>Ce<sub>0.7</sub>Y<sub>0.1</sub>Yb<sub>0.1</sub>O<sub>3-δ</sub> (BZCYb) has still been reported to occur in wet H<sub>2</sub> and CO<sub>2</sub> [21]. This hinders the implementation of H-SOFC in CH<sub>4</sub> dry reforming in which ideally 50% CO<sub>2</sub> is present as shown in Reaction (1).

The proposed syngas and electricity co-generation process could be feasible as well in the conventional O-SOFC if we can identify a selective catalyst for H<sub>2</sub> oxidation. Other than the selectivity for H<sub>2</sub> oxidation, such an O-SOFC should have good activity for DRM. However, the development of O-SOFC for DRM is still in its infancy with many problems to be solved. Using the commercialized YSZ anode for DRM is confronted with some tough challenges, including coking [22,23] that will cause catalyst deactivation as well as large thermal gradients causing thermal stress [24]. Ni-YSZ catalyst is well known for promoting severe carbon deposition, which originates mainly from the endothermic methane decomposition and Boudouard reactions. Excessive carbon formation on the anode surface leads to rapid deterioration of cell performance, eventually resulting in damage to the cells. Besides these technical issues, an H<sub>2</sub> selective catalyst is rarely reported in the field of O-SOFC technologies.

## 5.2. Technology development, installation and commissioning

### 5.2.1. Novel catalysts

We have developed a layered H-SOFC with multiple-twinned Ni<sub>0.8</sub>Co<sub>0.2</sub> nanoparticles. The novel catalyst showed greatly improved sintering resistance and the SOFC design enabled us to successfully achieve three milestones: (1) CO<sub>2</sub> utilization, (2) generation of electricity and (3) production of syngas.

As for the O-SOFC, the proposed syngas and electricity co-generation process could be feasible as well if we have a selective catalyst for H<sub>2</sub> oxidation. As well acknowledged, gas oxidation on the Ni-YSZ electrode is mainly comprised of two consecutive processes, that is, adsorption, dissociation and diffusion, followed by charge transfer over the Ni/YSZ interface. The property of electro-catalysis promises to be effective for selectively oxidizing H<sub>2</sub>. CO electro-oxidation over a Ni-YSZ anode can be simply described by Eq. 4 (adsorption, dissociation and diffusion) and Eq. 5 (charge transfer).



The CO molecule has “reactive orbitals” enabling its adsorption on transition metals more likely than a H<sub>2</sub> molecule; however, the rate of its adsorption is controlled by its diffusion. According to a previous study, adsorption of S on the Ni surface would lead to most CO molecules adsorbing on the same Ni atom, subsequently hindering the diffusion of CO<sub>ads,Ni</sub> to the three phase boundary (TPB). Therefore, sulfur adsorbed Ni is a potential catalyst for H<sub>2</sub> selective oxidation. Furthermore, we can also speculate that Ni alloys, especially Ni surface alloys, could alter the adsorption and desorption properties of CO during the CO electro-oxidation, making Ni alloys another potential route for H<sub>2</sub> selective oxidation. Based on the above, we have also developed a novel O-SOFC with a selective anode catalyst for application in concentrating syngas and electricity with zero CO<sub>2</sub> emissions.

### 5.2.2. Design and testing of a short stack under CH<sub>4</sub>-CO<sub>2</sub> gas mixtures

We fabricated a short stack composed of six cells (Figure 5-1a) and studied its electrochemical performance under different electrical connection configurations (parallel, series and parallel-series) at intermediate temperatures. The stack was tested in a horizontal tube furnace (Figure 5-1b). Two cells were in the Ni-YSZ/YSZ/Pr<sub>2</sub>NiO<sub>4</sub>-YSZ system (C1 and C4) and four were in the Ni-YSZ/YSZ/Nd<sub>2</sub>NiO<sub>4</sub>-YSZ configuration (C2, C3, C5 and C6), of which one (C6) failed following testing at 600°C. The reason of C6 failure was due to the crack in the electrolyte which propagated during operation. Overall, individual cells had similar performance delivering 202, 302 and 340 mW/cm<sup>2</sup> at 600, 650 and 700°C, respectively (Figure 5-2). The stack delivered a maximum of 7.40, 10.32 and 11.56 W at these temperatures. No significant differences were found among different electrical arrangements (Figure 5-1). However, as expected, the stack performance was most affected by the malfunctioning cell under a series arrangement at 600°C. Since the parallel-series configuration delivers an intermediate voltage and current and similar power to the parallel or series connections, it can be more suitable for the stack assembly. Such an arrangement also offers the possibility of replacement of a stack module in case a cell fails in that module during operation.



Figure 5-1 (a) Tubular SOFC stack after test, (b) anode and cathode wire leads

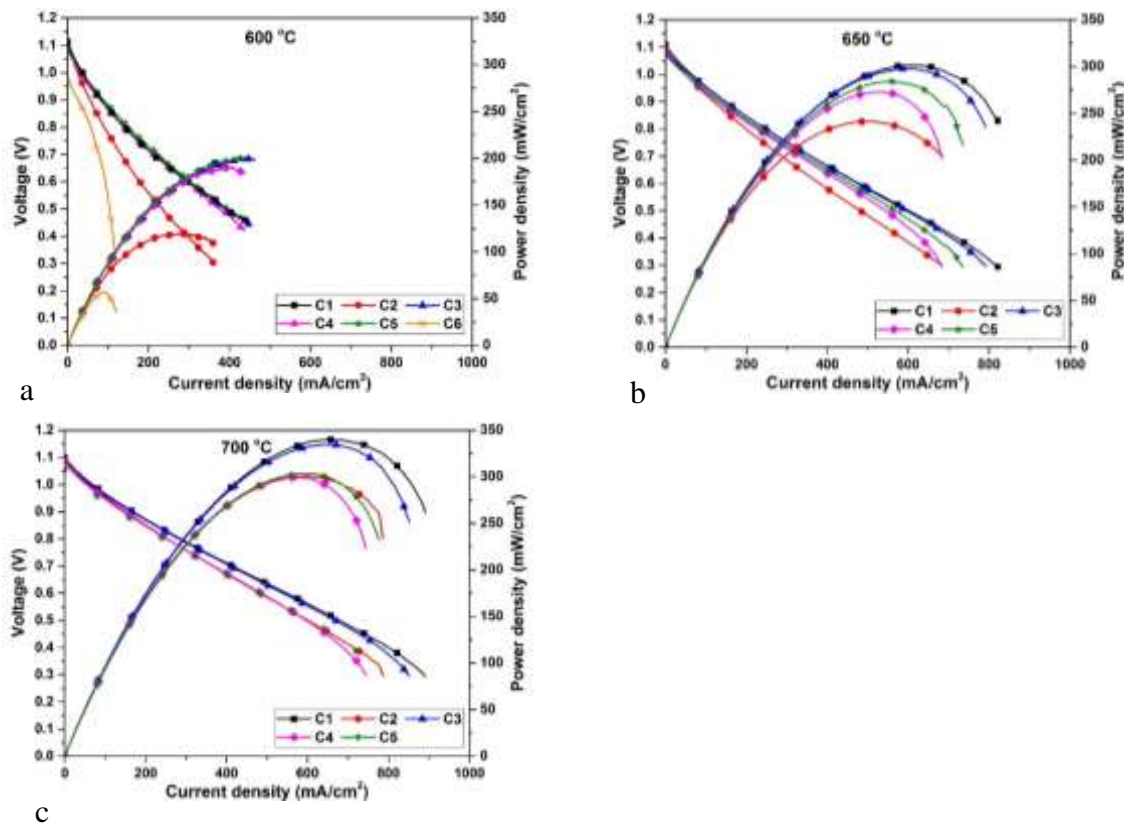


Figure 5-2 Individual fuel cell performance under humid hydrogen at (a) 600°C, (b) 650°C and (c) 700°C

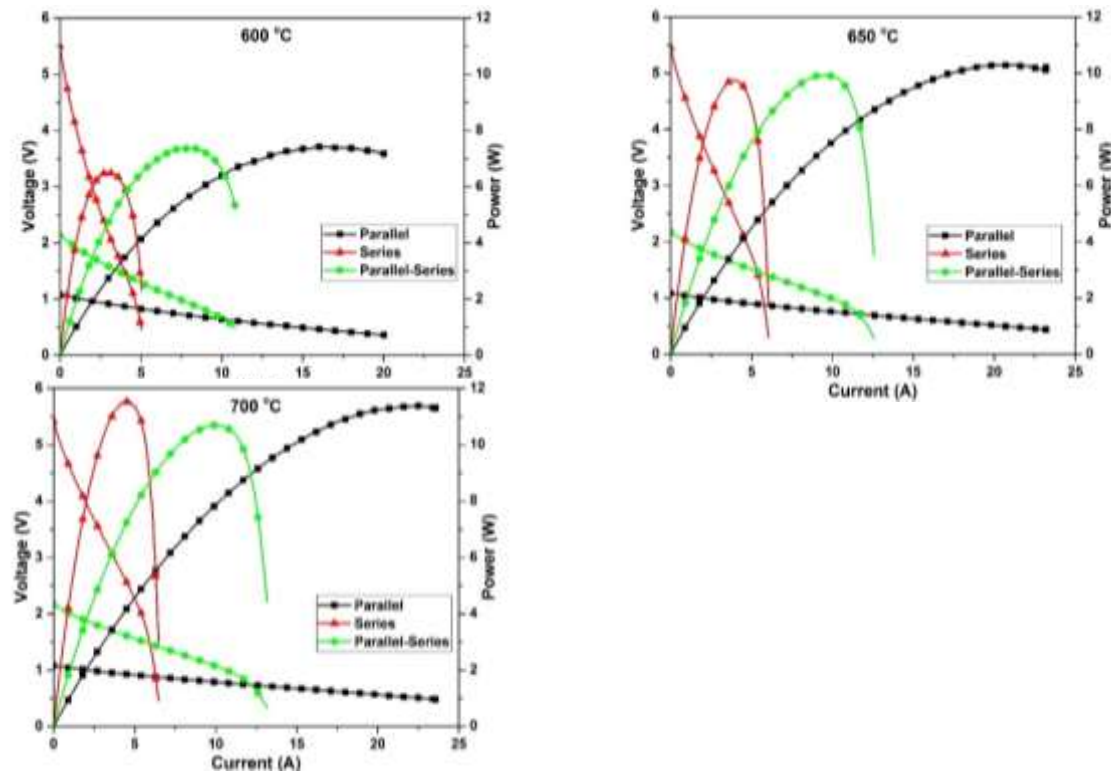


Figure 5-3 Electrochemical performance of the stack under different electrical arrangements at (a) 600°C, (b) 650°C and (c) 700°C

In our next effort we tried to fabricate a stack containing 12 tubular SOFCs in order to obtain a higher power performance (~25 W). The stack consisted of two modules with each module consisting of six cells (Figure 5-4). We found that there was significant power loss due to the resistance of different components specifically the measuring wires. We managed to obtain a maximum of 15 W from the new stack. We have modified our testing set up and changed to larger measuring wires hoping to achieve the target power. We observed that there was a 30% power loss in comparison to testing under H<sub>2</sub> when a CH<sub>4</sub>-CO<sub>2</sub> mixture was used as the fuel.



Figure 5-4 Tubular SOFC stack containing 12 cells

### 5.2.3. New current collector for anode

Current collectors are always problematic in tubular SOFCs. A good current collector needs to have a high conductivity, no reactivity and maintain close contact with the anode wall. Usually a total resistance of less than 1 ohm/cm<sup>2</sup> is acceptable. Using a new smaller mesh (30 mesh copper gauze with a 0.69 mm width of opening) gave us the ability to have resistances less than 0.25 ohm/cm<sup>2</sup> and much less reactance compared to the old mesh (Figure 5-5). From a cost perspective on an industrial scale, using less mesh could result in considerable savings.

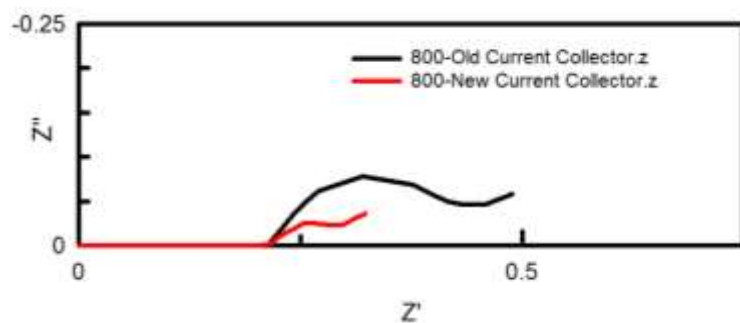


Figure 5-5 Impedance spectroscopy of both old and new current collectors

We have now managed to significantly improve the troublesome current collection system in tubular fuel cells using tubes open at both ends rather than closed at one end. Although cell performance is very similar in both cases, open-ended tubes show more stable performance and considerably less degradation after 45 h testing (Figure 5-6).

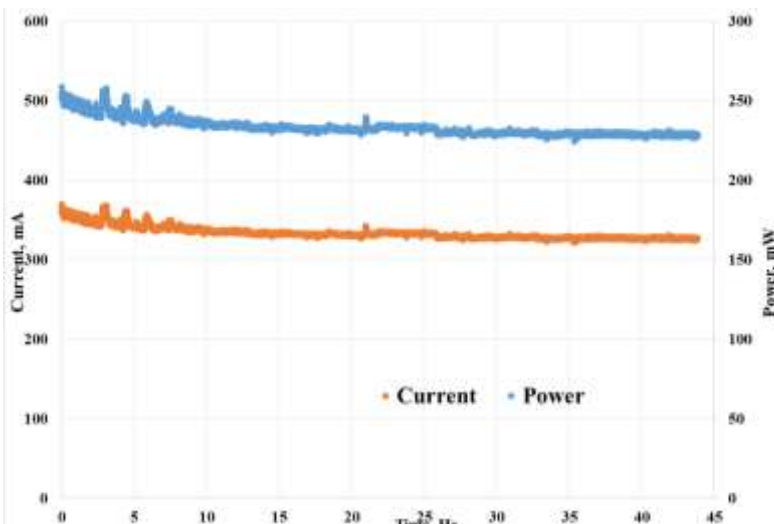


Figure 5-6 Stability check of open ended configuration at 600°C and 0.7 V

#### 5.2.4. Microwave sintering

Sintering is crucial to good fuel cell performance. The electrolyte needs to be dense and leak-free. Conventional sintering is time consuming and expensive. Also, side reactions and the difficulty of sintering some materials need to be considered. Microwave sintering opens up new possibilities, both for rapid sintering close to theoretical density values and also due to the volumetric heating nature, could be a very cost-effective process.

Most oxides are transparent to regular microwave generators (900 MHz and 2.45 GHz) since these waves are not in the range of their phonons. Increasing the temperature rapidly changes this and causes the specimen to absorb the waves. That is why it is convenient to use a material called a susceptor that can absorb the microwaves at low temperatures and heat up the specimen. Above a certain temperature, the specimen itself starts to absorb the waves. For example, Figure 5-7 shows a setup that uses SiC rods as the susceptor.

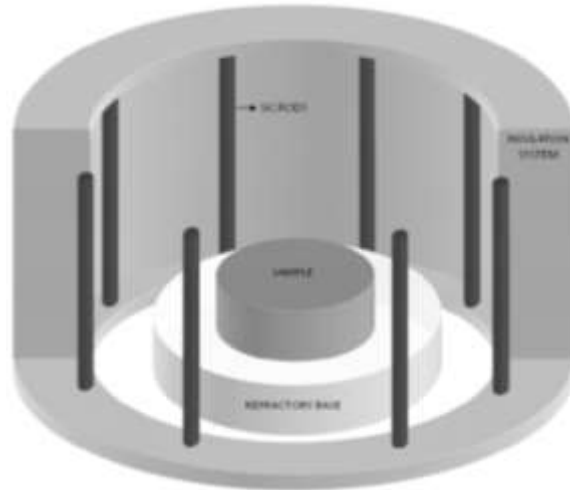
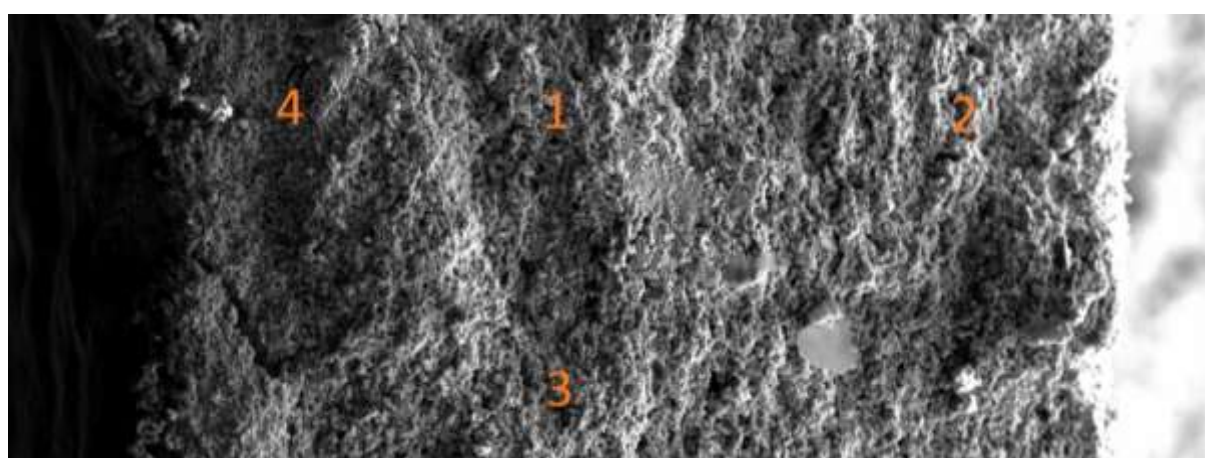


Figure 5-7 Hybrid microwave sintering. SiC rods are used to heat up the sample initially

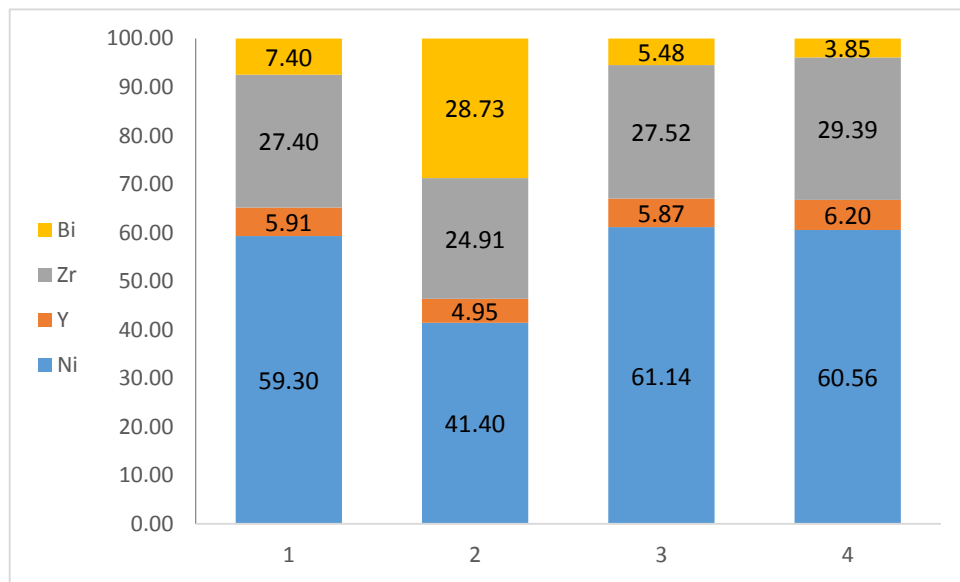
Our unique method consists of using the nickel metal-YSZ as support due to the fact that it can absorb the microwaves and act as a susceptor to heat up the BZY ( $\text{BaZr}_{0.8}\text{Y}_{0.2}\text{O}_{3-\delta}$ ) electrolyte until it can absorb the waves itself. Then due to fast sintering process, enhanced grain growth is expected. Also NiO–GDC ( $\text{Ce}_{0.8}\text{Gd}_{0.2}\text{O}_{1.90}$ ) can absorb the waves at room temperature which opens up another possible candidate.

#### 5.2.5. Using Ni as a pore former

A current investigation is being focused on a new approach to making porous scaffolds by effectively using nickel as a pore former. Nickel nitrate is soaked into the structure, decomposed to NiO, later reduced to Ni and finally leached out with nitric acid. SEM and EDX showed much better distribution and a higher weight gain of Ni on subsequent infiltration. Figure 5-8 shows an anode prepared using the above procedure and infiltrated using bismuth nitrate. A respectable weight gain was observed over the entire anode. A study of the performance enhancement of the cell in comparison to previous methods is in progress.



(a)



(b)

Figure 5-8 (a) Cross section of the anode after infiltration and labelling where EDX measurements were conducted, (b) corresponding composition of each label

### 5.2.6. Thermally coupled SOFC dry reforming technology

In the current project, dry reforming using SOFC technology is investigated whereby the SOFC cell is thermally and chemically coupled with the dry reforming process. A new idea is being proposed where the dry reforming is only thermally and not chemically coupled with the SOFC cell. This concept is schematically shown in Figure 5-9. In this instance, a dry reforming reactor (DRR) is inserted inside a tubular SOFC cell. There is no gas/chemical exchange between the SOFC cell and the DRR, meaning they are not chemically coupled but still thermally coupled and the product is syngas.

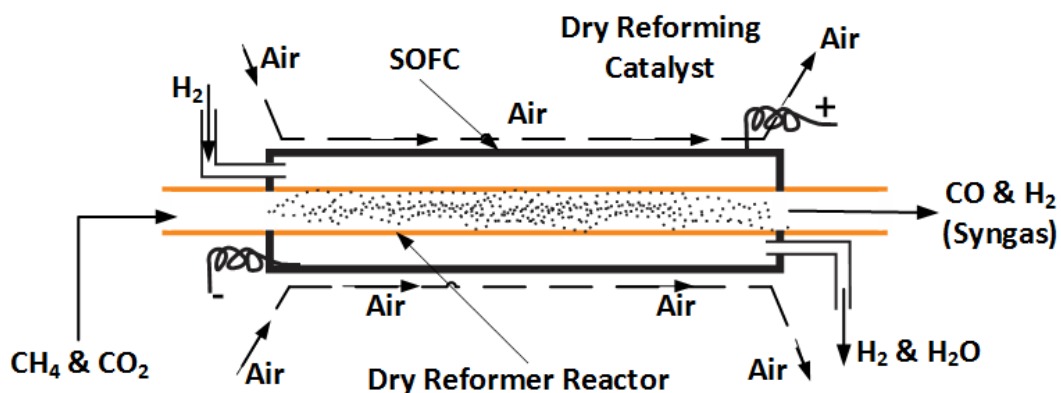


Figure 5-9 Dry reforming reactor embedded in a tubular solid oxide fuel cell

During operation, the SOFC generates heat. In a thermally coupled system, the heat generated by the SOFC can be used for the endothermic dry reforming of methane. A preliminary estimate of the heat generated during operation of the SOFC with 40% electrical

efficiency at 800°C that is available for the dry reforming of methane was calculated. In this scheme, the SOFC is operated with hydrogen fuel. This initial analysis showed that the heat energy from a 1 MW SOFC system can eliminate 22 tonnes of CO<sub>2</sub> per day.

A future vision would be to integrate CO<sub>2</sub> capture by solid sorbents with SOFC dry reforming technology which is illustrated in Figure 5-10. In this integrated system, CO<sub>2</sub> capture will be performed using solid sorbent technology being developed in Alberta.

The syngas produced by dry reforming is a crucially important building block of the chemical industry. Syngas is used in a variety of downstream processes like methanol production, Fischer-Tropsch synthesis processes, carbonylation, hydrogenation, hydro-formylation, etc.

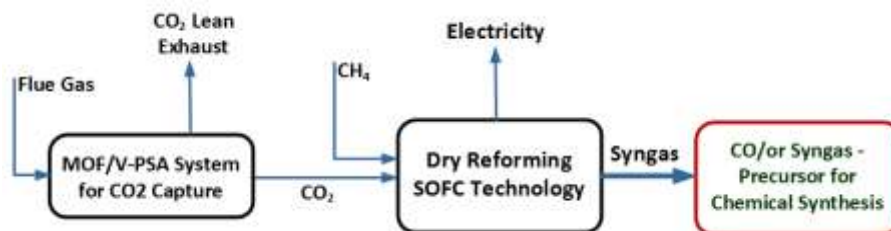


Figure 5-10 Block diagram of integrated CO<sub>2</sub> capture and dry reforming SOFC technology for CO<sub>2</sub> utilization

### 5.3. Experimental procedures/methodology

#### 5.3.1. NiO-YSZ anode supported tubular fuel cell fabrication

The tubular ceramic SOFC was fabricated by slip casting of a NiO-YSZ anode support, followed by dip coating of a thin YSZ electrolyte and a thin porous layer for cathode infiltration. Nd<sub>2</sub>NiO<sub>4+δ</sub> or Pr<sub>2</sub>NiO<sub>4+δ</sub> were infiltrated into the thin porous YSZ layer of the cells to form the cathode.

NiO (Baker Chemicals) and YSZ (TZ-8Y, 8 mol% Y<sub>2</sub>O<sub>3</sub>, Tosoh) were mixed at a ratio of 65:35 wt% and milled for 72 h in a ball mill. The solid loading of the slip was set to 40% by adjusting the water content and its final pH was set to 4 using 2% hydrochloric acid. To generate sufficient porosity, 30 vol.% graphite (Sigma Aldrich, <325 mesh) was added to the slip following pH adjustment, and then the suspension was mixed for 15 minutes prior to slip casting. To create the tubular support, the slip was cast into a plaster mold (previously prepared from a tubular mandrel) and left for about one minute, after which the excess slip was quickly poured out. The wet tube was then dried at room temperature for 1 h. The slip cast tubes were dried at 100°C, then heated at 700°C to burn off the graphite and then finally pre-sintered in air at 1000°C for 3 h. Further details regarding the slip casting procedure and fabrication of thin tubular support can be found in elsewhere [25].

The electrolyte and the thin porous YSZ layer formulas and their dip coating procedure

are available in other literatures [26,27]. Both layers were sintered at 1350°C for 3 h. The infiltration of  $\text{Nd}_2\text{NiO}_{4+\delta}$  (NNO) into a thin porous YSZ layer is addressed by Laguna-Bercero et al. and infiltration of  $\text{Pr}_2\text{NiO}_{4+\delta}$  (PNO) follows a similar process.

For the cathode current collection, a thin coating of silver alloyed with 10 wt% Pd paste was applied on the cell cathode, wrapped with silver mesh (Alfa Aesar) and secured with two 0.58 mm diameter silver wires. A rolled copper mesh current collector (Alfa Aesar) was tightly pushed inside the tube to ensure good contact with the anode wall. An Agilent electronic load (model N3301A) evaluated the open circuit voltage (OCV) and I-V curves. An Agilent scanner (model E4970A) monitored the thermocouples, and LabView software was used for automated measurements and data collection. AC impedance spectroscopy was carried out with a four probe configuration using a Solartron frequency response analyzer 1255 in combination with a Solartron electrochemical interface 1287. The assembly of a single tubular fuel cell and the testing setup have been depicted in Figure 5-11.

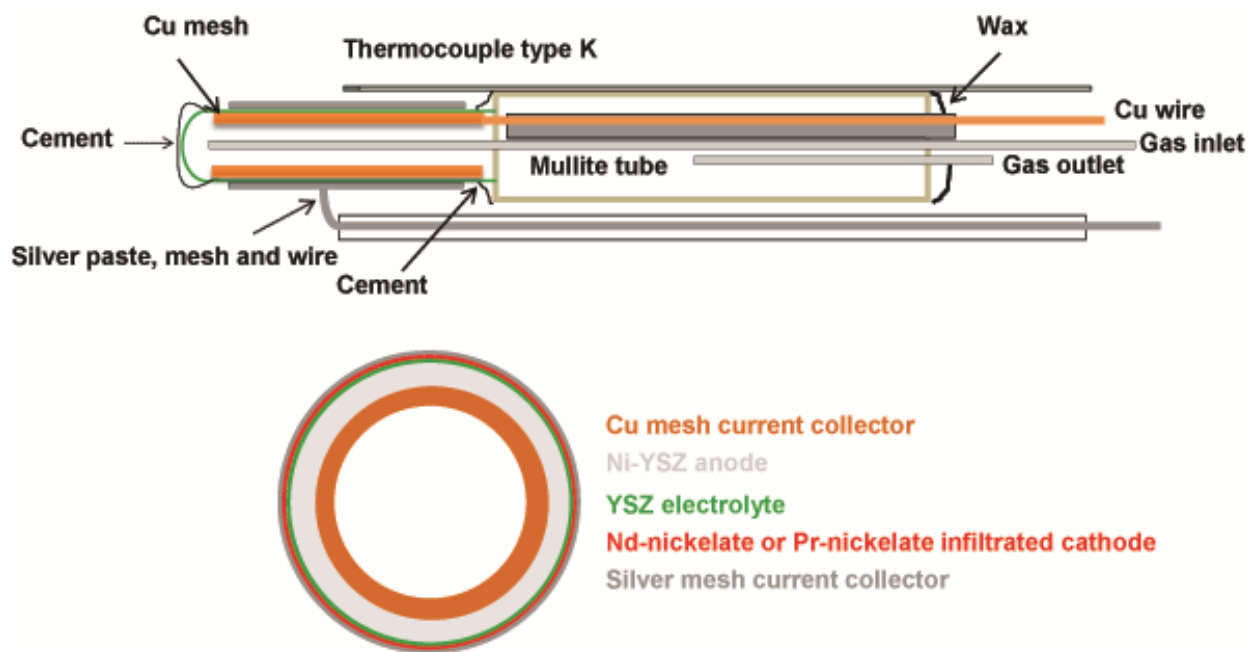


Figure 5-11 Cross section of the fuel cells used in the stack and the testing set up for a single cell

### 5.3.2. Proton conducting electrolyte (PCE) anode supported tubular fuel cell fabrication

Tubular anode supported proton conducting fuel cells were fabricated successfully based on a  $\text{Ni}-\text{BaZr}_{0.1}\text{Ce}_{0.7}\text{Y}_{0.1}\text{Yb}_{0.1}\text{O}_{3-\delta}$  (BZCYYb) composite anode. Fabrication of these fuel cells is challenging due to the high sintering temperature of the proton conducting electrolyte (same composition as the ceramic component of the anode). In order to improve the open circuit voltage (OCV) of the proton conducting fuel cells, fine NiO and proton conducting materials were synthesised through a sol-gel method and were used for cell fabrication. The cell

fabrication procedure was similar to the one for NiO-YSZ anode supported cells. The proton conducting electrolyte was sintered at 1450°C, followed by the application of a PCE-LSCF cathode [16]. The cathode was a 7:3 weight ratio of La<sub>0.6</sub>Sr<sub>0.4</sub>Co<sub>0.2</sub>Fe<sub>0.8</sub>O<sub>3-d</sub> (LSCF, Fuel Cell Materials)-BZCYYb powders, mixed with azeotropic solvent, binder and dispersant. It was dip coated on the electrolyte, followed by sintering at 1000 °C for 3 h to form a porous PCE-BZCYYb cathode.

### 5.3.3. H-SOFC

#### 5.3.3.1 Preparation of BZCYYb powder

BZCYYb powder with two distinct particle sizes was prepared using two different methods. For the solid-state reaction (SSR) process, stoichiometric amounts of BaCO<sub>3</sub>, ZrO<sub>2</sub>, CeO<sub>2</sub>, Y<sub>2</sub>O<sub>3</sub> and Yb<sub>2</sub>O<sub>3</sub> powders were initially mixed and ball milled in isopropyl alcohol, followed by calcination at 1100°C for 10 h. The wet ball milling and calcination steps were repeated until a pure perovskite phase was obtained. For the aqueous sol-gel process, stoichiometric amounts of Ba(NO<sub>3</sub>)<sub>2</sub>, ZrO(NO<sub>3</sub>)<sub>2</sub>·5H<sub>2</sub>O, Ce(NO<sub>3</sub>)<sub>3</sub>·6H<sub>2</sub>O, Y(NO<sub>3</sub>)<sub>3</sub>·6H<sub>2</sub>O and Yb(NO<sub>3</sub>)<sub>3</sub>·5H<sub>2</sub>O were initially dissolved in distilled water in a beaker. Suitable amounts of EDTA and citric acid were added into the solution sequentially as chelating agents. The aqueous solution was heated to 80°C with vigorous agitation until a viscous gel was formed. Then the beaker was transferred to an oven and dried at 300 °C to form a black foamy intermediate product. This foam was ground into a fine powder and then calcined at 1100°C for 5 h in air to obtain BZCYYb powder. In order to evaluate the stability of BZCYYb in different feedstocks at high temperature, the BZCYYb powder was placed in a crucible that was then inserted in a quartz tube subjected to either CH<sub>4</sub>-CO<sub>2</sub> or H<sub>2</sub>-CO treatment.

#### 5.3.3.2 Preparation of NBCaC cathode

To prepare an NdBa<sub>0.75</sub>Ca<sub>0.25</sub>Co<sub>2</sub>O<sub>5+δ</sub> (NBCaC) cathode, stoichiometric amounts of Nd(NO<sub>3</sub>)<sub>3</sub>·6H<sub>2</sub>O, Ca(NO<sub>3</sub>)<sub>2</sub>·4H<sub>2</sub>O, Ba(NO<sub>3</sub>)<sub>2</sub> and Co(NO<sub>3</sub>)<sub>2</sub>·6H<sub>2</sub>O were dissolved in distilled water with ethylene glycol/citric acid added as the chelating agent. After similar drying and grinding processes as those for BZCYYb preparation, the resulting powder was finally calcined in air at 900°C for 5 h to form the layered perovskite NBCaC.

#### 5.3.3.3 Preparation of the NiCo-LDC catalyst

NiCo-LDC catalyst was prepared by a glycine-nitrate auto combustion process (GNP). Initially, Ni(NO<sub>3</sub>)<sub>2</sub>·6H<sub>2</sub>O, Co(NO<sub>3</sub>)<sub>2</sub>·6H<sub>2</sub>O, La(NO<sub>3</sub>)<sub>3</sub>·6H<sub>2</sub>O and Ce(NO<sub>3</sub>)<sub>3</sub>·6H<sub>2</sub>O were dissolved in distilled water at a molar ratio of 6:1:2:8. Then glycine was added as both the chelating agent and the fuel. This solution was then heated on a hot plate at 200°C until auto combustion occurred. The collected powder was finally calcined at 800°C for 2 h to remove residual carbon and to form Ni<sub>0.8</sub>Co<sub>0.2</sub>O-La<sub>0.2</sub>Ce<sub>0.8</sub>O<sub>1.9</sub> (NiCoO-LDC) powder. The NiCo-LDC catalyst was obtained via *in situ* reduction in H<sub>2</sub> during the designated experiment.

In addition to the GNP method, we also prepared NiCo-LDC catalyst through a conventional wet impregnation method. Firstly, La<sub>0.2</sub>Ce<sub>0.8</sub>O<sub>1.9</sub> (LDC) nano powder was prepared via the GNP method detailed above. Stoichiometric amounts of Ni(NO<sub>3</sub>)<sub>2</sub>·6H<sub>2</sub>O and Co(NO<sub>3</sub>)<sub>2</sub>·6H<sub>2</sub>O were dissolved in distilled water in a beaker. Sequentially, a suitable amount of LDC nano powder was added to the solution under gentle agitation. The weight ratio of NiCo: LDC was kept at 19.5:80.5. The suspension was then stirred and dried in a water bath at 80°C. After water evaporation, the obtained powder was calcined at 800°C for 2 h.

#### **5.3.3.4 Cell fabrication**

The anode-supported cells were prepared by using a dry pressing-spin coating-sintering process. To prepare the anode support, the powder mixture, containing NiO and SSR-derived BZCYYb at a weight ratio of 65:35, was ball milled in isopropyl alcohol with 10 wt% corn starch as the pore former. After homogenization and drying, 1 g of the mixed powder was used to fabricate the anode support substrate using dry pressing in a cylindrical die. A sequential 2 h pre-sintering at 1050°C was applied to acquire strong substrates.

The thin BZCYYb electrolyte film on the NiO-BZCYYb anode substrate was prepared by an optimized slurry coating technique. Initially, GNP-derived BZCYYb-containing slurry was prepared by dispersing 2 g BZCYYb powder in 6 g ethanol in a vial. 0.04 g cellulose and 1g triethanolamine were added as the binder and dispersant, respectively. A homogenous slurry was then obtained using an ultrasonic processor in which the vial was cooled using a water bath. A BZCYYb membrane then was prepared by spin coating the BZCYYb suspension. The thickness of the BZCYYb membrane was controlled by the time of coating. Finally, the electrolyte coated substrate was densified at 1420°C for 5 h.

To prepare the cathode layer, NBCaC-BZCYYb (GNP derived, weight ratio of 60:40) paste was prepared by adding a suitable amount of home-made binder and then ground using a mortar-pestle. The paste was brush painted on the surface of the sintered BZCYYb electrolyte with an area of 0.316 cm<sup>2</sup>. This membrane electrolyte assembly was finally calcined in air at 950°C for 4 h to complete the fabrication of the anode-supported cell. For the layered H-SOFC, the NiCoO-LDC layer was also prepared using the paste method via brushing the NiCoO-LDC paste on the anode support surface of the cell, followed by calcination at 900°C in air for 2 h.

#### **5.3.3.5 Preparation of the NBCaC-BZCYYb and NiCo-LDC catalyst slurries**

The cathode and the NiCoO-LDC pastes were prepared by ball milling the powder and a home-made binder with a weight ratio of 50:50 for 1 h. The home-made binder was prepared via mixing 4 wt% cellulose and 96 wt% terpineol. The full dissolution of cellulose was achieved by heating the mixture to 80°C under vigorous agitation.

### 5.3.3.6 Reforming activity evaluation procedure

To compare the CH<sub>4</sub>-CO<sub>2</sub> reforming activities of Ni-BZCYYb and NiCo-LDC, catalyst powders of NiO-BZCYYb (weight ratio of 65:35) and NiCoO-LDC were calcined at 1420°C (5 h) and 900°C (2 h), respectively. The higher calcination temperature of the former is to simulate the particle agglomeration effect during the fuel cell fabrication process. Then, the obtained powders were sieved using 30 to 60 mesh. 0.2 g of each catalyst was mixed with 0.4 g of catalytically inert SiO<sub>2</sub>, and then packed into a quartz tube for activity measurements at temperatures from 700 to 550°C after initial reduction in H<sub>2</sub> at 700°C for 2 h. CH<sub>4</sub> and CO<sub>2</sub> were concurrently fed to the tubular reactor at a flow rate of 10 mL min<sup>-1</sup>. The composition of the effluent gas was analyzed using a gas chromatograph (GC, Hewlett Packard Series two). CO<sub>2</sub> conversion and CO selectivity were calculated by Equations (6) and (7), respectively.

$$\text{CO}_2 \text{ conversion} = \frac{1/2[\text{CO}]}{1/2[\text{CO}]+[\text{CO}_2]} \times 100\% \quad (6)$$

$$\text{CO selectivity} = \frac{[\text{CO}]}{[\text{CO}]+[\text{CO}_2]} \times 100\% \quad (7)$$

### 5.3.3.7 Electrochemical performance evaluation procedure

During an SOFC test, Au and Pt pastes were painted on the anode and cathode of the cells, respectively, as the current collectors, which were initially baked in air at 800°C for 2 h. Pt meshes were used as the secondary current collector on top of those pastes, which were connected with Pt wires. The cell was then sealed on the anode side to an alumina tube using a Ceramabond® glass sealant (Aremco Products, Inc.). After the sealant curing, the cell was reduced in H<sub>2</sub> at 700°C for 2 h prior to the electrochemical measurements. Open-circuit electrochemical impedance spectra (EIS) and current density-voltage (I-V) curves were obtained at temperatures ranging from 550 to 700°C in H<sub>2</sub>, H<sub>2</sub>-Ar, H<sub>2</sub>-CO and CH<sub>4</sub>-CO<sub>2</sub> (molar ratios of the mixed gases were 1:1); the fuel flow rate ranged from 20 to 40 mL min<sup>-1</sup>. Ambient air (relative humidity = (40±10) %) was used as the oxidant. An impedance/gain phase analyzer (Solartron 1255) and an electrochemical interface (Solartron 1287) were used to record the electrochemical performance. Stability and syngas production tests were carried out via applying a constant current load, and simultaneously monitoring the voltage response as well as the effluent gas composition using a GC. H<sub>2</sub> selectivity during the electro-oxidation process was calculated by Equation (8).

$$\text{H}_2 \text{ selective oxidation} = \frac{[\text{H}_2 \text{ converted}]}{[\text{H}_2 \text{ converted}]+[\text{CO converted}]} \times 100\% \quad (8)$$

### 5.3.3.8 Materials characterization

All the powder materials were subjected to X-ray diffraction analyses (XRD, Rigaku Rotaflex) for phase identification by using Cu K $\alpha$  radiation generated at 40 kV and 44 mA.

The scan was conducted within a  $2\Delta$  range between  $20^\circ$  and  $80^\circ$  at a rate of  $1^\circ \text{ min}^{-1}$ . The NiCo-LDC was further analyzed by transmission electron microscopy (TEM, JEOL 2200 FS). The microstructures of the cells were examined using scanning electron microscopy (SEM, JEOL 6301F). X-ray photoelectron spectroscopy (XPS, Kratos AXIS Ultra) was used to study the surface chemistry of NiCo-LDC powder referenced to adventitious carbon (C 1s with binding energy = 284.5 eV).

### 5.3.3.9 CO<sub>2</sub>-TPD

The CO<sub>2</sub>-TPD (temperature-programmed desorption) was carried out to test the effect of the preparation method on the surface basicity of the NiCo-LDC catalysts. The samples were first treated in Ar at  $500^\circ\text{C}$  for 1 h to remove the adsorbed species, and then cooled to room temperature, followed by exposing to CO<sub>2</sub> for 2 h. The treated samples were purged with Ar at room temperature for 1 h and heated linearly at  $10\text{-}800^\circ\text{C}$  in a constant flow of Ar. The CO<sub>2</sub> signal was monitored and recorded continuously as a function of temperature by the QIC-20 (Atmospheric Gas Analysis System).

## 5.3.4. O-SOFC

### 5.3.4.1 O-SOFC based on a Ni-S selective catalyst

#### 5.3.4.1.1 Preparation of the catalysts

NiCu-Ce<sub>0.8</sub>Zr<sub>0.2</sub>O<sub>2</sub> (ZDC) catalyst was prepared by a glycine-nitrate process (GNP). Ni(NO<sub>3</sub>)<sub>2</sub>·6H<sub>2</sub>O, Cu(NO<sub>3</sub>)<sub>2</sub>·3H<sub>2</sub>O, Zr(NO<sub>3</sub>)<sub>4</sub>·5H<sub>2</sub>O and Ce(NO<sub>3</sub>)<sub>3</sub>·6H<sub>2</sub>O were dissolved in distilled water at a molar ratio of 6:1:2:8 with glycine added. This solution was then combusted at  $200^\circ\text{C}$  and calcined at  $800^\circ\text{C}$  for 2 h to form NiCuO-Ce<sub>0.8</sub>Zr<sub>0.2</sub>O<sub>2</sub> powder, which was *in-situ* reduced in H<sub>2</sub> to form a NiCu-Ce<sub>0.8</sub>Zr<sub>0.2</sub>O<sub>2</sub> catalyst. The volume percentage of metal phase (Ni-Cu alloy) in the NiCu-ZDC cermet is around 23.3%, ensuring adequate electronic conductivity for SOFC operation. In a control group, we also prepared Ni-ZDC (molar ratio of Ni:Zr:Ce is 7:2:8), NiCo-ZDC (molar ratio of Ni:Co:Zr:Ce is 6:1:2:8) and NiFe-ZDC (molar ratio of Ni:Fe:Zr:Ce is 6:1:2:8) using the same method.

#### 5.3.4.1.2 Preparation of the cathode

To prepare La<sub>0.6</sub>Sr<sub>0.4</sub>Co<sub>0.2</sub>Fe<sub>0.8</sub>O<sub>3-δ</sub> (LSCF) cathode material, La(NO<sub>3</sub>)<sub>3</sub>·6H<sub>2</sub>O, Sr(NO<sub>3</sub>)<sub>2</sub>, Co(NO<sub>3</sub>)<sub>2</sub>·6H<sub>2</sub>O and Fe(NO<sub>3</sub>)<sub>3</sub>·9H<sub>2</sub>O were dissolved in distilled water with EDTA/citric acid added as the chelating agent. The aqueous solution was heated at  $80^\circ\text{C}$  under agitation to a viscous gel, and then dried at  $180^\circ\text{C}$  to form a black foamy intermediate product, which was ground into fine powder and calcined at  $800^\circ\text{C}$  for 2 h in air to obtain the perovskite structure LSCF.

### 5.3.4.1.3 Cell fabrication

Tape-casting/screen printing/sintering processes were used for fabrication of the anode supported cells. NiO (Type A Standard, Inco) and YSZ (TZ8YS, Tosoh) in a 57:43 weight ratio were ball milled for 24 h in toluene/ethanol solvent with fish oil as the dispersant and corn starch as the pore former. It was further milled for another 24 h after adding polyvinyl butyral (Richard E. Mistler Inc., USA) as the binder and polyethylene glycol (Richard E. Mistler Inc., USA) as the plasticizer. Such a prepared slurry was cast into sheet (anode support layer) by using a tape casting machine, then dried in air to obtain the anode support (16 mm in diameter  $\times$ 1.4 mm thick), to which functional NiO-YSZ (60:40 wt%, Type F Standard, Inco-TZ8Y, Tosoh) and electrolyte (TZ8Y, Tosoh) were then screen printed in sequence, prior to sintering at 1390 °C for 3 h. To prepare the baffle and cathode, Ce<sub>0.9</sub>Gd<sub>0.1</sub>O<sub>1.9</sub> (GDC, NIMTE, CAS) and LSCF-GDC (70:30) pastes were then screen printed successively on the surface of the sintered YSZ electrolyte, followed by sintering separately in air at 1300°C and 950°C for 2 h to complete the fabrication of the anode-supported cells. The size of the obtained SOFC button cell was about 13 mm in diameter  $\times$ 1 mm thick with an active area of 0.5 cm<sup>2</sup> (cathode). The NiCuO-Ce<sub>0.8</sub>Zr<sub>0.2</sub>O<sub>2</sub> slurry was painted on the outer surface of anode and sintered at 900°C for 2 h in air.

### 5.3.4.1.4 Preparation of the LSCF-GDC cathode and NiCuO-ZDC catalyst slurry

The cathode and the catalyst pastes were prepared by ball milling the powder and a self-made binder with a weight ratio of 50:50 for 1 h. The self-made binder was prepared by adding 4 wt% cellulose into 96 wt% terpineol, followed by stirring and heating at 80°C to completely dissolve the cellulose.

### 5.3.4.1.5 Catalytic activity evaluation

The catalytic activity and sulfur tolerance of Ni-YSZ (57:43, sintered at 1390°C) and Ni- and NiM (M =none, Co, Cu, Fe)-ZDC were compared. Catalytic activity measurements for the DRM reaction were performed at atmospheric pressure using a compound of 0.2 g catalysts and 0.4 g catalytically inactive quartz powder, which was sieved into the particle size ranging from 30 to 60 mesh and packed in a bed in a quartz tube. Prior to the catalytic evaluation, the samples were heated up to 850°C and reduced in H<sub>2</sub> for 5 h. Regarding the assessment of sulfur tolerance, the reduced catalysts were exposed to H<sub>2</sub>-500 ppm H<sub>2</sub>S for 5 h prior to the test. The gas mixtures of sweet CH<sub>4</sub>-CO<sub>2</sub> (mole ratio=1:1) or sour CH<sub>4</sub>-CO<sub>2</sub> (mole ratio=1:1, balanced with 50 ppm H<sub>2</sub>S) were fed into the reactor at a flow rate of 20 mL min<sup>-1</sup>. Compositional analysis of the effluent gases was performed with a gas chromatograph (GC, Hewlett Packard Series two). The catalytic reactions were performed at the temperatures ranging from 550 to 800°C up to 48 h. The percentages of CH<sub>4</sub> conversion and CO selectivity were calculated according to Eq.6 and 7, respectively.

#### 5.3.4.1.6 Carbon deposition resistance evaluation

The carbon deposition resistance of the catalysts was evaluated by analyzing the nature of the carbon deposited on the catalyst through Raman spectroscopy. To accelerate the rate of carbon formation on the catalyst, we exposed the as-reduced/treated catalysts to pure CH<sub>4</sub> at 800°C for 30 min and cooled them down to room temperature in H<sub>2</sub>, followed by carrying out the Raman tests.

#### 5.3.4.1.7 Other Characterizations

In addition to the XRD, SEM and TEM mentioned in Section 5.3.1, Raman spectrometry (Thermo Nicolet Almega XR Raman Microscope) was employed to detect the graphitization degree of deposited carbon on the catalyst. A SDT-Q600 (TA Instruments, USA) machine was used to carry out the thermogravimetric analysis (TGA) experiments of the catalyst reduction process. Carbon deposition on the catalysts was quantitatively investigated by using temperature programmed oxidation [TPO via coupled TGA-Mass Spectrometer (MS, Pfeiffer Vacuum GmbH)].

### 5.3.4.2 O-SOFC based on a Ni-Sn alloy selective catalyst

#### 5.3.4.2.1 Micro reformer preparation and single cell fabrication

NiSn nanoparticles (NPs) were deposited onto Al<sub>2</sub>O<sub>3</sub> (Fisher Scientific) supports through the wet impregnation technique. Stoichiometric amounts (mole ratio of Ni<sup>2+</sup>/Sn<sup>2+</sup> is 9/1) of Ni(NO<sub>3</sub>)<sub>2</sub> and SnCl<sub>2</sub> (Fisher Scientific) were dissolved in deionized water with trace amounts of hydrochloric acid added. A targeted amount (weight ratio of Al<sub>2</sub>O<sub>3</sub>/NiSn is 85/15) of Al<sub>2</sub>O<sub>3</sub> powder was added into this solution, followed by heating and stirring until the water was completely evaporated. The mixture was ground to loose powder, which was then calcined at 650°C in air for 2 h. The Ni foams were pre-treated in H<sub>2</sub>-500 ppm H<sub>2</sub>S at 850°C for 2 h in order to enhance their carbon deposition resistance. The micro reformer was prepared by filling the pre-treated Ni foam with the NiSn/Al<sub>2</sub>O<sub>3</sub> catalysts. Firstly, a paste of tungsten carbide was applied to one side of the Ni foam and dried in air at 80°C in order to seal the Ni foam. Then, the Ni foam was filled with NiSn/Al<sub>2</sub>O<sub>3</sub> catalyst from the other side. The typical weight ratio of Ni foam/catalyst was approximately 1/2. Finally, the tungsten carbide paste was applied to the other side of the Ni foam and dried in air at 80°C to complete the preparation of the micro reformer.

The NiO-YSZ/YSZ anode/electrolyte substrates were fabricated through a co-sintering (1390°C) method, which was detailed in our former work [19]. In the present study, the diameter of the sintered NiO-YSZ/YSZ substrate is approximately 20 mm. The (La<sub>0.8</sub>Sr<sub>0.2</sub>)<sub>0.95</sub>MnO<sub>3-δ</sub> (LSM, Fuel Cell Materials)-YSZ (TZ-8YS, weight of LSM/YSZ is 60/40) cathode slurry was screen printed on the YSZ electrolyte with an area of 0.8 cm<sup>2</sup>, followed by sintering at 1000°C in air for 2 h. The above NiSn-containing solution was then infiltrated into

the NiO-YSZ anode of the prepared single cells, and calcined at 650°C in air for 2 h. The infiltration and calcination processes were repeated to get 3 wt% weight gain for the single cell.

#### **5.3.4.2.2 Evaluation of the chemical and electrochemical activities**

Pt paste, mesh and wire were used as the current collector and measuring lead for the LSM-YSZ cathode. For the anode, a paste of tungsten carbide served as the current collecting layer and was used to make a good contact between the NiSn-YSZ anode and the micro reformer. Scheme S1 (electronic supporting information, ESI) and Figure 4-1a show the arrangement of all the components in the biogas reactor. The reactor was then sealed to an alumina tube by using a Ceramabond® glass sealant. The cell was heated to 850°C in 10% H<sub>2</sub>-90% N<sub>2</sub>, and then reduced in H<sub>2</sub> at 850°C prior to the chemical and electrochemical tests. Its activity for IRB reaction was evaluated in a feed stream of CH<sub>4</sub>-CO<sub>2</sub> (1:1) with a total flow rate of 20 mL min<sup>-1</sup>. To evaluate the effect of H<sub>2</sub>S poison on the activity for DRM and electrochemical performance, the fresh cell (F-C) and the cell contaminated in H<sub>2</sub>-500 ppm H<sub>2</sub>S at 850°C (S-C) were tested in CH<sub>4</sub>-CO<sub>2</sub> and 200 ppm H<sub>2</sub>S-containing CH<sub>4</sub>-CO<sub>2</sub>, respectively. Compositional analysis of the exhausts was carried out via gas chromatography (GC, Hewlett Packard Series two). The catalytic reactions took place at temperatures between 600 and 850°C. The values of CH<sub>4</sub> conversion and CO selectivity were calculated by Equations 6 and 7, respectively. Current-voltage (I-V) curves in H<sub>2</sub> (0~200 ppm of H<sub>2</sub>S, 40 mL min<sup>-1</sup>) and biogas (CO<sub>2</sub>:CH<sub>4</sub>=1:1, 0~200 ppm of H<sub>2</sub>S, 20 mL min<sup>-1</sup>) were also collected. The performance durability of the reactor in biogas was estimated under 1.25 A cm<sup>-2</sup> and at 850°C. The LSM-YSZ cathode was fed with 500 mL min<sup>-1</sup> dry air. The exhausts from the anode side were analyzed by the GC machine.

#### **5.3.4.2.3 Characterization**

As described in Section 5.3.1, XRD, XPS and TEM were used to characterize the samples. A field emission scanning electron microscope (FESEM, Zeiss Sigma 300 VP) was also used to examine the microstructures of the samples.

### **5.4. Results, discussions and outcomes**

#### **5.4.1. Lab scale extruder for tubular fuel cell manufacturing**

Extrusion is a suitable method for high-speed manufacture of the porous tubular support components of a solid oxide fuel cell. It is an effective and efficient method of forming tubular ceramics semi-continuously and is accordingly well accepted by the ceramic industry for mass production. Extruders can be categorized in three basic types: pug mill-auger, screw-fed and ram or piston. In pug mill-augers, the machine mixer and extruder are in one unit. This type is typically used for softer pastes. Screw-fed extruders are typically used for plastic extrusion. Piston extruders are common for extruding technical ceramics with stiffer extruding pastes.

Typical commercially available extruders are not suitable for the scale of research work since each extruder throughput needs a significant amount (kilograms) of extrusion paste. Therefore, a lab scale extruder which can operate with small batch sizes (~50 g) was designed and fabricated. Figure 5-12a is the Solidworks 3-D assembly arrangement of a lab scale piston extruder showing its different components. Figure 5-12b is a photograph of the actual unit. The inner diameter of the barrel is 3 cm and it has a length of 15 cm. Extrusion of one-barrel worth of paste will provide around 20 SOFC tubular supports 15 cm long and 1.0 cm OD with a wall thickness of 0.01 cm.

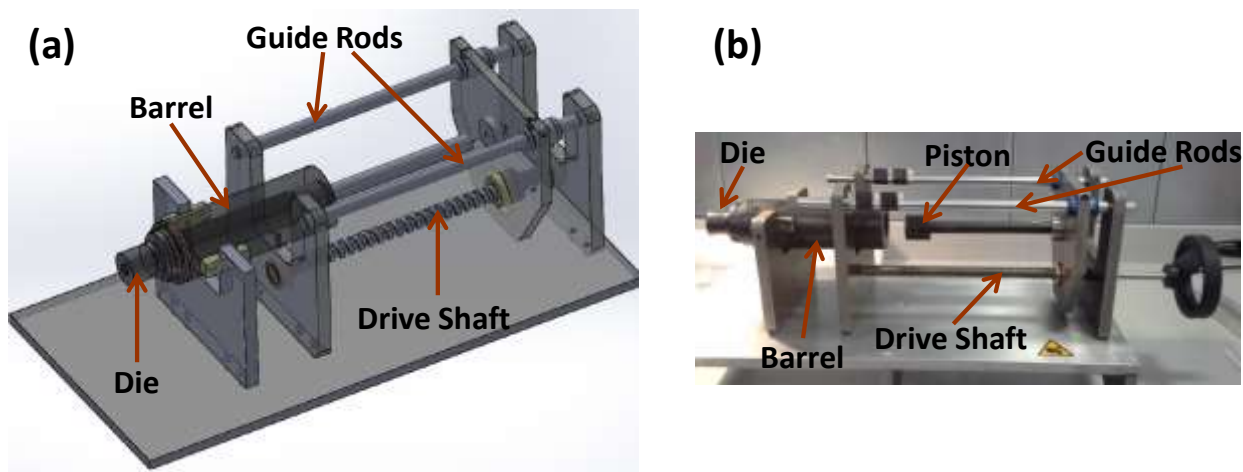


Figure 5-12 (a) Drawing of 3-D assembly and (b) photograph of built lab scale piston extruder

As shown in the figures, during the extrusion operation, the piston is pushed into the die using an Acme threaded shaft and drive. Guide rods are used to ensure alignment of the piston and drive system. Figure 5-13a is a cross sectional view of the extruder die to produce a tube with an outer diameter of 11.5 mm and a wall thickness of 1.5 mm. Figure 5-13b shows tube extrusion using common Play-Doh. Two types of commercial modeling clays (common Play-Doh (softer) & Craft Smart Plastalina (stiffer)) were used in the extruder evaluation. Figure 5-13c shows a photo of some of the extruded tubes. It was observed that extrusion of the stiffer Plastalina was difficult with the extruder and it needs improvement to handle stiff paste.

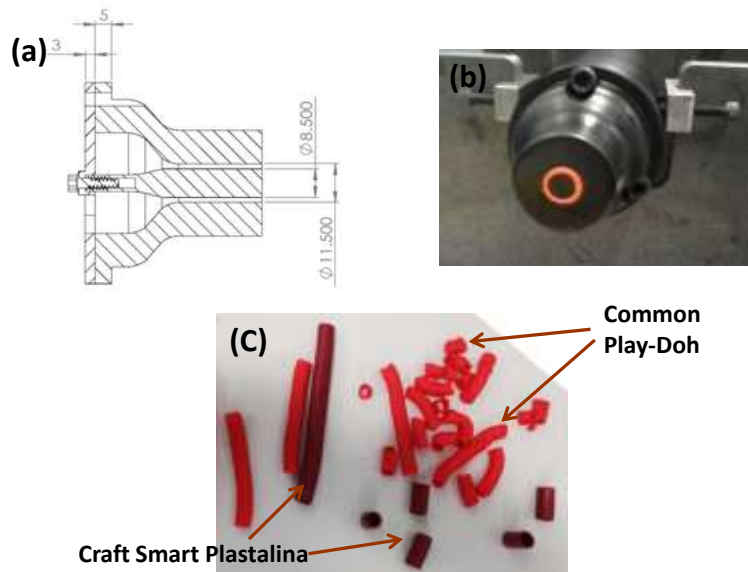


Figure 5-13 (a) Cross sectional view of the die for tube extrusion, (b) photograph of extrusion of the tube during operation and (c) photo of several extruded tubes using two different commercial modeling clays

A photograph of the modified extruder is shown in Figure 5-14a. The drive shaft diameter has been increased and it has been moved to the center position to align with the piston axis. In the improved extruder, the number of guide rods was increased from two to three and the guide rod diameters were also increased to enhance the stability of the piston drive system. A clamp was also added to keep the die in its position during high pressure extrusion operation. A drive stopper was added to stop the piston when it reached the end of the barrel; otherwise it can potentially damage the front part of the die. Figure 5-14b shows a University of Alberta SOFC researcher and an AITF technical staff member working on SOFC tube fabrication. Figure 5-14c is a picture of the extrusion of an YSZ support tube using the extruder. Aqueous based pastes (YSZ and YSZ/NiO) using methyl cellulose binder were chosen for the fabrication of tubular SOFC supports. Typical paste formulation and the function of the ingredients are provided in Table 5-1. The initial step consisted of dissolving 5-7 wt% methyl cellulose binder in water. The paste is prepared in an automated mortar and pestle by slowly adding the methyl cellulose solution to the ceramic powder. The remaining ingredients of the paste are then added. It was found that approximately 30 g of YSZ or YSZ/NiO provides enough paste to run the extruder and evaluate the paste.

Table 5-1 Typical composition of extrusion paste

| Materials  | Wt%   |
|--|-------|
| Ceramic Powder (e.g., yttria-stabilized zirconia (YSZ), YSZ/NiO, etc.) | 55-70 |
| Methyl Cellulose – typical viscosity 400 cp - binder                   | 1-5   |
| Polyethylene Glycol (PEG) - plasticizer                                | 0-3   |
| Stearic Acid - lubricant   | 0-4   |
| Vegetable Oil- improve plasticity & lubrication                        | 0-3   |

Water –solvent

20-35

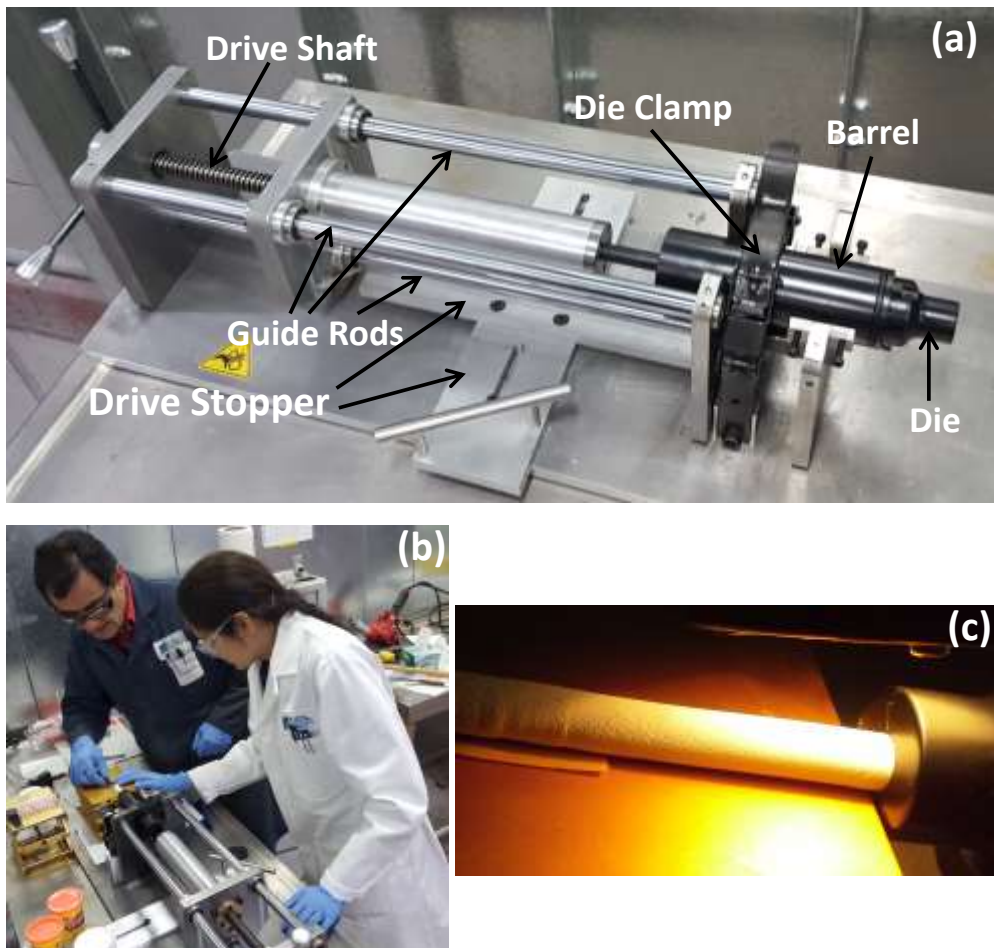


Figure 5-14 (a) Photograph of the modified extruder for manufacturing of tubular SOFCs, (b) SOFC researchers operating the extruder and (c) photograph of a YSZ extruded support tube during an extrusion run

#### 5.4.2. Development of the basic tubular fuel cell structure for a proton conducting solid electrolyte

It is clear that a successful proton conductor will ensure complete separation of H<sub>2</sub> and CO since only H<sub>2</sub> will be able to participate in the anode reaction. The tubular cell behaves relatively well under hydrogen and produces a high power density. The power density results obtained are higher than some of the results reported in recent publications. Maximum power densities in the range of 320–420 mW/cm<sup>2</sup> were generated by these cells between 600–700°C, under H<sub>2</sub> carrying 3 vol% moisture (Figure 5-15). The performance of the proton conducting cell under a mixture of H<sub>2</sub> and CO at 700°C is about 130 mW/cm<sup>2</sup> which is lower than that of the humidified hydrogen fuel since the CO gas does not contribute in the overall power performance. The impedance of a PCE cell is shown in Figure 5-16 where both a lower ohmic resistance and activation polarization are observed in the cell with increasing operating

temperature while concentration polarization remains relatively unchanged. A higher ohmic resistance and activation polarization were also observed when the cell was operating under the H<sub>2</sub> and CO gas mixture. Figure 5-17 presents SEM images of the cross section of the studied proton conducting cell. As shown in Figure 5-17a and b, there is a 25  $\mu\text{m}$  PCE covering the Ni-PCE anode support while the PCE-LSCF cathode is relatively thick (90  $\mu\text{m}$ ). The brighter phase in Figure 5-17b represents the PCE phase and the darker phase is the Ni phase in the anode microstructure.

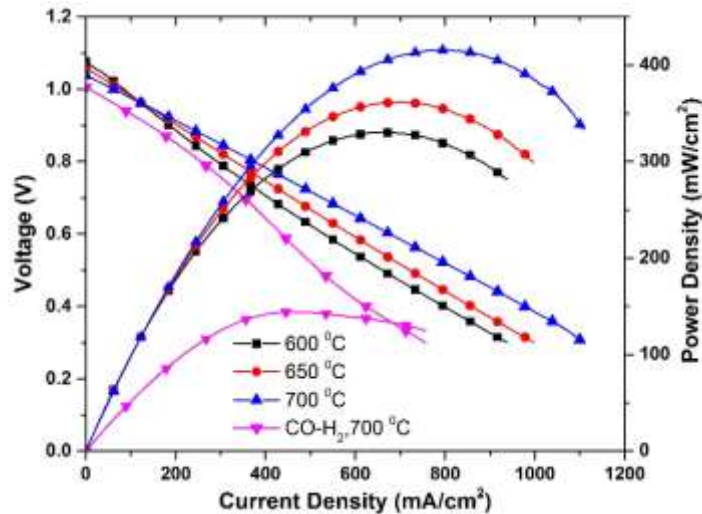


Figure 5-15 Performance of a proton conducting electrolyte based tubular SOFC under humid H<sub>2</sub> and its mixture with CO gas

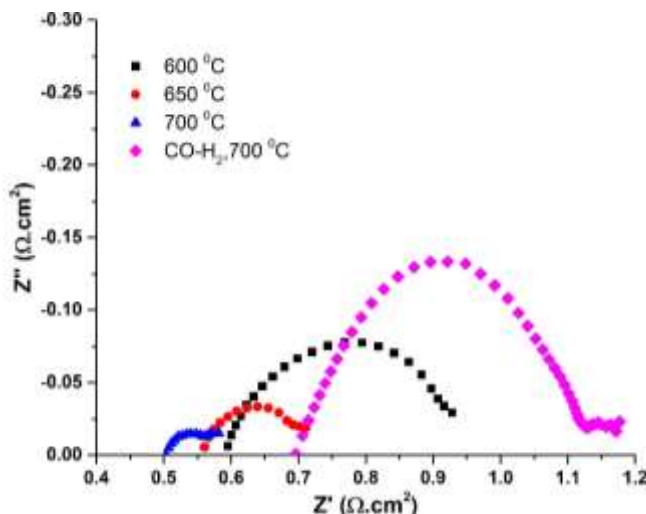


Figure 5-16 Impedance spectra of the proton conducting tubular SOFC

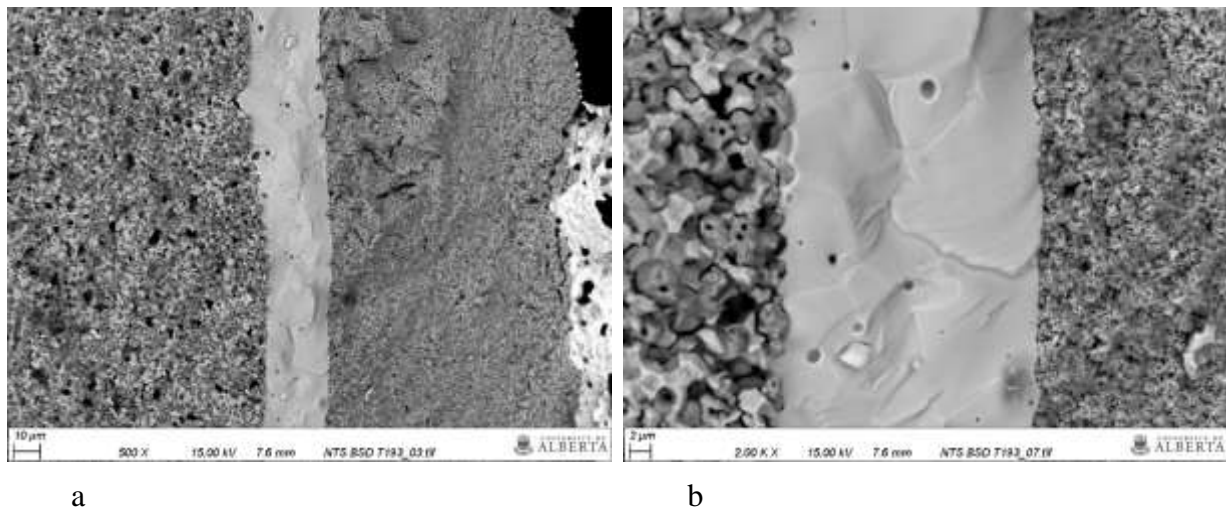


Figure 5-17 SEM images of the cross section of the proton conducting fuel cell

Efforts were then made to coat a dense proton conducting electrolyte on a Ni-YSZ anode which has far superior mechanical strength and resistance under hydrocarbons compared with proton conducting anodes. We managed to fabricate such a proton conducting fuel cell for the first time. This cell showed a power density of 160-280 mW/cm<sup>2</sup> within 600-700°C (Figure 5-18), which is a lower power than the proton conducting anode supported cell shown above. This might be due to a larger active functional area in the Ni-PCE anode support compared with the Ni-YSZ anode support coated with a thin layer of Ni-PCE material that is responsible for the electrochemical reactions.

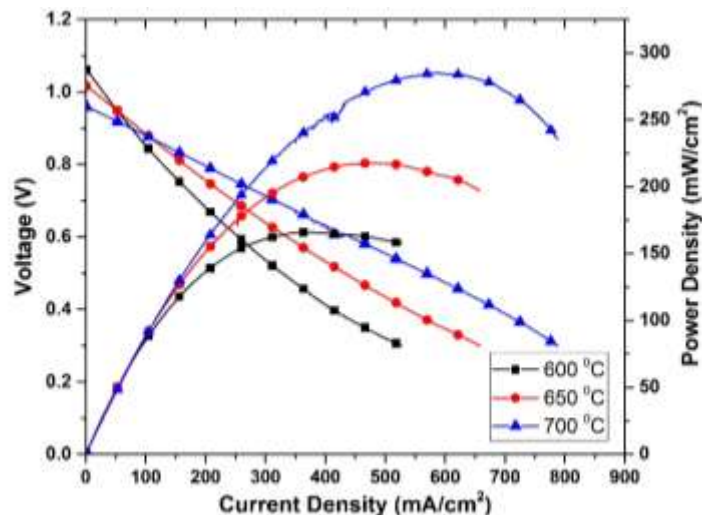


Figure 5-18 Performance of a proton conducting electrolyte tubular SOFC based on Ni-YSZ anode support under humid H<sub>2</sub>

#### 5.4.3. Redox and thermal cycling of the infiltrated electrodes and the suitability of the porous support to accommodate an anode catalyst

Our research group has previously shown that a fuel cell having nickel infiltrated porous YSZ as its anode is highly resistant against redox and thermal cycling. However, it suffers from

a lack of long term stability due to nickel agglomeration. Efforts were made to develop a porous YSZ microstructure which is more stable upon nickel infiltration. This will help to improve cell stability when a nickel based catalyst is also infiltrated into the porous YSZ microstructure. We observed that the pore size of the porous YSZ matrix has an important influence on the growth of nickel particles. Two different microstructures were developed. In the first sample (the reference), 30 vol.% graphite and calcined-milled YSZ were mixed, slip cast as a disk and sintered at 1350°C. Pores of about 1-2 microns due to the presence of calcined YSZ and 5-7 microns due to the presence of the graphite pore former were formed. In the second sample, as received YSZ powder was slip cast at pH 4 and the resulting disk was sintered at 1100°C which led to formation of submicron pores. Both samples showed about 50% open porosity after sintering. When 20 wt% NiO was infiltrated into both samples, very different microstructures were developed. While nickel agglomeration led to larger nickel particles in the reference sample, (Figure 5-19a), a uniform network of connected nickel particles appeared in the second sample having fine pores (Figure 5-19b). Since the nickel particles join each other through the free spacing (open pores) in the microstructure, the narrower pores of the second sample do not provide the required spacing for them to agglomerate. Therefore, a uniform network of fine nickel particles form within the porous YSZ structure. This should significantly improve the cell long term stability and solve a long term problem among the fuel cell community.

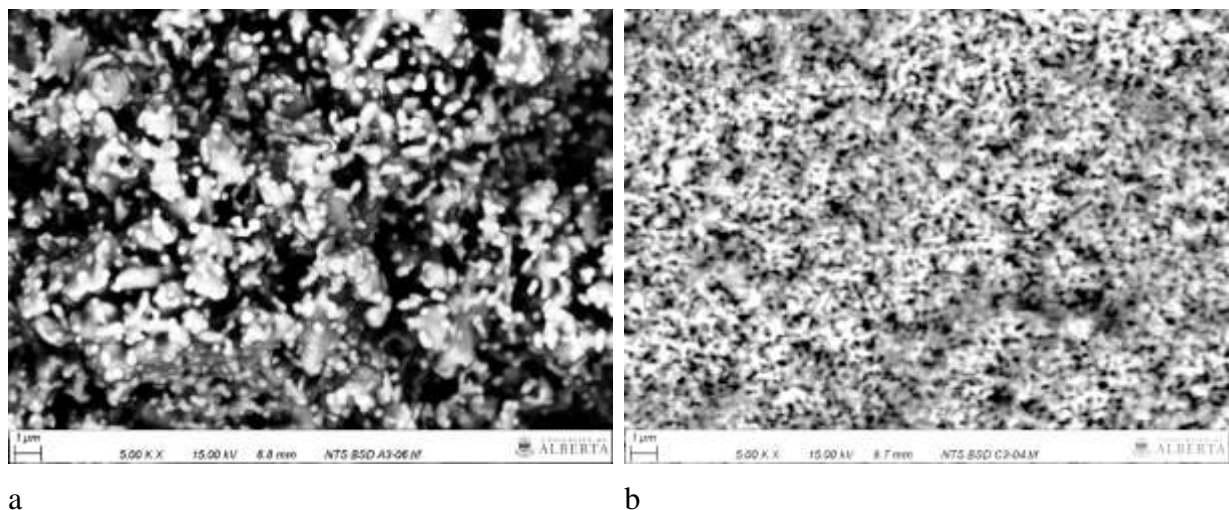


Figure 5-19 . Porous YSZ microstructure infiltrated with 20 wt% NiO. (a) initial slip contained calcined-milled YSZ and graphite, (b) initial slip contained as received YSZ and was cast at pH 4

#### **5.4.4. Impact of structure parameters of the porous support and the concentration and particle size of the infiltrate on the power output**

We have managed to engineer the Ni-YSZ anode microstructure by controlling the particle size of the YSZ for reversible applications under both fuel cell (SOFC) and electrolysis (SOEC) modes. This has led to unique fuel cell performance especially under SOEC mode where the highest ever reported output current densities have been achieved. For this purpose,

two different types of cells were prepared based on a Ni-YSZ/YSZ/Nd<sub>2</sub>NiO<sub>4+δ</sub>-YSZ configuration. For the anode preparation, a suspension was prepared by mixing NiO and YSZ in a ratio of 65:35 wt% (Ni-YSZ 50:50 vol.%) with 30 vol.% graphite as the pore former. As received Tosoh YSZ or its calcined form (heated at 1500°C for 3 h) was used in the anode support as the YSZ source. Electrochemical results showed that optimization of the fuel electrode microstructure is essential for the optimal distribution of gas within the support of the cell, especially under electrolysis operation where the performance for an optimized cell (calcined YSZ) was enhanced by a factor of two (Figure 5-20). In comparison with a standard cell (as received YSZ), at 1.5 V and 800°C the measured current density was -1380 mA/cm<sup>2</sup> and -690 mA/cm<sup>2</sup> for the cells containing calcined and as received YSZ, respectively. The anode supported fuel cells with as received Tosoh YSZ and calcined YSZ in their Ni-YSZ anode support are referred to as “TY” and “CY”, respectively.

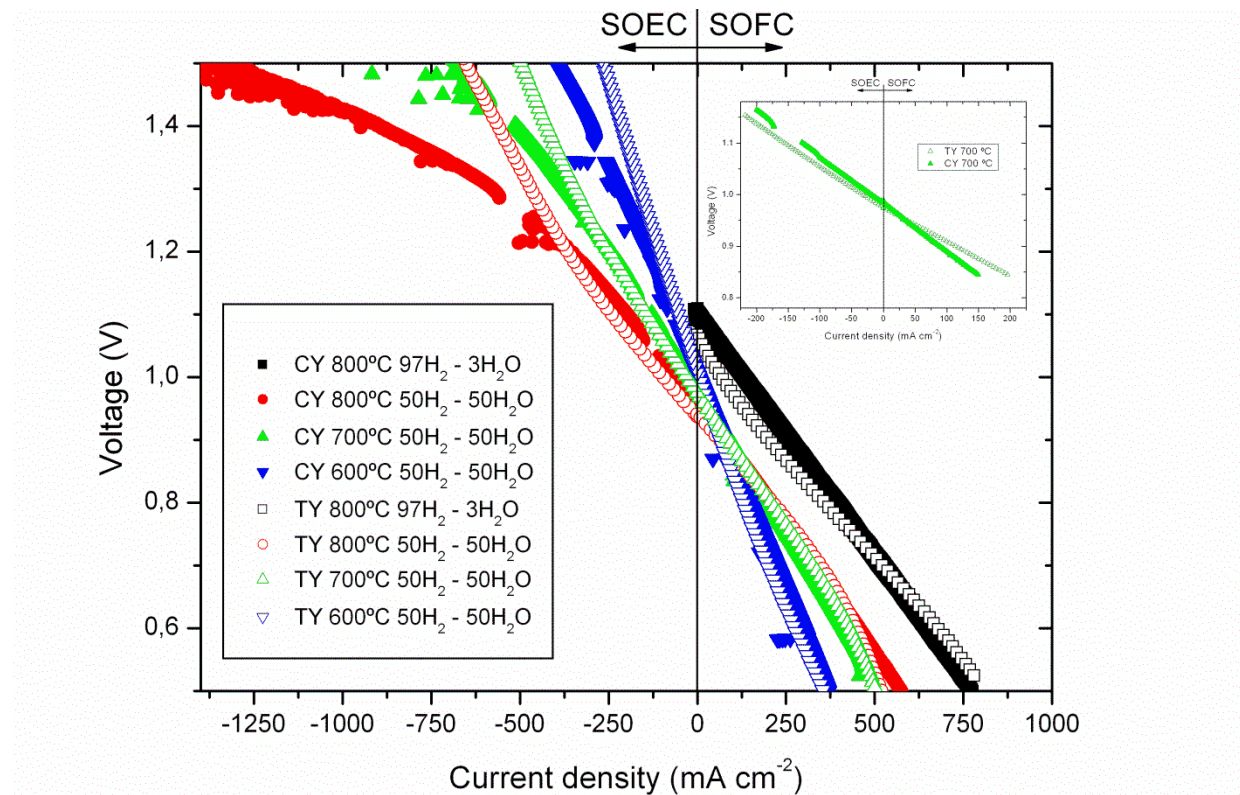


Figure 5-20 Electrochemical galvanodynamic studies in SOFC and SOEC modes for the cell containing as received Tosoh YSZ (TY) and calcined YSZ (CY) in its anode structure. Solid symbols correspond to the CY cell and hollow symbols to the TY cell. Black: measured at 800°C using RT humidified hydrogen as fuel. All the rest were measured using 50% steam – 50% hydrogen as fuel. Red: measured at 800°C; Green: measured at 700°C; Blue: measured at 600°C. The inset corresponds to a magnification for both samples at low current densities (700°C).

Table 5-2 shows the porosity of the TY and CY anodes before and after reduction. Following sintering at 1350°C, both microstructures have a significant amount of closed pores

(see Figure 5-21a and Figure 5-21c). After reduction, the amount of closed porosity in both microstructures decreases and open porosity increases (see Figure 5-21b and Figure 5-21d). The CY anode microstructure remains more porous than the TY anode both before and after reduction. The pores caused by the pore former are larger (5-20  $\mu\text{m}$ ) than the intergranular pores and the porosity caused by NiO reduction ( $\sim 1 \mu\text{m}$ ). These finer pores have more impact on the triple phase boundary length than the large pores formed by graphite. However, larger pores provide excellent channels for gas diffusion into the reaction points. Comparing the high magnification images shown in Figure 5-21e and f reveals that the less porous TY anode contains finer pores. The distribution of the pores (not formed by the graphite pore former) and their average in both anodes presented in Table 5-2 confirms this. This might be the reason for its similar surface area (see Table 5-2) to the CY anode despite the fact that the former anode is less porous.

We have previously shown that following 72 h ball milling of as received Tosoh YSZ, its particle size (250 nm for as received powder and 240 nm following milling) and surface area (13.19  $\text{m}^2/\text{g}$  for as received powder and 12.38  $\text{m}^2/\text{g}$  following milling) remain relatively constant. However, the particle size of 1500°C calcined YSZ (75  $\mu\text{m}$ ) shows a significant decrease following 72 h ball milling (760 nm) and its surface area after calcining (0.03  $\text{m}^2/\text{g}$ ) increases following milling (3.23  $\text{m}^2/\text{g}$ ). Therefore, the milled-calcined YSZ maintains larger particles and a lower surface area compared with the as received powder. The increased particle size of calcined-milled YSZ compared with as received powder is a major reason for the reduced sinterability, higher porosity and larger pores in the anode microstructures containing calcined powder. This is also confirmed by the lower shrinkage rate of this sample following sintering (see Table 5-2).

Table 5-2 Porosity, surface area, pore size and shrinkage of the TY and CY anodes before and after reduction

| Sample              | Open porosity (%) | Closed porosity (%) | Surface area ( $\text{m}^2/\text{g}$ ) | Pore size range ( $\mu\text{m}$ ) | Average pore size ( $\mu\text{m}$ ) | Shrinkage (%) |
|---------------------|-------------------|---------------------|--|-----------------------------------|-------------------------------------|---------------|
| TY before reduction | 8 $\pm$ 1         | 18 $\pm$ 0.5        | -                                      | -                                 | -                                   | 20.3          |
| TY after reduction  | 33 $\pm$ 1        | 3 $\pm$ 0.5         | 0.89                                   | 0.3-1.85                          | 0.86                                | -             |
| CY before reduction | 33 $\pm$ 1        | 11 $\pm$ 0.5        | -                                      | -                                 | -                                   | 15.7          |
| CY after reduction  | 46 $\pm$ 1        | 3 $\pm$ 0.5         | 0.71                                   | 0.3-3                             | 1.25                                | -             |

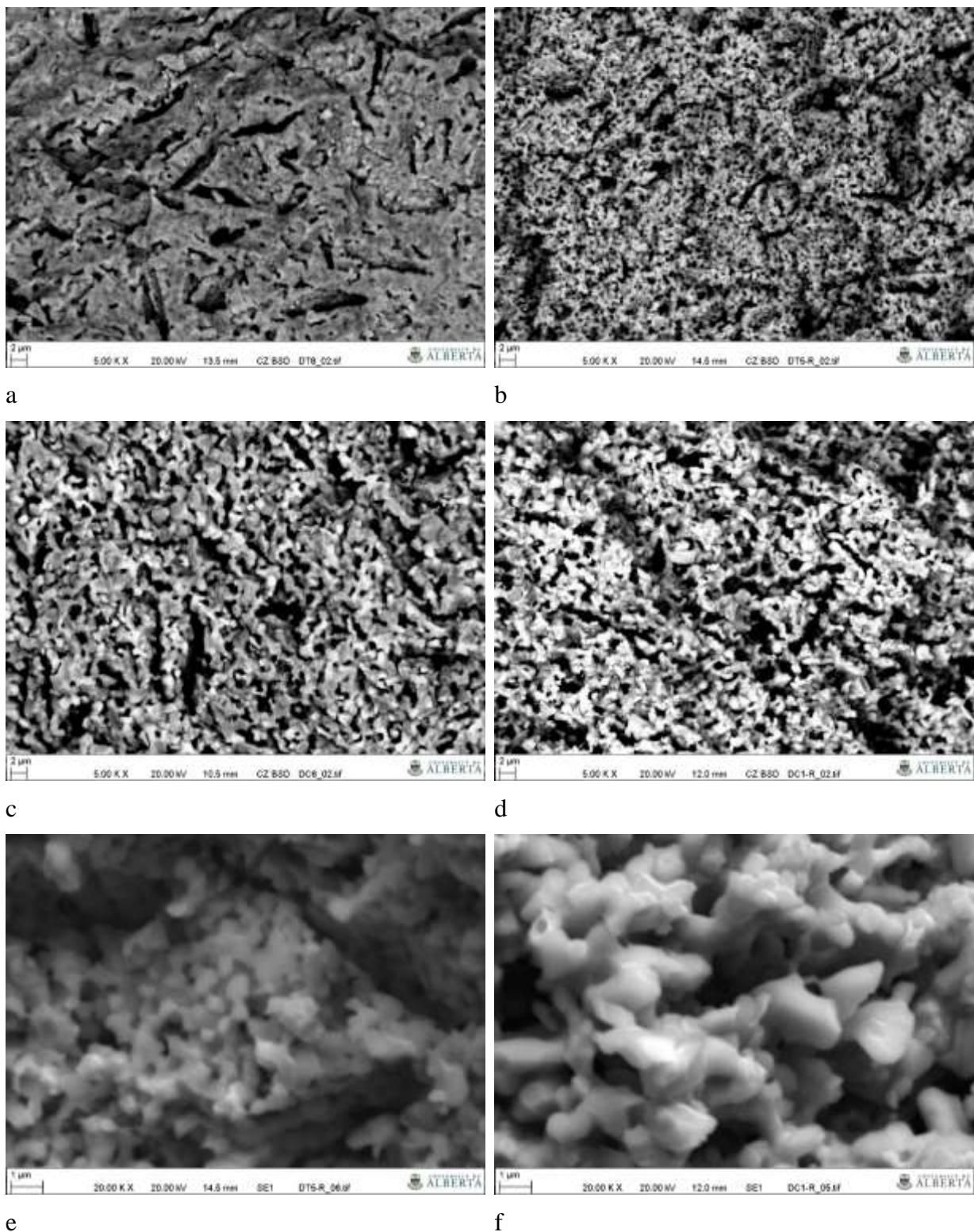


Figure 5-21 SEM image of (a) TY anode before reduction, (b) TY anode after reduction, (c) CY anode before reduction, (d) CY anode after reduction, (e) pores of TY anode, (f) pores of CY anode

#### 5.4.5. Evaluation of infiltrated $\text{Pr}_2\text{NiO}_4$ as a cathode material

The  $\text{Pr}_2\text{NiO}_4$  cathode delivered a very similar power performance to that of the  $\text{Nd}_2\text{NiO}_4$  cathode and we observed only a minor improvement. The cathode was used on tubular cells in a short stack. Cost would undoubtedly dictate which oxide was preferable.

#### 5.4.6. Development of a fuel cell with higher performance in syngas compared to hydrogen

Usually a fully stabilized zirconia (8% yttria doped) and nickel oxide mixture are used for fabrication of the fuel cell support due to their suitable mechanical properties and electrical conductivity. Reactions take place near the triple point boundary where oxygen ions, electrons and fuel meet which is within a 10  $\mu\text{m}$  distance from the electrolyte.

3YSZ (3 mol % yttria doped zirconia) possesses not only excellent mechanical properties but also shows suitable electronic and ionic conductivity. As shown in Figure 5-22, although the performance of a fuel cell fabricated based on Ni-3YSZ under pure hydrogen is less than the Ni-8YSZ cell, under syngas the performance increases more than 30% which is quite interesting. In addition, no degradation was observed over 72 h.

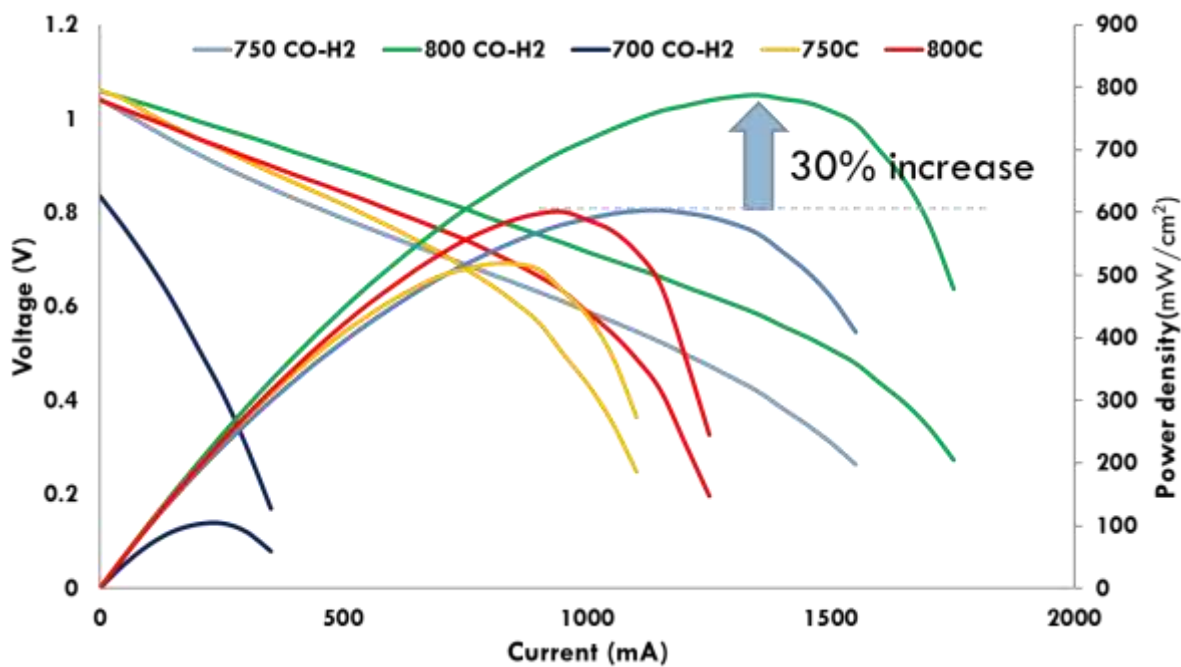


Figure 5-22 Performance of a cell using 3YSZ in the anode under hydrogen and syngas

These results open up new horizons for using fuel cells under hydrocarbons. The SEM cross-section image of this fuel cell appears in Figure 5-23.

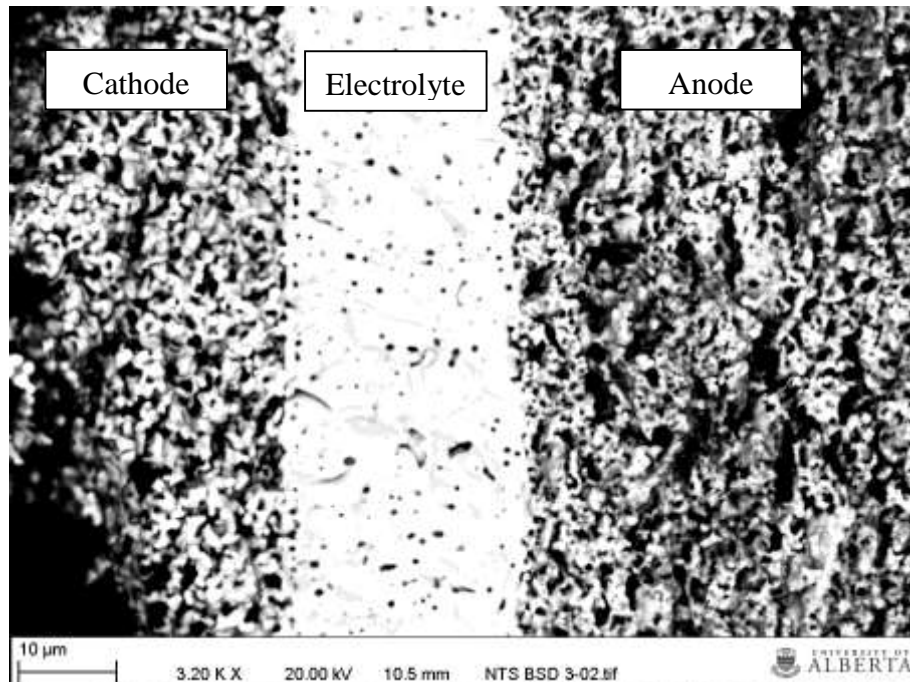


Figure 5-23 Cross-section of cell with 3YSZ in the anode

#### 5.4.7. In-situ dry reforming catalyst

Using the conventional Ni-based cermet anode of a SOFC for in-situ DRM is confronted with great challenges, including coking and sulfur poisoning that will cause catalyst deactivation as well as large thermal gradients causing thermal stress. Ni-based cermet catalysts are well known for promoting severe carbon deposition, which originates mainly from the endothermic methane decomposition and Boudouard reactions. Excessive carbon formation on the anode surface leads to rapid deterioration of the cell performance, eventually resulting in damage to the cells. Another critical issue for in-situ DRM is that the Ni-based anode is insufficiently active for complete conversion of CH<sub>4</sub> and CO<sub>2</sub> after a high temperature fabrication process. Thus, we designed a layered anode by incorporating a catalyst layer onto the anode via a low temperature sintering process.

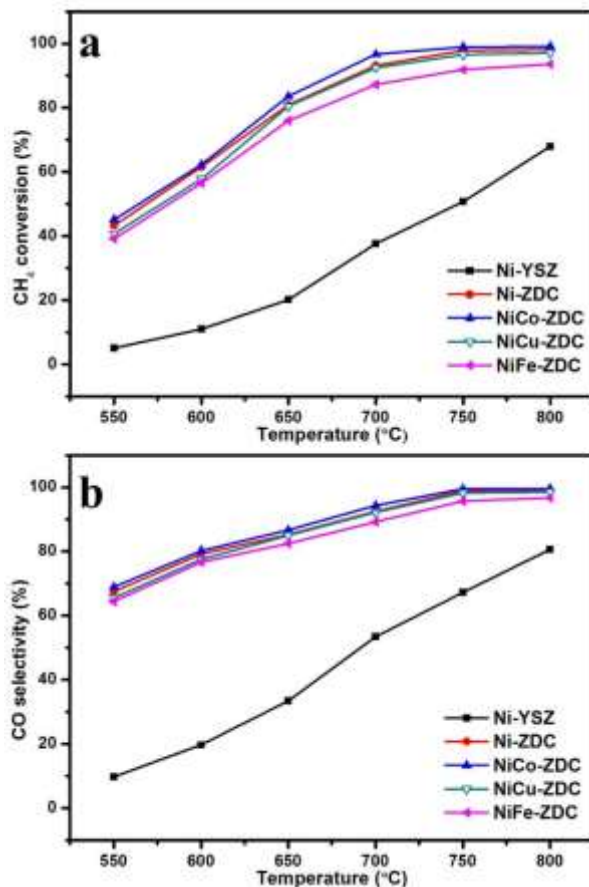


Figure 5-24 CH<sub>4</sub> conversion and CO selectivity for methane dry reforming over Ni-YSZ and NiM-Ce<sub>0.8</sub>Zr<sub>0.2</sub>O<sub>2</sub> catalysts at temperatures from 550°C to 800°C

We investigated a series of Ni and Ni alloy catalysts, i.e., supported NiM (M = none, Co, Cu, Fe) for DRM. The performance of NiM catalysts, in terms of catalytic activity and coke/sulfur resistance, for the DRM reaction was evaluated. State-of-the-art Ni-YSZ electro-catalyst (calcined at 1390°C to simulate the sintered state of an SOFC anode) was also included in this examination. Figure 5-24 compares the CH<sub>4</sub> conversion and CO selectivity when different catalysts were applied in sweet CH<sub>4</sub>-CO<sub>2</sub> from 550 to 800°C. Apparently, CH<sub>4</sub> conversion and syngas yield increase rapidly with an increase of temperature. NiM-Ce<sub>0.8</sub>Zr<sub>0.2</sub>O<sub>2</sub> (ZDC) catalysts showed excellent activities towards DRM, and >90% methane conversion was recorded for all catalyst series at temperature higher than 750°C. Conversely, CH<sub>4</sub> conversion and syngas yield over the Ni-YSZ catalyst were rather poor in the temperature range of interest, most likely as a result of the sintering effect causing agglomeration of Ni particles.

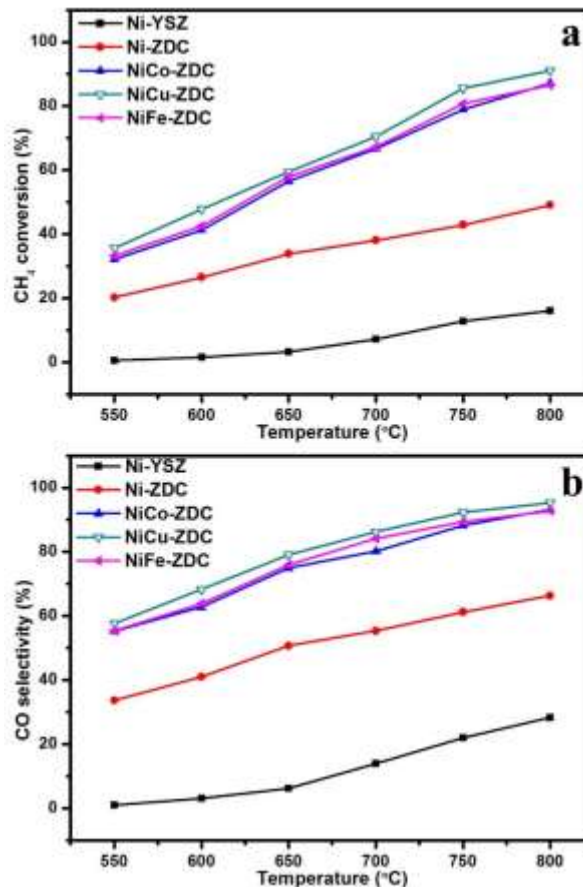


Figure 5-25 CH<sub>4</sub> conversion and CO selectivity for methane dry reforming over Ni-YSZ and NiM-Ce<sub>0.8</sub>Zr<sub>0.2</sub>O<sub>2</sub> catalysts after H<sub>2</sub>S treatment at temperatures ranging from 550°C to 800°C

A sequential sulfur tolerance test was carried out by initially exposing the catalyst to H<sub>2</sub>-500 ppm H<sub>2</sub>S at 850°C for 5 h. Although the H<sub>2</sub>S treatment deactivated all the investigated catalysts for the DRM reaction, Ni alloy-ZDC demonstrated superior sulfur resistance, achieving roughly identical CH<sub>4</sub> conversion and syngas yield in comparison with those obtained in the sulfur-free feeds at temperature above 750°C (Figure 5-25). This advantage was more prominent over Ni-YSZ. At 800°C, the methane conversion on H<sub>2</sub>S treated Ni alloy-ZDC was approximately 4-fold higher than that of Ni-YSZ given the same treatment.

Other than catalytic activity and sulfur tolerance, coke resistance is a pivotal parameter when designing a DRM catalyst because of the strong preference for carbon formation during the DRM reaction. Therefore, we further evaluated the carbon resistance of the catalysts after exposure to pure CH<sub>4</sub> at 800°C for 30 min. The Raman spectra of Ni-YSZ, NiM-ZDC and H<sub>2</sub>S treated catalysts are shown in Figure 5-26.

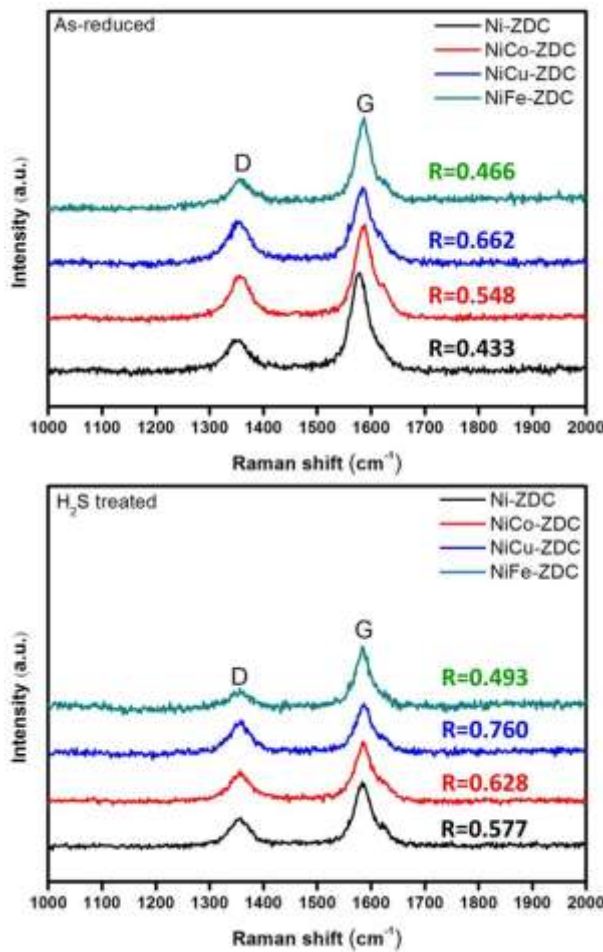


Figure 5-26 Raman spectra of fresh and  $\text{H}_2\text{S}$  treated catalysts after exposing to dry  $\text{CH}_4$  at  $800^\circ\text{C}$  for 30 min

Two intense bands related to the deposited carbon appeared in the spectra, i.e., the D (defect) band associated with the disordered structure of carbon, and the G (graphite) band featuring the graphitic layers and the tangential vibration of carbon atoms. Usually, D-band carbon can be readily removed via using oxidants (e.g.,  $\text{CO}_2$ ,  $\text{H}_2\text{O}$  or  $\text{O}^{2-}$ ). The intensity ratio  $R$  equaling  $I_{\text{D}}/I_{\text{G}}$  has been widely used to characterize the graphitization degree of carbon. A higher value of  $R$  indicates the presence of more active carbonaceous species with a lower degree of graphitization, which is preferred in DRM. NiCu-ZDC catalysts yielded the highest  $R$  value (0.662) compared with other effective bimetallic catalysts for DRM. This was ascribed to the surface dilution effects of nickel by copper atoms that were basically inert to carbon-carbon bond formation. Due to sulfur poisoning effects, the graphitization degree of the deposited carbon on the NiCu-ZDC catalysts further decreased after being treated in the  $\text{H}_2\text{S}$  atmosphere, which was also observed in other NiM-ZDC catalysts. Once again, NiCu-ZDC exhibited the highest  $R$  value (0.760).

Hence, after screening a series of DRM catalysts, we concluded that the conventional

Ni-YSZ electro-catalyst was not appropriate for in-situ dry reforming of methane due to its low activity and poor sulfur resistance. Alternatively, NiM-ZDC bimetallics exhibited greatly improved catalytic performance.

#### 5.4.8. Co-generating syngas-electricity from CO<sub>2</sub>-CH<sub>4</sub> in an H-SOFC

The adopted H-SOFC is based on the BZCYYb electrolyte. The prepared H-SOFC, i.e., Ni-BZCYYb/BZCYYb/NBCaC(NdBa<sub>0.75</sub>Ca<sub>0.25</sub>Co<sub>2</sub>O<sub>5+δ</sub>)-BZCYYb demonstrated superior performance in a H<sub>2</sub> feed stream, reaching 1,480 mW cm<sup>-2</sup> maximum power density at 700°C whereas the polarization resistance ( $R_p$ ) was as low as 0.031 Ω cm<sup>2</sup>. By using this state-of-the-art H-SOFC, we then evaluated its feasibility for the internal dry reforming involving CO<sub>2</sub> and CH<sub>4</sub>. In a control group, fuel cell performance in Ar diluted H<sub>2</sub> provides a benchmark to examine the possible negative influences of non-H<sub>2</sub> fuels (i.e., CO and CH<sub>4</sub>) over H<sub>2</sub> electrochemical oxidation.

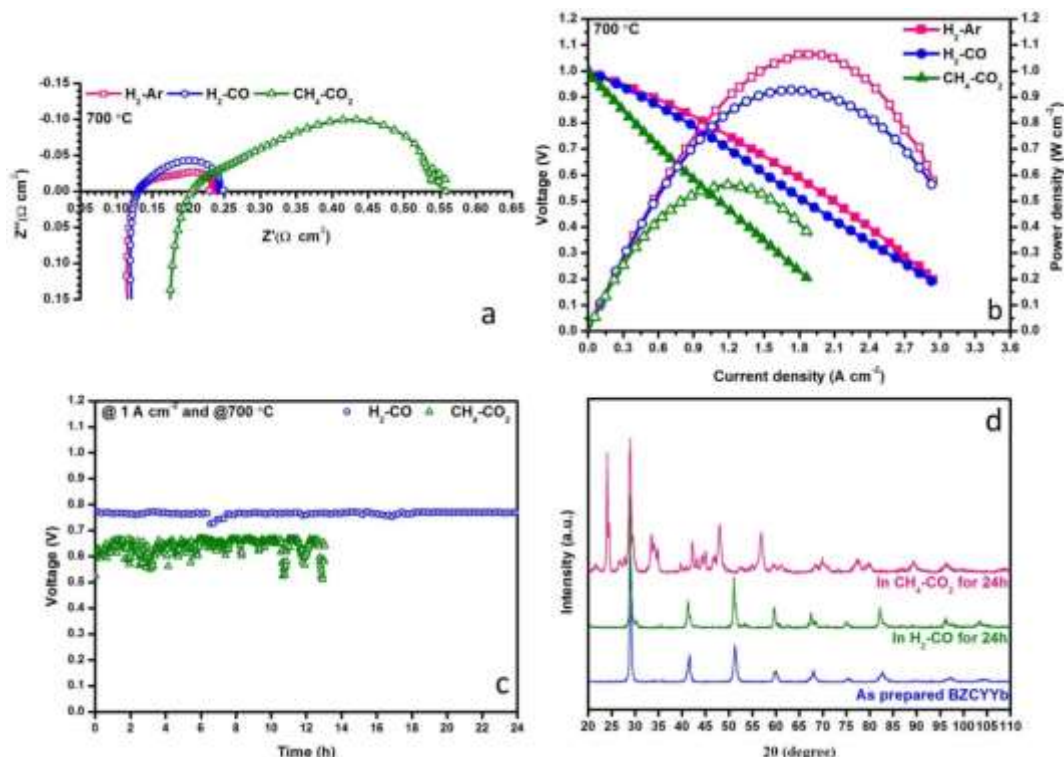


Figure 5-27 Electrochemical performance of conventional H-SOFC in various fuels at 700°C. (a) impedance spectra, (b) I-V and I-P curves, (c) galvanostatic test at a constant current of 1 A cm<sup>-2</sup>; (d) XRD patterns of BZCYYb powder after 24 h exposure to either H<sub>2</sub>-CO or CH<sub>4</sub>-CO<sub>2</sub> at 700°C

Figure 5-27a and Figure 5-27b show the electrochemical impedance spectra (EIS) and I-V(P) curves measured in H<sub>2</sub>-Ar, H<sub>2</sub>-CO and CH<sub>4</sub>-CO<sub>2</sub> at 700°C. The molar ratios of all mixed gases were fixed at 1:1. Remarkably, the  $R_p$  values of the cell in H<sub>2</sub>-Ar and H<sub>2</sub>-CO were essentially identical, 0.106 and 0.112 Ω cm<sup>2</sup>, respectively, implying that CO did not affect the

electrochemical activation and conversion of H<sub>2</sub> under this experimental condition. This, in turn, confirms the potential of using H-SOFC in a syngas feed stream. Surprisingly, when CH<sub>4</sub>-CO<sub>2</sub> was used as the fuel, which was supposed to yield syngas with an H<sub>2</sub>-CO ratio close to unity, the polarization resistance of the cell increased substantially to 0.347 Ω cm<sup>2</sup> whereas the ohmic resistance (R<sub>O</sub>) also grew to 0.201 Ω cm<sup>2</sup>. Apparently, these results imply that both the physical and the chemical properties of the TPB have been altered drastically during the internal dry reforming. Consequently, the maximum power density dropped to 562 mW cm<sup>-2</sup> and the cell suffered from degradation during a 12 h galvanostatic operation at 1 A cm<sup>-2</sup>.

Our conjecture was proven correct based on the impurities that appeared in the XRD patterns in Figure 5-27d. In particular, BZCYYb has reacted with CO<sub>2</sub> after exposure in CH<sub>4</sub>-CO<sub>2</sub> at 700°C for 24 h forming BaCO<sub>3</sub>. Accordingly, we now conclude that the electrochemical performance decrease in CH<sub>4</sub>-CO<sub>2</sub> was ascribed solely to the decomposition of BZCYYb rather than coke formation. Nevertheless, it is still encouraging to find that the BZCYYb based SOFC showed excellent stability in syngas (see Figure 5-27c), demonstrating the potential of fueling H-SOFC with dry reforming derived syngas.

Intuitively, one would imagine that in an H-SOFC, if the majority of CO<sub>2</sub> is converted via methane reforming, the integrity of the BZCYYb electrolyte can be sustained since there is no direct contact between them. Figure 5-28 is a schematic illustration of the novel layered H-SOFC. In this design, an additional reforming layer was incorporated onto the surface of the anode support. The CH<sub>4</sub>-CO<sub>2</sub> feed stream is fully reformed on the high performance NiCo-LDC (Ni<sub>0.8</sub>Co<sub>0.2</sub>-La<sub>0.2</sub>Ce<sub>0.8</sub>O<sub>2-δ</sub>) catalyst layer, yielding syngas, before entering the Ni-BZCYYb functional anode. The sequential selective oxidation of H<sub>2</sub> at TPBs not only generates electrical power and CO-enriched syngas, but also provides enough heat completely compensating that required for the internal dry reforming. Based on the thermodynamic data shown below, we found that the thermal independency can be acquired when H<sub>2</sub> utilization is higher than 52% (corresponding to the total fuel utilization of 26%). This can significantly counterbalance the energy input for conventional methane reforming. Following this design, we fabricated the layered H-SOFC.



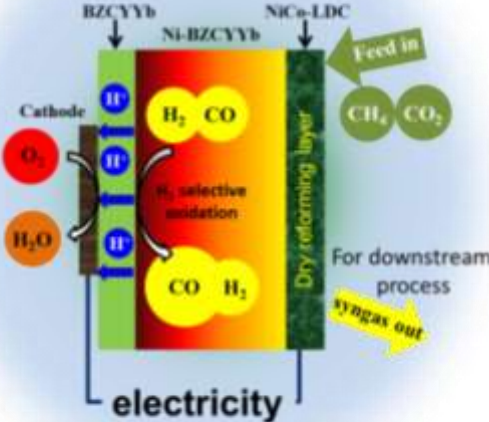


Figure 5-28 Schematic showing the configuration of the novel layered H-SOFC

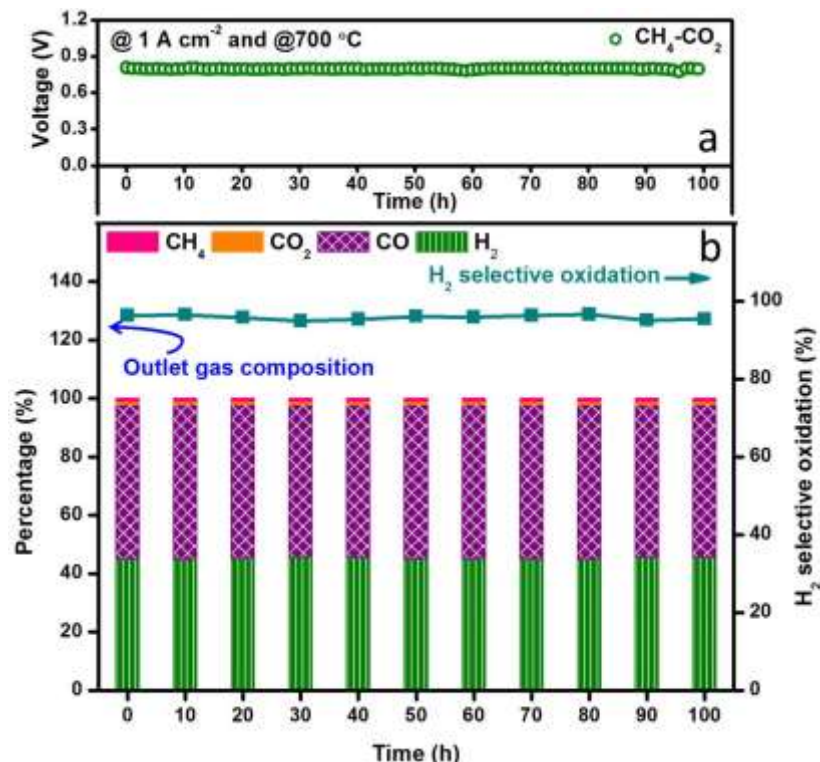


Figure 5-29 Stability test of in situ dry reforming in layered H-SOFC fueled with CH<sub>4</sub>-CO<sub>2</sub> at 700°C. (a) galvanostatic test under a constant load of 1 A cm<sup>-2</sup>, (b) exhaust gas composition

We finally examined the electrochemical stability of the layered H-SOFC for cogeneration of power and chemicals. Figure 5-29 displays the long-term performance of the cell under a constant current density load of 1 A cm<sup>-2</sup>. The voltage stabilized at ~0.8 V showing

negligible degradation and the power density was as high as  $800 \text{ mW cm}^{-2}$ . In the meantime, the gas composition of the anode effluent was examined every 10 h using GC. The  $\text{H}_2$  selectivity stabilized at around 95%, implying that the layered cell was fully capable of accomplishing internal dry reforming in the anode chamber (note that BZCYYb shows some oxygen-ion conductivity at  $700^\circ\text{C}$ ).

### 5.4.9. Co-generating syngas-electricity from $\text{CO}_2\text{-CH}_4$ in an O-SOFC

#### 5.4.9.1 Ni-S selective catalyst

In this design, an additional coke/sulfur resistant catalyst layer was incorporated onto the surface of the anode support layer to carry out the DRM process (Figure 5-30). Prior to entering the Ni-YSZ anode, the sour  $\text{CH}_4\text{-CO}_2$  feed stream is effectively reformed, yielding syngas with residue of reactants. Sequentially, the acquired syngas reaches the TPBs where  $\text{H}_2$  is preferentially oxidized without forming  $\text{CO}_2$  gas, as a result of the sulfur-nickel synergistic effect. This process generates electrical power from  $\text{CO}_2$  and, moreover, no  $\text{CO}_2$  can be readily produced from  $\text{CO}$  in an electrochemical reaction. The conventional DRM process is inevitably accompanied by catalyst deactivation caused by carbon formation that is thermodynamically favored. In an O-SOFC, however, the  $\text{H}_2\text{O}$  generated from the  $\text{H}_2$  electrochemical reaction suppresses carbon deposition. Moreover, the heat released during the energy conversion process can be used to partially compensate that required for DRM.

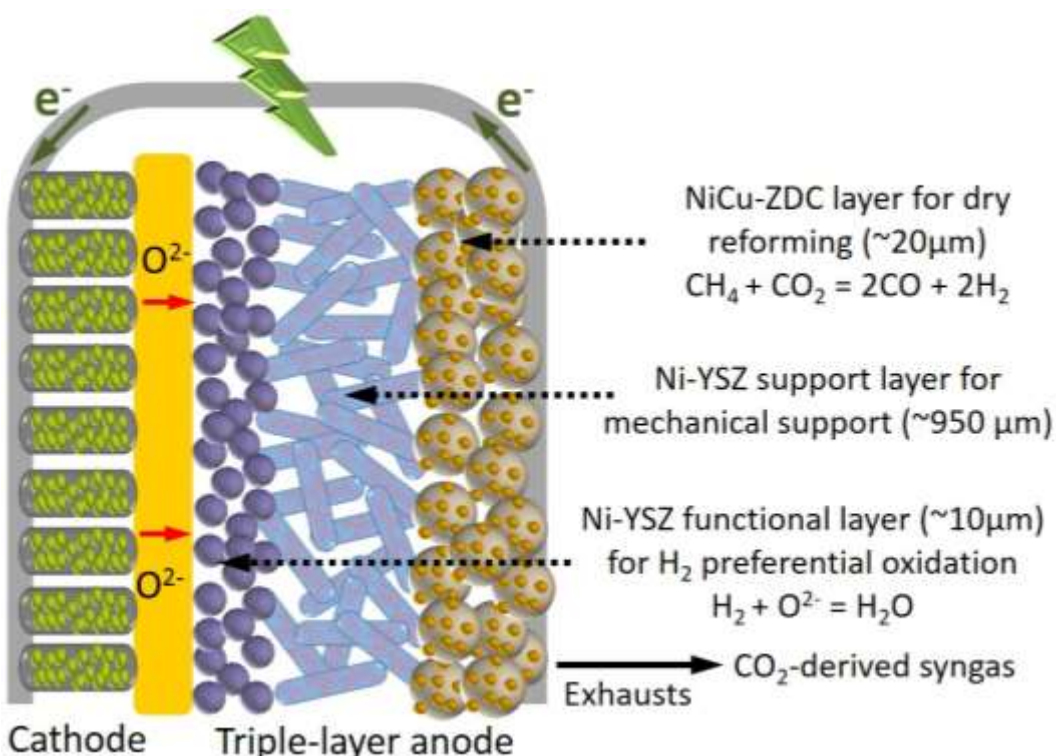


Figure 5-30 Schematically illustrating the CO<sub>2</sub> conversion process in a O-SOFC

Prior to electrochemical evaluation, the single cells were reduced in a H<sub>2</sub> atmosphere at 800°C for 2 h. Figure 5-31 shows the voltage and power density as a function of current density for a conventional SOFC (C-SOFC) and triple-layer anode SOFC (TA-SOFC) in various fuels at 800°C. The peak power densities (PPDs) of C-SOFC in H<sub>2</sub>, CO, CO-H<sub>2</sub> and CH<sub>4</sub>-CO<sub>2</sub> were 1.41, 1.06, 1.26 and 1.12 W cm<sup>-2</sup>, while the corresponding PPD values for TA-SOFC were 1.44, 1.07, 1.28 and 1.26 W cm<sup>-2</sup> for the same conditions. TA-SOFC exhibited identical performance in H<sub>2</sub>, CO and CO-H<sub>2</sub> to C-SOFC as the additional layer alters neither the inner morphological structure of the electrolyte-electrode-gas TPB nor the nature of these fuels. According to the previous catalyst evaluation, the conversion of CH<sub>4</sub> and CO<sub>2</sub> over a Ni-YSZ catalyst is not high enough, which eventually leads a lower PPD of C-SOFC in CH<sub>4</sub>-CO<sub>2</sub> than that in CO-H<sub>2</sub>. Conversely, the PPD in CH<sub>4</sub>-CO<sub>2</sub> was improved by adding a NiCu-Ce<sub>0.8</sub>Zr<sub>0.2</sub>O<sub>2</sub> on-cell reforming layer, implying a high conversion of CH<sub>4</sub> and CO<sub>2</sub> is achieved over the NiCu-Ce<sub>0.8</sub>Zr<sub>0.2</sub>O<sub>2</sub> catalyst, which is supported by the results of the catalytic evaluation.

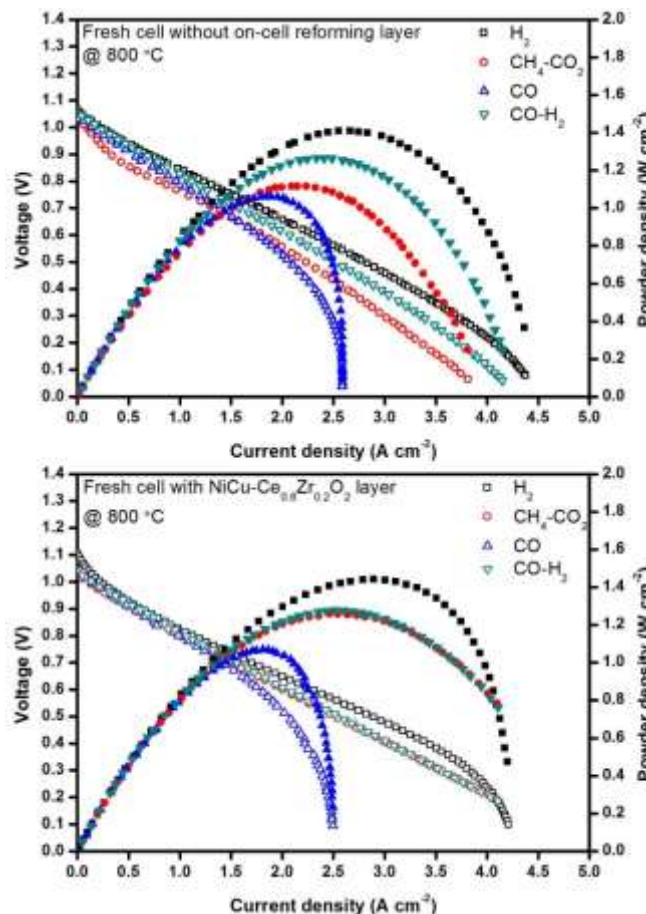


Figure 5-31 I-V and I-P curves of C-SOFC and TA-SOFC in various fuels at temperatures between 650°C and 800°C

Comparing the electrochemical performance of fresh SOFCs in H<sub>2</sub> and CO, it is obviously seen that a fresh Ni-YSZ anode is not feasible to achieve H<sub>2</sub> selective oxidation because of its high catalytic activity for the CO electrochemical oxidation reaction. To attain the objective of H<sub>2</sub> selective oxidation, the reduced C-SOFC and TA-SOFC were polarized in H<sub>2</sub>-500 ppm H<sub>2</sub>S

at 850°C and at 0.8 V prior to the electrochemical evaluation to form a Ni+S-YSZ anode in the inner TPB area. Thermodynamic calculation confirmed metallic Ni is the stable phase under the experimental conditions, which is in compliance with our XPS data of an H<sub>2</sub>S-treated anode indicating no nickel sulfide had formed. The performance of sulfured C-SOFC and TA-SOFC in the fuels of interest is shown in Figure 5-32. The PPDs of sulfured C-SOFC in H<sub>2</sub> and CO-H<sub>2</sub> were 1.03 and 0.88 W cm<sup>-2</sup>, which are respectively 27% and 30% lower than those before sulfur treatment. As for the performance of sulfured C-SOFC in CO and CH<sub>4</sub>-CO<sub>2</sub>, the PPDs were dramatically decreased to 0.30 and 0.29 W cm<sup>-2</sup>, resulting from the formation of Ni-S catalyst suppressing its adsorption ability for CO as well as the catalytic activity for methane dry reforming. Regarding the sulfured TA-SOFC, it showed similar performance in H<sub>2</sub>, CO and CO-H<sub>2</sub> to sulfured C-SOFC with the PPD in these fuels achieving at 1.06, 0.28 and 0.94 W cm<sup>-2</sup>, respectively. As evidenced in the catalytic evaluation, the NiCu-Ce<sub>0.8</sub>Zr<sub>0.2</sub>O<sub>2</sub> on-cell reforming layer is quite tolerant to H<sub>2</sub>S. Therefore, sulfured TA-SOFC showed a much better performance in CH<sub>4</sub>-CO<sub>2</sub> compared to sulfured C-SOFC.

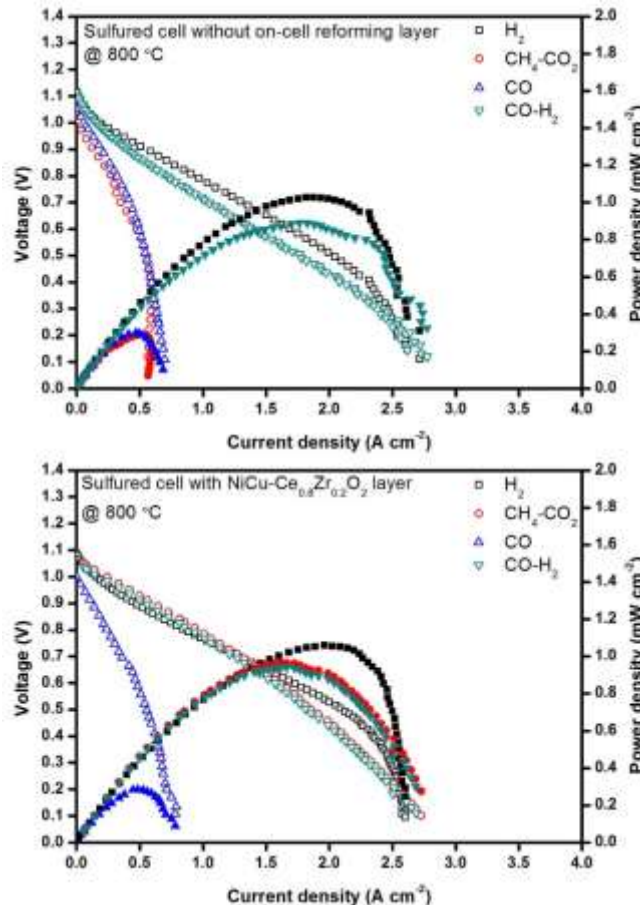


Figure 5-32 I-V and I-P curves of sulfured C-SOFC and TA-SOFC in various fuels at temperatures between 650°C and 800°C

It is obviously seen from Figure 5-33 that CH<sub>4</sub> and CO<sub>2</sub> are almost completely converted into CO and H<sub>2</sub>, showing the DRM reaction is stable over the NiCu-Ce<sub>0.8</sub>Zr<sub>0.2</sub>O<sub>2</sub> on-cell reforming layer in the actual fuel cell. Moreover, in accordance with the previous analysis, at

the given current density ( $1.5 \text{ A cm}^{-2}$ ) almost all the  $\text{O}^{2-}$  participated in the  $\text{H}_2$  oxidation process due to the presence of the Ni+S electro-catalyst, confirmed by the GC analysis of the outlet gas. These results demonstrate a steady DRM reaction and CO separation process are achieved during the 50 h test, implying the combination of the on-cell reforming layer and Ni+S electro-catalyst shows long term stability for CO production from a  $\text{CH}_4$  and  $\text{CO}_2$  mixture.

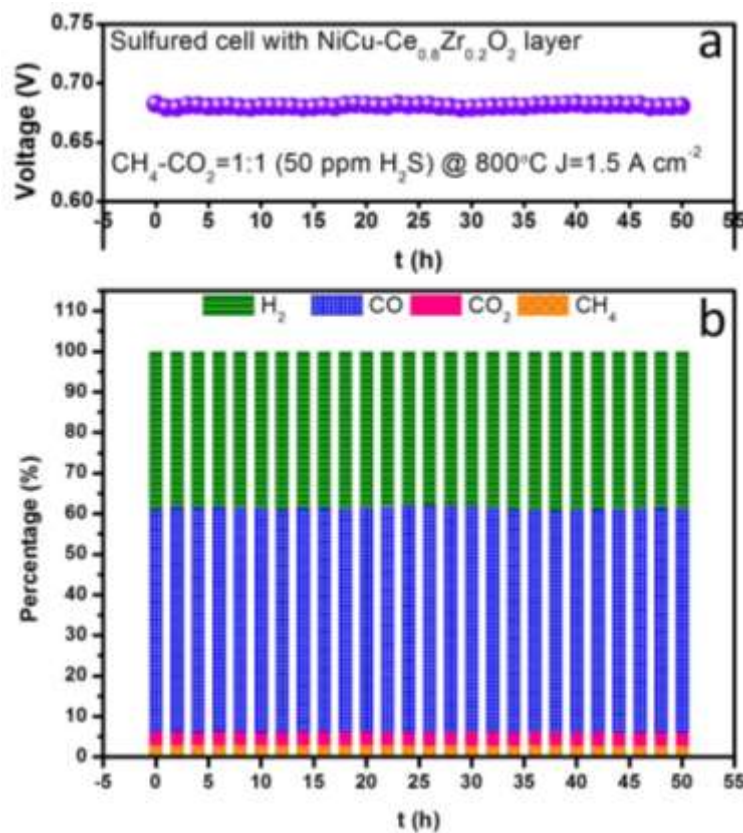


Figure 5-33 (a) Time dependent voltage of TA-SOFC in  $\text{CH}_4\text{-CO}_2$  atmosphere at  $800^\circ\text{C}$  and at  $1.5 \text{ A cm}^{-2}$  and (b) the corresponding time dependent exhaust gas composition

#### 5.4.9.2 Ni-Sn alloy catalyst

In this work, a novel on-cell micro reformer, *i.e.*, the noble-metal free  $\text{NiSn}/\text{Al}_2\text{O}_3$  catalyst embedded Ni foam was designed for efficient internal reforming of biogas. The micro reformer introduces an efficient internal reforming process, which is attractive in terms of the system simplification, significant cost reduction, higher energy efficiency and faster load response. Additionally, the  $\text{NiSn}$  bimetallic alloys have been developed and characterized as potential anode materials and biogas reforming catalysts to enhance both the carbon deposition resistance and sulfur tolerance, and simultaneously achieve excellent chemical and electrochemical performance.

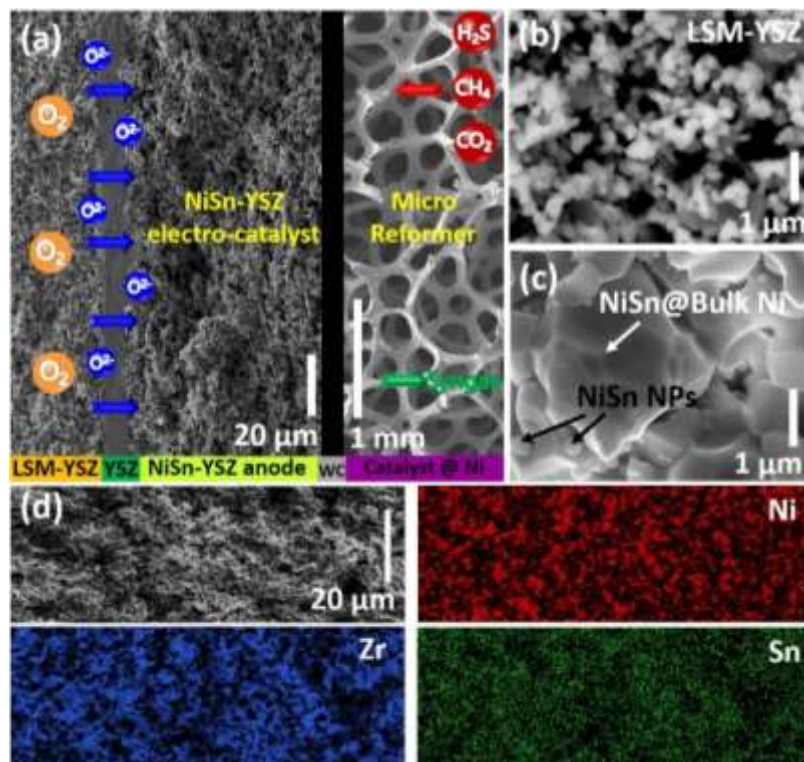


Figure 5-34 (a) SOFC for biogas conversion, (b) microstructure of the prepared LSM-YSZ composite cathode, (c) microstructure of the NiSn-YSZ anode, (d) EDX mappings showing the element distribution in the anode

Single cells were using a NiSn bimetallic alloy as the anode and reforming catalyst to acquire high fuel utilization, high power density and good coke/sulfur tolerance in biogas. Figure 5-34a shows a cross-sectional SEM image of an anode-supported single cell and the Ni foam. Typically, the single cell was composed of multiple layers, an oxygen conductive and fairly dense YSZ electrolyte (~10 μm) layer was sandwiched between the two porous layers of LSM-YSZ (~30 μm) cathode and Ni-YSZ (~1 mm) anode. The LSM-YSZ cathode was fabricated by a conventional mechanical mixture method to achieve uniform distribution of solid phases and adequate porosity for oxygen transport (Figure 5-34b). Compared to the conventional Ni-YSZ anode, one main change in the NiSn-YSZ anode was the presence of spherical NiSn NPs ranging from 100 to 500 nm on the YSZ electrolyte (Figure 5-34c); these NPs had a richer Sn content than the large bulk of Ni. The infiltrated NiSn NPs, dispersed on the inert YSZ support, dramatically extended the active areas of the anode. In the conventional anode, the electro-oxidation processes are mainly restricted within the gas, YSZ and Ni TPBs. Moreover, research has shown that the carbon deposition resistance of the bulk Ni particles can be effectively improved by adding tin, which remained preferentially on the surface of the NiSn alloy. To further check the distribution of Sn, we performed EDX mapping in the anode regions. Figure 5-34d shows that Sn was uniformly distributed in the anode.

Figure 5-35a to Figure 5-35d present the initial chemical and electrochemical performance of the novel reactor for biogas conversion. Dry reforming is an endothermic

reaction and, for that reason, CO<sub>2</sub> and CH<sub>4</sub> conversions improve as the temperature increases under all conditions. At open circuit condition (no current was applied) and fed with CH<sub>4</sub>-CO<sub>2</sub>, an as-reduced reactor (only Ni foam was treated in H<sub>2</sub>S) gave the highest conversion of CH<sub>4</sub> and the highest selectivity of CO, which are high enough for practical applications. For example, at 800 and 850°C, the conversion of CH<sub>4</sub> reached up to 96.5 and 97.5 %, respectively. After pre-contaminating in H<sub>2</sub>-500 ppm H<sub>2</sub>S, this reactor still offered excellent activity for catalyzing the IRB reaction: 97.5 % CH<sub>4</sub> could be eventually converted at 850°C in a CH<sub>4</sub>-CO<sub>2</sub> feed stream. This good performance should be attributed to the outstanding sulfur tolerance of the NiSn bimetallic. In a 200 ppm H<sub>2</sub>S-containing CH<sub>4</sub>-CO<sub>2</sub>, the conversion of CH<sub>4</sub> over a pre-contaminated reactor was still as high as 95.6%. These results clearly demonstrate that the designed reactor is a promising technology for practical utilization, since H<sub>2</sub>S is an inevitable component of the raw gas. Moreover, because of the anti-correlation between the reaction energy barrier and temperature, both the IRB and electrochemical reactions need to take place at the high temperatures (e.g., 800 and 850°C) in order to get reasonable values of biogas conversions and syngas yields.

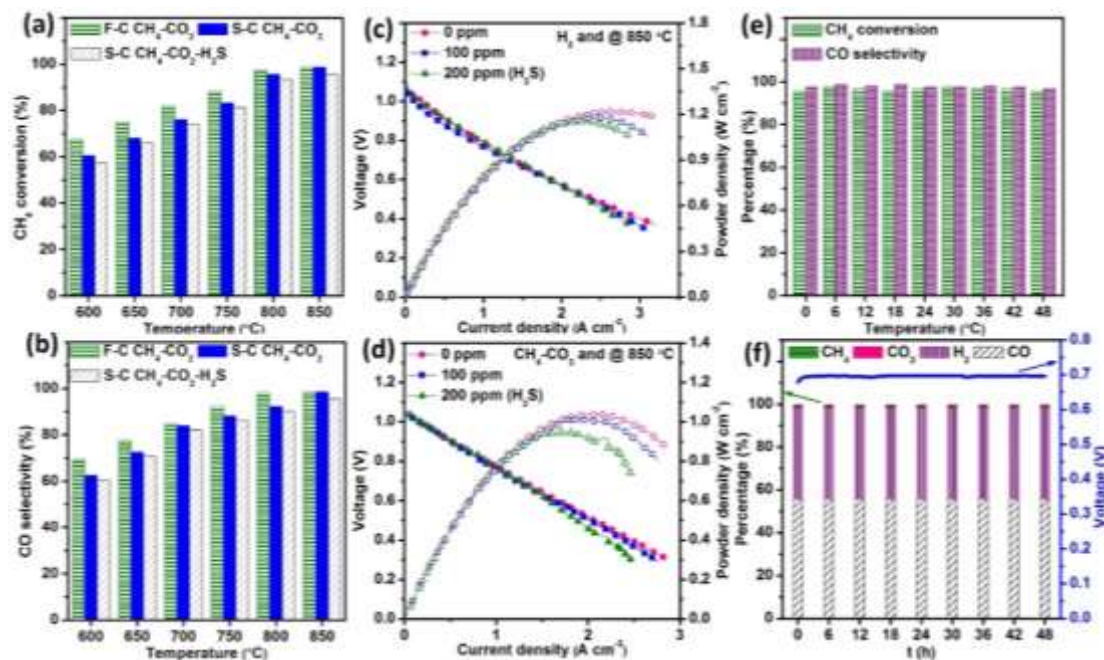


Figure 5-35 (a) CH<sub>4</sub> conversion and (b) CO selectivity during CH<sub>4</sub>-CO<sub>2</sub> (0 or 200 ppm H<sub>2</sub>S) dry reforming of biogas under various conditions [fresh cell (F-C) and the cell pre-treated in H<sub>2</sub>-500 ppm H<sub>2</sub>S (S-C)], (c) I-V and I-P curves of the cell in H<sub>2</sub> (0~200 ppm H<sub>2</sub>S), (d) I-V and I-P curves of the cell in CH<sub>4</sub>-CO<sub>2</sub> (0~200 ppm H<sub>2</sub>S), (e) CH<sub>4</sub> conversion and CO selectivity during dry reforming of biogas at open circuit condition, (f) voltage and outlet gas composition during dry reforming of biogas under 1.25 A cm<sup>-2</sup>. The feeding stream during the long term test is equal amounts of CH<sub>4</sub> and CO<sub>2</sub> balanced with 200 ppm H<sub>2</sub>S for a total flow rate of 20 mL min<sup>-1</sup>

Therefore, we conducted the initial electrochemical tests at 850°C to obtain high power output and biogas conversion. Figure 5-35c and Figure 5-35d are the profiles of voltage/power density versus current for the reactor in different test conditions. To independently evaluate the effect of sulfur contamination on the electrochemical performance, H<sub>2</sub>S-containing H<sub>2</sub> was used as the feed gas. It can be seen that the reactor could deliver a peak power density (PPD) of 1.22 W cm<sup>-2</sup> in pure H<sub>2</sub>, which is comparable to the best SOFCs reported so far. Moreover, our reactor can continue to provide high PPDs in 100 ppm (1.17 W cm<sup>-2</sup>) and 200 ppm (1.15 W cm<sup>-2</sup>) H<sub>2</sub>S. Notably, a PPD as high as 0.946 W cm<sup>-2</sup> was achieved in a 200 ppm H<sub>2</sub>S-containing CH<sub>4</sub>-CO<sub>2</sub>, demonstrating the simultaneously excellent activity and sulfur tolerance that has been rarely reported. Generally, most SOFCs described in the literature exhibited greatly inferior performances in H<sub>2</sub>S-containing fuels, especially when the H<sub>2</sub>S concentration reached several hundred ppm. In fact, it has been a big challenge to find practical solution(s) for solving the H<sub>2</sub>S contamination issue and simultaneously offer good electrochemical performance in the SOFCs.

Figure 5-35e and Figure 5-35f show the results from a 48 h test of the reactor operating in CH<sub>4</sub>-CO<sub>2</sub>-200 ppm H<sub>2</sub>S under 1.25 A cm<sup>-2</sup>. The CH<sub>4</sub> conversion and CO selectivity continuously were maintained at around 95%. The output voltage (0.69 V) and exhaust gas composition did not apparently change with runtime, indicating that the reactor is quite stable and has no significant performance deterioration. The excellent stability of the reactor allows its operation in the biogas atmosphere and is very crucial for its practical implementation in industry.

#### 5.4.10. Performance of a small stack using CH<sub>4</sub>-CO<sub>2</sub>

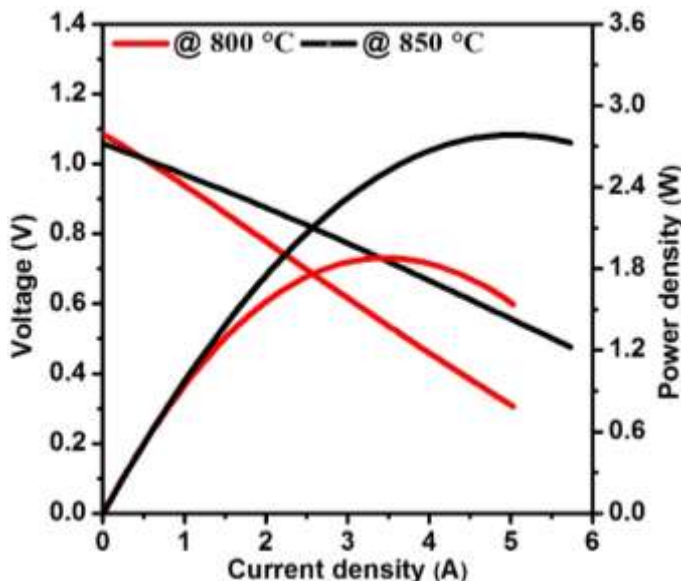


Figure 5-36 The voltage-current/power curves of a stack based on three cells

Finally, we tested an SOFC stack consisting of three single cells based on a NiSn-YSZ anode, LSM-YSZ cathode and YSZ electrolyte. Figure 5-36 shows the I-V (P) of this SOFC stack. For a stack based on three single cells, we can obtain a PPD of 2.8 W at 850°C in CH<sub>4</sub>-CO<sub>2</sub>. We also evaluated the exhaust gas composition. At open circuit, the exhaust gas composition is 10% CO<sub>2</sub>, 11% CH<sub>4</sub>, 40% H<sub>2</sub> and 39% CO. The CO<sub>2</sub> concentration in the exhaust decreased dramatically.

## 5.5. Summary and project outcomes

### 5.5.1. Summary of catalytic work

The present work firstly discussed the feasibility of converting CO<sub>2</sub> to CO by reforming with CH<sub>4</sub> and selectively electro-oxidizing H<sub>2</sub> in an H-SOFC configured as Ni-BZCYYb/BZCYYb/NBCaC-BZCYYb, in which the anode was coated with a novel NiCo-LDC internal reforming layer to facilitate the reforming process. According to the results obtained, the following conclusions can be made. We found that (1) the as-prepared cell exhibited excellent performance and stability in H<sub>2</sub>, suggesting satisfactory electrochemical stability of the cell. However, the state-of-the-art H-SOFC was incapable of completing internal dry reforming due to the reaction of BZCYYb with CO<sub>2</sub> in a CH<sub>4</sub>-CO<sub>2</sub> atmosphere; (2) the multiple-twinned Ni<sub>0.8</sub>Co<sub>0.2</sub> bimetallic nanoparticles showed superior activity towards *in situ* dry reforming. In comparison to the conventional design, the layered SOFC demonstrated drastically improved reforming efficiency with CO<sub>2</sub> conversion up to 91.5 % at 700°C, and up to 100 h galvanostatic stability in a CH<sub>4</sub>-CO<sub>2</sub> feed stream at 1 A cm<sup>-2</sup>. More importantly, by coating the anode with a NiCo-LDC layer, the potential reaction between BZCYYb and CO<sub>2</sub> is inhibited; (3) in the layered SOFC, CO<sub>2</sub> was fully converted to CO and H<sub>2</sub> was effectively and exclusively oxidized to H<sup>+</sup> during electrochemical reactions, yielding no CO<sub>2</sub> but only valuable syngas in the anode effluent.

Furthermore, we have demonstrated this process is also feasible in a novel O-SOFC with sandwiched-architecture consisting of a triple-layer anode. The novel process and the tailored structure-architecture enabled us to co-produce the CO<sub>2</sub>-derived syngas and energy in an efficient and coke/sulfur resistant way. The conventional O-SOFC only shows the potential of a simultaneous DRM process to coproduce syngas. The insufficient reforming efficiency of this one-pot chemical/electrochemical reaction in a conventional Ni-YSZ anode, as we have well displayed, is the major obstacle for the practical implementation of this scientifically and industrially significant process. Besides, the Ni-YSZ catalyst also demonstrated a strong preference for carbon formation and poor sulfur tolerance.

Thus after carefully screening a series of DRM catalysts, we chose an alternative catalyst for *in-situ* dry reforming of methane. The greatly improved catalytic performance and coke/sulfur resistance of a NiCu-ZDC bimetallic catalyst made it a superior reforming catalyst for DRM in SOFC. To cope with the difficulty of applying the low-melting-point NiCu

bimetallic to the SOFC anode, which is usually fabricated at high temperature ( $> 1300^{\circ}\text{C}$ ), we designed a triple-layer anode architecture, in which an extra NiCu-ZDC catalyst layer was applied to the anode by using a low temperature process, sustaining both the nano structure of the catalyst and the stoichiometry of NiCu bimetallic. The add-on catalyst layer allowed the CH<sub>4</sub>-CO<sub>2</sub> feed stream to effectively reform prior to entering the Ni-YSZ anode, yielding syngas with residue of reactants. In the novel EDRM process shown here, H<sub>2</sub>S is no longer a poison for the chemical/electrochemical catalyst. We transformed this unfavorable sulfur poison into a catalyst for the H<sub>2</sub> selective oxidation reaction and an enhancement for carbon deposition resistance without significantly decreasing both the chemical and electrochemical activity of the tailored SOFC. Thus, the whole process not only generates electrical power while utilizing CO<sub>2</sub>, but also provides sufficient energy completely compensating that required by the DRM process. Thanks to the sulfur-nickel synergetic effects, we achieved syngas and electricity free of CO<sub>2</sub> emissions. Additionally, the H<sub>2</sub>O generated from the H<sub>2</sub> electrochemical reaction promoted the suppression of carbon deposition. We also performed thermodynamic calculations, demonstrating that this EDRM was completely thermally self-sustained and coke-free when the H<sub>2</sub> conversion was reasonably high at 52%. Although such a high H<sub>2</sub> conversion leads to an H<sub>2</sub>/CO ratio close to  $\sim 1/2$ , it could be adjusted to unity or other targeted values by combining the SRM and DRM together in this one-pot electrochemical reforming of methane (ERM) process.

The Ni-S catalysts resulted in low performance. To cope with this obstacle, we then developed a Ni-Sn anode for the O-SOFC to co-generate syngas and electricity from CO<sub>2</sub>. The NiSn bimetallic alloys have been developed and characterized as both the potential anode material and biogas reforming catalyst. Sn remained preferentially on the surface of the NiSn alloy to enhance both the carbon deposition resistance and sulfur tolerance. The novel reactor delivers high biogas conversion rate, syngas yield and peak power density as well as outstanding tolerance to sulfur poisoning and coking in the biogas atmosphere. This work offers a promising method for biogas utilization in the context of efficient energy conversion technologies.

### **5.5.2. Project outcomes**

1. Our group has the expertise to develop anodes based on infiltration of nickel-based catalysts into porous YSZ microstructures. This is critical to fabricating robust crack-resistant fuel cells. We have determined how the fine pore size of the porous microstructure can control nickel particle growth. Our group is able to infiltrate different anode or cathode materials into the porous YSZ structures and develop high performing electrodes.
2. We have also managed to develop a suitable Ni-YSZ anode microstructure for conventional (un-infiltrated) fuel cells using calcination and milling of YSZ. This had led to unique fuel cell performance especially under SOEC mode where the highest ever reported output current densities were achieved.

3. Anode supported proton conducting tubular fuel cells based on Ni-BaCe<sub>0.7</sub>Zr<sub>0.1</sub>Y<sub>0.1</sub>Yb<sub>0.1</sub>O<sub>3</sub> were developed which perform well under humidified hydrogen and its mixture with carbon monoxide.

4. Novel proton conducting fuel cells were also developed by our research group for the first time which are based on a Ni-YSZ anode support which provides significantly higher mechanical strength for the cell.

5. We have managed to fabricate and test tubular SOFC stacks of 6-12 cells delivering about 15 W power. We have identified our system resistance losses and lowered them. We are hoping to improve our stack power performance by a factor of two.

6. We are ready to incorporate the new catalyst material developed by our research group into the tubular design and fabricate and test the new stack.

7. 3YSZ shows magnificent results under syngas without undergoing coke formation. It can be the next candidate to use as the support in SOFCs which need to run under hydrocarbon.

8. Microwave sintering could pave the way for a faster and more cost-effective solution to fabricating SOFCs.

9. The new current collector does have better conductivity. Accordingly, now less current collector can have the same performance as the old current collector resulting in further cost savings.

## **5.6. Important lessons learned**

1. Loss of power output from the fuel cells is predominantly due to resistance from the testing equipment wiring.
2. Challenges in the successful fabrication of a NiO-PCE anode support. Different particle sizes of precursors for BaZr<sub>0.1</sub>Ce<sub>0.7</sub>Y<sub>0.1</sub>Yb<sub>0.1</sub>O<sub>3-δ</sub> and NiO composite were tested in the slip casting stage. This also influenced the compatibility of the support with the proton conducting electrolyte, due to different shrinkage rates of the anode and electrolyte at 1450°C.

## **5.7. References**

- [1] A. W. Budiman, S.-H. Song, T.-S. Chang, C.-H. Shin, and M.-J. Choi, "Dry Reforming of Methane Over Cobalt Catalysts: A Literature Review of Catalyst Development," *Catal. Surv. from Asia*, vol. 16, no. 4, pp. 183–197, Dec. 2012.
- [2] C. Guerra, A. Lanzini, P. Leone, M. Santarelli, and N. P. Brandon, "Optimization of dry reforming of methane over Ni/YSZ anodes for solid oxide fuel cells," *J. Power Sources*, vol. 245, pp. 154–163, 2014.

- [3] R. J. Gorte, S. Park, and J. M. Vohs, “Direct oxidation of hydrocarbons in a solid-oxide fuel cell,” *Nature*, vol. 404, no. 6775, pp. 265–267, Mar. 2000.
- [4] A. Lanzini, P. Leone, C. Guerra, F. Smeacetto, N. P. Brandon, and M. Santarelli, “Durability of anode supported Solid Oxides Fuel Cells (SOFC) under direct dry-reforming of methane,” *Chem. Eng. J.*, vol. 220, pp. 254–263, 2013.
- [5] X.-M. Ge, S.-H. Chan, Q.-L. Liu, and Q. Sun, “Solid Oxide Fuel Cell Anode Materials for Direct Hydrocarbon Utilization,” *Adv. Energy Mater.*, vol. 2, no. 10, pp. 1156–1181, Oct. 2012.
- [6] W. Wang, C. Su, Y. Wu, R. Ran, and Z. Shao, “Progress in Solid Oxide Fuel Cells with Nickel-Based Anodes Operating on Methane and Related Fuels,” *Chem. Rev.*, vol. 113, no. 10, pp. 8104–8151, Oct. 2013.
- [7] S. E. Evans, J. Z. Staniforth, R. J. Darton, and R. M. Ormerod, “A nickel doped perovskite catalyst for reforming methane rich biogas with minimal carbon deposition,” *Green Chem.*, vol. 16, no. 10, pp. 4587–4594, Jul. 2014.
- [8] K. T. Lee, C. M. Gore, and E. D. Wachsman, “Feasibility of low temperature solid oxide fuel cells operating on reformed hydrocarbon fuels,” *J. Mater. Chem.*, vol. 22, no. 42, pp. 22405–22408, 2012.
- [9] B. Hua, M. Li, J. Pu, B. Chi, and L. Jian, “BaZr 0.1 Ce 0.7 Y 0.1 Yb 0.1 O 3–δ enhanced coking-free on-cell reforming for direct-methane solid oxide fuel cells,” *J. Mater. Chem. A*, vol. 2, no. 31, pp. 12576–12582, Jun. 2014.
- [10] Z. Zhan and S. A. Barnett, “An octane-fueled solid oxide fuel cell.,” *Science*, vol. 308, no. 5723, pp. 844–7, May 2005.
- [11] L. Yang, S. Wang, K. Blinn, and M. Liu, “Enhanced sulfur and coking tolerance of a mixed ion conductor for SOFCs: BaZr(0.1)Ce(0.7)Y(0.2-x)Yb(x)O(3-delta).,” *Science*, vol. 326, no. 5949, pp. 126–9, Oct. 2009.
- [12] M. Li, B. Hua, S. P. Jiang, J. Pu, B. Chi, and L. Jian, “BaZr0.1Ce0.7Y0.1Yb0.1O3–δ as highly active and carbon tolerant anode for direct hydrocarbon solid oxide fuel cells,” *Int. J. Hydrogen Energy*, vol. 39, no. 28, pp. 15975–15981, 2014.
- [13] M. Li, B. Hua, J. Pu, B. Chi, and L. Jian, “Electrochemical performance and carbon deposition resistance of M-BaZr0.1Ce0.7Y0.1Yb0.1O3–δ (M = Pd, Cu, Ni or NiCu) anodes for solid oxide fuel cells,” *Sci. Rep.*, vol. 5, Jan. 2015.
- [14] C. Zuo, S. Zha, M. Liu, M. Hatano, and M. Uchiyama, “Ba(Zr0.1Ce0.7Y0.2)O3–δ as an Electrolyte for Low-Temperature Solid-Oxide Fuel Cells,” *Adv. Mater.*, vol. 18, no. 24, pp. 3318–3320, Dec. 2006.

- [15] L. Bi, S. Boulfrad, and E. Traversa, “Steam electrolysis by solid oxide electrolysis cells (SOECs) with proton-conducting oxides,” *Chem. Soc. Rev.*, vol. 43, no. 24, pp. 8255–8270, Aug. 2014.
- [16] B. H. Rainwater, M. Liu, and M. Liu, “A more efficient anode microstructure for SOFCs based on proton conductors,” *Int. J. Hydrogen Energy*, vol. 37, no. 23, pp. 18342–18348, 2012.
- [17] E. Fabbri, L. Bi, D. Pergolesi, and E. Traversa, “Towards the next generation of solid oxide fuel cells operating below 600 °C with chemically stable proton-conducting electrolytes.,” *Adv. Mater.*, vol. 24, no. 2, pp. 195–208, Jan. 2012.
- [18] E. Fabbri, L. Bi, D. Pergolesi, and E. Traversa, “High-performance composite cathodes with tailored mixed conductivity for intermediate temperature solid oxide fuel cells using proton conducting electrolytes,” *Energy Environ. Sci.*, vol. 4, no. 12, pp. 4984–4993, 2011.
- [19] T. Hibino, A. Hashimoto, M. Suzuki, and M. Sano, “A Solid Oxide Fuel Cell Using Y-Doped BaCeO<sub>3</sub> with Pd-Loaded FeO Anode and Ba<sub>0.5</sub>Pr<sub>0.5</sub>CoO<sub>3</sub> Cathode at Low Temperatures,” *J. Electrochem. Soc.*, vol. 149, no. 11, pp. A1503–A1508, 2002.
- [20] N. Zakowsky, S. Williamson, and J. T. S. Irvine, “Elaboration of CO<sub>2</sub> tolerance limits of BaCe<sub>0.9</sub>Y<sub>0.1</sub>O<sub>3</sub>–δ electrolytes for fuel cells and other applications,” *Solid State Ionics*, vol. 176, no. 39, pp. 3019–3026, 2005.
- [21] R. Kannan, K. Singh, S. Gill, T. Fürstenhaupt, and V. Thangadurai, “Chemically Stable Proton Conducting Doped BaCeO<sub>3</sub> -No More Fear to SOFC Wastes,” *Sci. Rep.*, vol. 3, pp. 294–303, Jul. 2013.
- [22] S. Fang, K. S. Brinkman, and F. Chen, “Hydrogen permeability and chemical stability of Ni–BaZr<sub>0.1</sub>Ce<sub>0.7</sub>Y<sub>0.1</sub>Yb<sub>0.1</sub>O<sub>3</sub>–δ membrane in concentrated H<sub>2</sub>O and CO<sub>2</sub>,” *J. Memb. Sci.*, vol. 467, pp. 85–92, 2014.
- [23] J. Ma, C. Jiang, P. A. Connor, M. Cassidy, and J. T. S. Irvine, “Highly efficient, coking-resistant SOFCs for energy conversion using biogas fuels,” *J. Mater. Chem. A*, vol. 3, no. 37, pp. 19068–19076, 2015.
- [24] J. B. Robinson, L. D. Brown, R. Jervis, O. O. Taiwo, T. M. M. Heenan, J. Millichamp, T. J. Mason, T. P. Neville, R. Clague, D. S. Eastwood, C. Reinhard, P. D. Lee, D. J. L. Brett, and P. R. Shearing, “Investigating the effect of thermal gradients on stress in solid oxide fuel cell anodes using combined synchrotron radiation and thermal imaging,” *J. Power Sources*, vol. 288, pp. 473–481, 2015.
- [25] A. R. Hanifi, M. A. Laguna-Bercero, T. H. Etsell, and P. Sarkar, “The effect of electrode

infiltration on the performance of tubular solid oxide fuel cells under electrolysis and fuel cell modes," *Int. J. Hydrogen Energy*, vol. 39, no. 15, pp. 8002–8008, 2014.

[26] A. R. Hanifi, A. Torabi, X. Chen, S. Hill, P. Sarkar, and T. H. Etsell, "Development of Redox Resistant Fully Infiltrated Tubular SOFCs," *J. Electrochem. Soc.*, vol. 161, no. 4, pp. F391–F397, Jan. 2014.

[27] A. R. Hanifi, S. Paulson, A. Torabi, A. Shinbine, M. C. Tucker, V. Birss, T. H. Etsell, and P. Sarkar, "Slip-cast and hot-solution infiltrated porous yttria stabilized zirconia (YSZ) supported tubular fuel cells," *J. Power Sources*, vol. 266, pp. 121–131, 2014.

## 6. GREENHOUSE GAS AND NON-GHG IMPACTS

### 6.1. Greenhouse gas impact

The system developed will offer an effective means for recycling CO<sub>2</sub> by using CO<sub>2</sub> as a resource to generate electricity. The process consumes CO<sub>2</sub>, and generates no greenhouse gases. At the same time, CO<sub>2</sub> and CH<sub>4</sub> are converted to a useful feedstock (syngas) for various chemical syntheses. The power generated from the fuel cell reactor replaces in part the need for burning fossil fuels, thus further reducing the emission of greenhouse gases.

#### 6.1.1. Greenhouse gas impact of O-SOFC

In the case of O-SOFC based on a NiSn-YSZ anode with the 2.4 cm<sup>2</sup> working area of the cell, fed with CH<sub>4</sub> (30 mL min<sup>-1</sup>) and CO<sub>2</sub> (30 mL min<sup>-1</sup>) balanced with 200 ppm H<sub>2</sub>S, we obtained a current density of 1.25 A cm<sup>-2</sup> at a voltage of 0.635 V. Within 1 min, 8.4 mL CO<sub>2</sub> remained in the outlet gas.

The net CO<sub>2</sub> consumed in 1 hour in the SOFC with 2.4 cm<sup>2</sup> working area is

$$\text{CO}_{2\text{in}} - \text{CO}_{2\text{remained}} = [30 \left( \frac{\text{mL}}{\text{min}} \right) - 8.4 \left( \frac{\text{mL}}{\text{min}} \right)] \times 10^{-3} \left( \frac{\text{L}}{\text{mL}} \right) \times 60 \left( \frac{\text{min}}{\text{h}} \right) = 1.296 \left( \frac{\text{L}}{\text{h}} \right)$$

The net CO<sub>2</sub> consumed/MWh is

$$\frac{\frac{1.296 \left( \frac{\text{L}}{\text{h}} \right)}{2.4 \left( \text{cm}^2 \right)}}{0.635 \left( \text{V} \right) \times 1.25 \left( \frac{\text{A}}{\text{cm}^2} \right)} = 0.683 \left( \frac{\text{L}}{\text{Wh}} \right)$$

At 25 °C and 1 atm, the volume of 1 mole of ideal gas

$$\frac{V}{n} = \frac{RT}{P} = \frac{0.082 \left( \frac{L \cdot atm}{mol \cdot K} \right) \times 298 (K)}{1 (atm)} = 24.44 \left( \frac{L}{mol} \right)$$

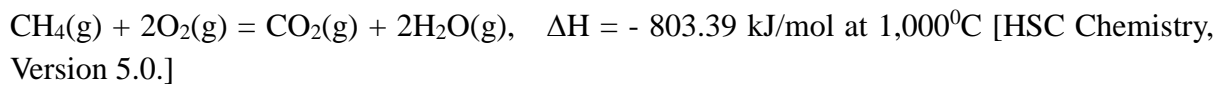
The molecular mass of CO<sub>2</sub> = 44 g/mol. Therefore, the density of CO<sub>2</sub> at 25 °C and 1 atm is

$$\frac{44 \left( \frac{g}{mol} \right)}{24.44 \left( \frac{L}{mol} \right)} = 1.80 \left( \frac{g}{L} \right)$$

CO<sub>2</sub> conversion in tonnes/MWh

$$0.683 \left( \frac{L}{Wh} \right) \times 1.801 \left( \frac{g}{L} \right) \times \frac{10^{-6} \left( \frac{\text{tonne}}{g} \right)}{10^{-6} \left( \frac{MWh}{Wh} \right)} = 1.225 \left( \frac{\text{tonnes of } CO_2}{MWh} \right)$$

Based on the following calculation, generating 1 MWh of energy through combustion of methane at a power plant releases 0.438 tonnes of CO<sub>2</sub> at 45% efficiency (maximum).



$$\text{Amount of } CO_2 \text{ released/MWh} = \frac{44 \left( \frac{g}{mol \text{ } CO_2} \right)}{803.39 \left( \frac{kJ}{mol \text{ } CO_2 \text{ released}} \right) \times 0.2778 \left( \frac{Wh}{kJ} \right) \times 45\%} = 0.438 \text{ (tonnes)}$$

The total CO<sub>2</sub> reduction/MWh

$$\begin{aligned} &= 1.225 \text{ (tonnes of } CO_2 \text{ consumed/MWh)} + 0.438 \text{ (tonnes of } CO_2 \text{ released/MWh)} \\ &= 1.663 \text{ (tonnes of } CO_2 \text{/MWh).} \end{aligned}$$

$$\text{Energy generated for reduction of 1MT of } CO_2 = \frac{10^6 \left( \frac{T \text{ } CO_2}{year} \right)}{1.663 \left( \frac{T \text{ } CO_2}{MWh} \right)} = 6.013 \times 10^5 \left( \frac{MWh}{year} \right)$$

Bloom Energy has recently sold 500 kW units. The energy generated by each unit in one year is

$$= 500 \left( \frac{kW}{unit} \right) \times 24 \left( \frac{h}{day} \right) \times 365 \left( \frac{day}{year} \right) = 4.38 \times 10^3 \left( \frac{MWh}{unit \cdot year} \right)$$

Total converted CO<sub>2</sub> using our anode catalyst on Bloom Energy's SOFC per unit per year will

be

$$\begin{aligned}\frac{\text{Total CO}_2 \text{ reduction}}{\text{unit} \cdot \text{year}} &= 4.38 \times 10^3 \left( \frac{\text{MWh}}{\text{unit} \cdot \text{year}} \right) \times 0.846 \left( \frac{\text{tonnes of CO}_2}{\text{MWh}} \right) \\ &= 7,284 \left( \frac{\text{tonnes of CO}_2}{\text{unit} \cdot \text{year}} \right)\end{aligned}$$

Therefore, the number of units to eliminate 1MT of CO<sub>2</sub>/year

$$= \frac{10^6 \left( \frac{\text{T CO}_2}{\text{year}} \right)}{7,284 \left( \frac{\text{T CO}_2}{\text{unit} \cdot \text{year}} \right)} = 138 \text{ units of 500 kW O-SOFC.}$$

### 6.1.2. Greenhouse Gas Impact of H-SOFC

For our H-SOFC with the 0.316 cm<sup>2</sup> working area of the cell, fed with CH<sub>4</sub> (10 mL min<sup>-1</sup>) and CO<sub>2</sub> (10 mL min<sup>-1</sup>), we obtained a current density of 1 A cm<sup>-2</sup> at a voltage of 0.8 V. Within 1 min, 36.3 mL gas remained in the outlet and 0.4 mL CO<sub>2</sub> in the outlet gas.

Using the same equations as for the O-SOFC, we can get the following values:

$$\text{CO}_2 \text{ conversion in tonnes/MWh} = 4.103 \left( \frac{\text{tonnes of CO}_2}{\text{MWh}} \right)$$

Considering CO<sub>2</sub> generated through combustion of methane at a power plant, the total CO<sub>2</sub> reduction/MWh = 4.541 (tonnes of CO<sub>2</sub>/MWh)

$$\text{Energy generated for reduction of 1MT of CO}_2 = 2.202 \times 10^5 \left( \frac{\text{MWh}}{\text{year}} \right)$$

If using Bloom Energy's 500 kW units with our anode catalyst and proton electrolyte, the number of units to eliminate 1MT of CO<sub>2</sub>/year would = 51 units of 500 kW H-SOFC.

### 6.1.3. Summary of Greenhouse Gas Impact

In summary, the overall reductions in CO<sub>2</sub> emission for every MWh of power generated by our O-SOFC and H-SOFC processes will be 1.663 tonnes/MWh and 4.541 tonnes/MWh, respectively. Consequently, the process can contribute significantly to achieving the target of reducing greenhouse gas emissions in Alberta.

## 6.2. Non-GHG Impact

There are four distinct value propositions (market impact) of this technology: (1) Direct alignment with the Alberta Industrial Heartland's vision of capturing the economic impacts of

additional hydrocarbon value added processing in Alberta; (2) Low parasitic thermal load for the process compared with the steam methane reforming process; (3) Sequesters carbon in CO<sub>2</sub> as carbon in a value added product which could stay in the chemical value chain for a long time; (4) Carbon free electricity generation as a by-product; the electricity could be used onsite reducing the overall GHG impact of the facility.

Schlenker Consulting (2013) has determined that 900 kilotonnes/year (a total of \$270 million in GDP over ten years) of methanol production capacity could be made available in Alberta based on the feedstock availability during the next decade. Methanol demand is increasing worldwide. Although the proposed technology would not capture all of that value, it is reasonable to assume that business drivers exist in Alberta for new technology adoption for methanol and other chemicals production, and that the proposed technology would capture some of the \$270 million value. As well, the technology is not limited to just Alberta; it could be deployed globally, but it would be premature to quantify the potential value at this time in the development stage of the technology.

The GHG benefit of the technology can also be quantified. See Section 6.1 of the developed technology for the GHG benefit values. Additionally, the electricity generated as a by-product has value for reducing the overall GHG intensity of the process. It can be determined that 1 tonne of consumed CH<sub>4</sub> generated 3.66 MWhE as the by-product of the process. Given that 1 tonne CH<sub>4</sub> produces 3.50 tonnes CO, 1 tonne CO production using this technology will produce 1.05 MWhE. Also, given that Alberta has a grid emission intensity factor of 0.65 tonnes of GHG emitted per MWh of electricity produced, the generated electricity would be equivalent to \$10.242 of offset credits under the existing \$15 carbon tax in Alberta. This value will, of course, increase with the coming increase in the value of the carbon tax.

Scalability of the proposed technology has been shown by Siemens Westinghouse and Mitsubishi Heavy Industries via long term testing of 100-220 kW tubular systems with a 300 kW unit under development by Mitsubishi. Bloom Energy has been selling 100-500 kW planar systems for five years. As for replicability, it is interesting to note that 4.5 month tests by both Siemens Westinghouse and Mitsubishi on pressurized 220 kW and 200 kW systems, respectively, yielded very similar results as to electrical efficiency and performance degradation.

There is heavy demand for syngas as a feedstock for refining of metals and production of hydrocarbon fuels as well as petrochemicals.

Carbon monoxide (CO) is used to provide a reducing atmosphere in metallurgical processes such as reduction of iron ore to pig iron or sponge iron. Some transition metals react under pressure with carbon monoxide to yield metal carbonyls which are used as precursors for making homogeneous catalysts or for the preparation of very pure metals such as nickel.

CO is also an important raw material for the production of many industrial chemicals. The major use of CO is in carbonylation of alcohols to higher acids, anhydrides and related carboxylic chemicals, and production of widely used products such as dimethyl carbonate and methyl methacrylate. The cheapest process for the preparation of acetic acid is by catalytic carbonylation with methanol. This consumes more than 500,000 tonnes/year of CO. Analogously, a plant that uses the carbonylation of methyl acetate (Eastman Kodak-Halcon) is producing acetic anhydride at the rate of 250,000 tonnes/year. Other uses of CO include the production of formic acid and methyl formate. N,N-Dimethylformamide is prepared from dimethylamine under similar conditions. Acrylic acid and propanoic acid are also prepared by the hydroxyl carbonylation (Reppe carbonylation) of acetylene and ethylene, respectively.

Syngas is the starting material for the production of a large variety of chemicals, ranging from saturated hydrocarbons to oxygenated compounds. Specifically, the most important applications of syngas are in the production of:

Methanol (from CO+H<sub>2</sub>)

Hydrocarbons: gasoline and diesel fuels (by Fisher-Tropsch process)

Linear aliphatic aldehydes (by Oxo Synthesis)

The world market for the above chemicals is very large and thus CO can be considered as a value added CO<sub>2</sub> reduction intermediate.

## 7. OVERALL CONCLUSIONS

We have demonstrated that the internal dry reforming of methane can be achieved using H-SOFC with a layered structure, or using O-SOFC with an H<sub>2</sub> selective catalyst and a reforming catalyst. An additional internal reforming layer could effectively catalyze the in situ reforming of methane, yielding only syngas in the anode. Hence, both the H-SOFC and deactivated O-SOFC demonstrated excellent electrochemical performance in a CH<sub>4</sub>-CO<sub>2</sub> feed stream, coproducing CO-enriched syngas with little CO<sub>2</sub> as a by-product. The present work sheds light on the configuration optimizations of SOFCs in the context of energy-CO<sub>2</sub> conversions.

Over the past several years, we have made significant progress in the development of robust tubular SOFCs which have delivered some of the highest performances reported under both SOFC and SOEC modes. In part, this has been achieved through optimizing the Ni-YSZ anode microstructure by controlling the particle size of its constituents as well as infiltrating novel cathode materials. We are able to develop a microstructure of suitable porosity and pore size to infiltrate a special catalyst selective to hydrogen and not carbon monoxide. Moving towards scale up, we have fabricated both six and 12 tubular fuel cell stacks and have learned

how to reduce ohmic losses to improve power. We have determined that connecting the stack in a mixed series-parallel configuration not only balances voltage and current but is also most suitable for stack repair in case there is a malfunctioning tube. For the next phase, we hope to incorporate the new catalyst materials developed in the current phase into the tubular cells and fabricate a stack running under a mixture of methane and carbon dioxide. Although we managed to fabricate tubular proton conducting fuel cells with respectable power densities under hydrocarbon fuels, they may prove unsuitable for the current application as they are difficult to fabricate and have shown unacceptable performance degradation.

## 8. SCIENTIFIC ACHIEVEMENTS

### 8.1. Refereed journal papers

#### 8.1.1. Published

1. Amir Reza Hanifi, Benjamin Zahiri, David Mitlin, Adrien L. Vincent, Thomas H. Etsell, Partha Sarkar, "Effect of Washing and Calcination-Milling on Ionic Release and Surface Properties of Yttria Stabilized Zirconia", *Ceramics International*, 42(6), 6755-6760, 2016.
2. Amir Reza Hanifi, Miguel A. Laguna-Bercero, Navjot Kaur Sandhu, Thomas H. Etsell, Partha Sarkar, "Tailoring the Microstructure of a Solid Oxide Fuel Cell Anode Support by Calcination and Milling of YSZ" In press, *Scientific Reports*, 2016.
3. B. Hua, N. Yan, M. Li, Y.-Q. Zhang, Y.-F. Sun, J. Li, T. Etsell, P. Sarkar, K. Chuang, J.-L. Luo, "Novel layered solid oxide fuel cells with multiple-twinned Ni<sub>0.8</sub>Co<sub>0.2</sub> nanoparticles: the key to thermally independent CO<sub>2</sub> utilization and power-chemical cogeneration," *Energy Environ. Sci.*, 9 (2016) 207-215.
4. B. Hua, M. Li, Y.-F. Sun, Y.-Q. Zhang, N. Yan, J. Chen, J. Li, T. Etsell, P. Sarkar, J.-L. Luo, "Biogas to syngas: flexible on-cell micro-reformer and NiSn bimetallic nanoparticle implanted solid oxide fuel cells for efficient energy conversion," *J. Mater. Chem. A*, 4 (2016) 4603-4609.
5. B. Hua, N. Yan, M. Li, Y.-F. Sun, J. Chen, Y.-Q. Zhang, J. Li, T. Etsell, P. Sarkar, J.-L. Luo, "Toward highly efficient *in-situ* dry reforming of H<sub>2</sub>S contaminated methane in solid oxide fuel cells via incorporating coke/sulfur resistant bimetallic catalyst layer," *J. Mater. Chem. A*, (2016), DOI: 10.1039/c6ta02809h.

#### 8.1.2. To be submitted/in preparation

1. Navjot Kaur Sandhu, Amir Reza Hanifi, Andrew Woldnik, Taghi Amiri, Thomas H. Etsell, Jing Li Luo, Partha Sarkar, "Electrochemical Performance of a Short Tubular

Solid Oxide Fuel Cell Stack at Intermediate Temperatures”, Under review, Journal of Applied Energy.

2. Amir Reza Hanifi, Navjot Kaur Sandhu, Jing Li Luo, Thomas H. Etsell, Partha Sarkar, “Development of a Proton Conducting Tubular SOFC”, In preparation.
3. Amir Reza Hanifi, Navjot Kaur Sandhu, Jing Li Luo, Thomas H. Etsell, Partha Sarkar, “Nickel-YSZ anode Based Proton Conducting Fuel Cell”, In preparation.
4. B. Hua, M. Li, Y.-F. Sun, N. Yan, Y.-Q. Zhang, J. Li, T. Etsell, P. Sarkar, J.-L. Luo, “Embedding doped manganite into nickel anode to achieve superior performance and coke/sulfur tolerance for direct biogas solid oxide fuel cells,” To be submitted.

## **8.2. Conference presentations**

1. A. R. Hanifi, M. A. Laguna-Bercero, N. K. Sandhu, J. L. Luo, T. H. Etsell and P. Sarkar, “Tailoring The Microstructure of Anode Supported Microtubular Cells for Fuel Cell and High Temperature Electrolysis Applications”, 21st World Hydrogen Energy Conference, Zaragoza, Spain, June 13-16, 2016.
2. Navjot Kaur Sandhu, Amir Reza Hanifi, M. A. Laguna-Bercero, Andrew Woldnik, Jing Li Luo, Thomas H. Etsell and Partha Sarkar, “Fabrication and Testing of a Short Tubular Solid Oxide Fuel Cell Stack”, 21st World Hydrogen Energy Conference, Zaragoza, Spain, June 13-16, 2016.
3. P. Keyvanfar, A. R. Hanifi, P. Sarkar, T. H. Etsell and V. I. Birss, “Enhancing the Stability of Infiltrated Ni/YSZ Anodes”, SOFC-XIV, Glasgow, Scotland, July 26-31, 2015.
4. Partha Sarkar, Jing Li Luo and Thomas H. Etsell, “Novel Internal Dry Reforming Solid Oxide Fuel Cell Technology for CO<sub>2</sub> Utilization”, COSIA Innovation Summit, Banff, Alberta, March 31 – April 2, 2015.
5. Amir Reza Hanifi, Thomas H. Etsell and Partha Sarkar, “Advanced Electrodes for Tubular Ceramic Fuel Cells”, 39th International Conference and Exposition on Advanced Ceramics and Composites”, Daytona Beach, FL, January 25-30, 2015.
6. Amir Reza Hanifi, Thomas H. Etsell and Partha Sarkar, “Tubular Ceramic Fuel Cell Stack”, 39th International Conference and Exposition on Advanced Ceramics and Composites, Daytona Beach, FL, January 25-30, 2015.

## **9. NEXT STEPS**

Through Phase I of this project, the proposed core concept of the internal dry reforming

SOFC technology for CO<sub>2</sub> utilization has been validated. The technical team also developed another new concept of dry reforming that would produce syngas by inserting a dry reforming reactor in an SOFC cell. In the current project, internal dry reforming using SOFC technology was investigated whereby the SOFC cell is thermally and chemically coupled with the dry reforming process. However, for this new idea being proposed, dry reforming is only thermally but not chemically coupled with the SOFC cell. This concept is schematically shown in Figure 5-9. In this instance, a dry reforming reactor (DRR) is inserted inside a tubular SOFC cell. There is no gas/chemical exchange between the SOFC cell and DRR, so they are not chemically coupled (function independently) but they are thermally coupled and the product is syngas. The syngas produced by dry reforming is a crucially important building block of the chemical industry - it is used in a variety of downstream processes like methanol production, Fischer-Tropsch synthesis processes, carbonylation, hydrogenation, hydro-formylation, etc.

Dry reforming is a strongly endothermic process whereas the SOFC generates heat while operating. In this thermally coupled system, the heat generated by the SOFC will be used for the endothermic dry reforming of methane. The alumina dry reforming tubular reactor walls can be coated with an appropriate dry reforming catalyst as well as catalyst coated on a substrate can be placed inside the reactor chamber as shown in Figure 5-9. It is critical to match the optimum operating temperature of the dry reformer with that of the SOFC. The catalyst for the dry reformer will play a critical role in achieving a high conversion rate and avoiding coking that will deactivate the catalyst. Currently, the project's technical team is in discussion with a Western Canadian leading research group in dry reforming to develop a collaboration and work plan for a CCEMC Grand Challenge Phase II project.

A preliminary estimate of the heat generated during operation of an SOFC with 40% electrical efficiency at 800°C for dry reforming of methane was made. In this scheme, the SOFC is operated using hydrogen fuel. This initial analysis showed that the heat energy from a 1MW SOFC system can convert 22 tonnes of CO<sub>2</sub> per day.

The project team's vision for Phase II is to integrate CO<sub>2</sub> capture by solid sorbents with the SOFC dry reforming technology as shown in Figure 9-1. A research group based in Alberta has developed a sorbent for CO<sub>2</sub> capture with proven efficiency. This has been licensed by a small Alberta based company that is further developing this technology for CO<sub>2</sub> capture. This company is also establishing collaborating relationships with other R&D groups in the province to develop a hybrid Thermal Vacuum-Pressure Swing Adsorption (VPSA) system for CO<sub>2</sub> capture. Our project team is in contact with the company and other R&D groups to consider the process engineering of the system and how to integrate this CO<sub>2</sub> capture technology with the dry reforming SOFC technology.



Figure 9-1 Block diagram of integrated CO<sub>2</sub> capture and dry reforming SOFC technology for CO<sub>2</sub> utilization

### 9.1. High level plan for Phase II and the road map of dry reforming SOFC technology for CO<sub>2</sub> utilization

At the beginning of Phase II of the project a steering committee will be formed. This steering committee will convene every three months. Project progress and any critical issues will be discussed and the committee will provide guidance to tackle identified issues. Phase II also requires greater involvement of the technology provider. The project team has identified several research groups and industries whose participation in the program would be beneficial. The list of the groups/industries under consideration for the next phase of the project appears below:

- University of Alberta's SOFC groups (original developer of the dry reforming SOFC technology)
- Alberta Innovates – Technology Futures (original developer of the dry reforming SOFC technology)
- SOFC manufacturing company (new partner - an international company)
- R&D group with dry reforming expertise (new partner – Western Canadian R&D group)
- Alberta based SME with CO<sub>2</sub> capture technology (new partner)
- R&D group with solid sorbents for CO<sub>2</sub> capture expertise (new partner)
- R&D group with expertise in VPSA and process engineering (new partner)

The goal of this phase of the project is to design, build and operate a prototype in a

simulated environment. This prototype will be able to utilize ~25 kg of CO<sub>2</sub> per day. To build and run such a unit requires considerable facilities that are available at AITF in Edmonton. Some of the main work plan elements for Phase II of the project are:

1. Optimize single cell and short stack performance and perform parametric study for internal dry reforming (IDR) SOFC technology (chemically and thermally coupled);
2. Develop appropriate operating conditions and a catalyst system for thermally coupled dry reforming (TCDR) SOFC technology;
3. Optimize a single unit TCDR SOFC cell and a short bundle, and perform parametric study;
4. Perform a parametric study of the VPSA CO<sub>2</sub> capture system and integrate it with an SOFC.

These activities will occur in the first year of the project. Based on the outcomes from activities numbered 1 to 3, one of the dry reforming technologies (either IDR or TCDR) will be selected for building a kW level prototype system to be integrated with the VPSA based CO<sub>2</sub> capture system. This combined system will be built and tested at the AITF facilities for a parametric study and demonstration. The Phase II development strategy is illustrated in Figure 9-2. In year 1, three major parallel tasks, internal dry reforming technology, thermally coupled dry reforming technology and CO<sub>2</sub> capture technology development will be pursued. At the end of year 1, one of the dry reforming technologies will be selected for further development. The selected dry reforming fuel cell technology will be integrated with CO<sub>2</sub> capture technology and a prototype will be demonstrated.

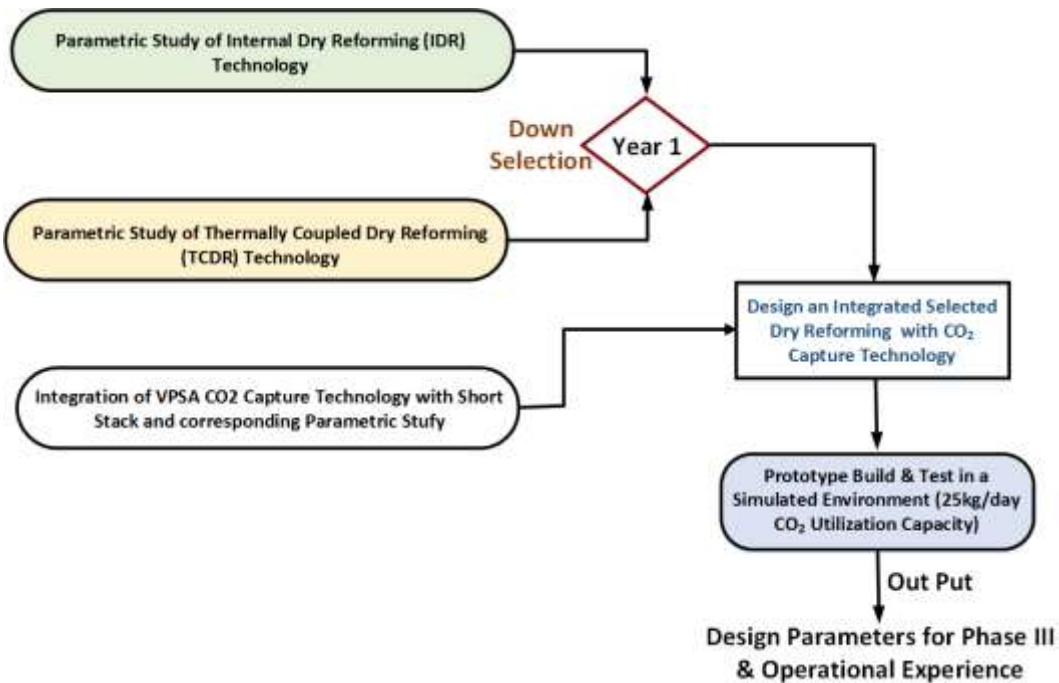


Figure 9-2 Phase II technology development scheme

A high level road map for dry reforming SOFC technology is provided in Figure 9-3. This has four two year segments. The first two-year segment (Phase I) is already completed and has validated the core concept of dry reforming fuel cell technology; the technology has reached TRL 3. The plan for the next two years (year 2016 to 2018 – Phase II) has been discussed in this section. In Phase II of the project, a prototype will be designed and built integrating a kW level SOFC with a VPSA based CO<sub>2</sub> capture unit to achieve a CO<sub>2</sub> utilization ~25 kg/day in a simulated environment (TRL6). In Phase III of the project, the technology will be demonstrated at a user site. This demonstration unit will be capable of utilizing ~500 kg/day CO<sub>2</sub>. This will promote the technology to TRL 7 and provide all the necessary data to design and build a commercial unit. In Phase IV (year 2020), commercialization will begin, led by an SOFC manufacturer and CO<sub>2</sub> technology companies.

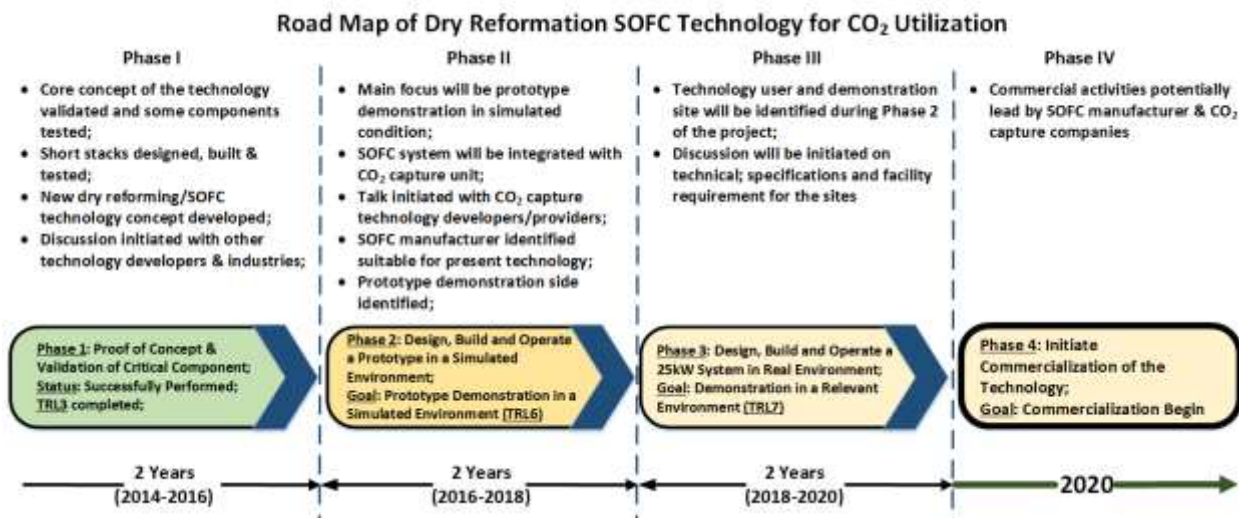


Figure 9-3 Multiyear development road map for dry reforming SOFC technology

## 10. COMMUNICATIONS PLAN

The current technical progress and status of the project was reported through several technical presentations in various Alberta based and international conferences. One of the project's principal investigators gave an oral presentation at the COSIA Innovation Summit in Banff, Alberta on April 2, 2015. The full list of conference presentations has been provided in Section 8. Several technical articles have been published in reputed international journals to validate and disseminate the project results. They are also given in Section 8.

A project-specific communications plan will be developed and implemented as the Phase II proposal is prepared. Some of the strategies, channels, activities and events the project team will use to communicate include:

- **Use social media channels** (Twitter, Instagram, Vine and YouTube) to increase public awareness and attract media attention
- **Conduct media interviews** (specialty and mainstream media outlets) to increase public awareness of the project itself, CCEMC and project partners (University of Alberta, AITF, etc.)
- **Give presentations** at conferences, workshops and other relevant events to increase understanding of the project, promote 'Made in Alberta' technologies and spread the word about CCEMC's ongoing efforts to reduce GHG emissions
- **Create a web presence** for the project (University of Alberta, AITF and CCEMC websites) to enable people to learn more about it and the talented experts involved

- **Host a technical workshop** that, among other things, provides an update on the project and invites participants to contribute or collaborate
- Represent the project at Government of Alberta and CCEMC events on an ‘as requested’ basis
- **Submit project update articles** to scientific journals for publication to provide other researchers with some technical details about the project